

PHOTOCATALYTIC DEGRADATION OF DICLOFENAC USING DIFFERENT MIXED OXIDE CATALYSTS

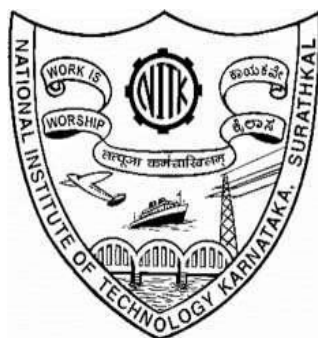
THESIS

Submitted in partial fulfilment of the requirements for the degree of

DOCTOR OF PHILOSOPHY

by

MUGUNTHAN E



DEPARTMENT OF CHEMICAL ENGINEERING
NATIONAL INSTITUTE OF TECHNOLOGY KARNATAKA
SURATHKAL, MANGALORE, INDIA - 575025

JANUARY, 2021

DECLARATION

I, **Mr. Mugunthan E.**, hereby *declare* that the Research Thesis entitled “**Photocatalytic degradation of diclofenac using different mixed oxide catalysts**” which is being submitted to the National Institute of Technology Karnataka, Surathkal in partial fulfilment of the requirements for the award of the Degree of **Doctor of Philosophy** in the Department of Chemical Engineering, is a *bonafide report of the research work carried out by me*. The material contained in this Research Thesis has not been submitted to any University or Institution for the award of any degree.

Place: NITK, Surathkal

Date:

Name: MUGUNTHAN E

Register Number: 148022CH14F07

Department of Chemical Engineering

CERTIFICATE

This is to certify that the Research Thesis entitled “**Photocatalytic degradation of diclofenac using different mixed oxide catalysts**” submitted by **Mr. Mugunthan E. (Register Number: 148022CH14F07)** as the record of the research work carried out by him, is *accepted as the Research Thesis submission* in partial fulfillment of the requirements for the award of degree of **Doctor of Philosophy**.

Research supervisors

Dr. M. B. Saidutta

Professor

Dept. of Chemical Engineering

NITK, Surathkal

Dr. P. E. JagadeeshBabu

Associate Professor

Dept. of Chemical Engineering

NITK, Surathkal

Chairman – DRPC

Dr. Prasanna B. D.

Head of the Department

Dept. of Chemical Engineering

NITK, Surathkal

ACKNOWLEDGEMENT

With great pleasure and immense gratitude, it is my privilege to extend my heartfelt thanks to all the people who helped to finish the research thesis. First and foremost, I express my earnest gratitude to my Research supervisors Prof. M. B. Saidutta and Dr. P. E. JagadeeshBabu, Assoc. Professor, Department of Chemical Engineering, NITK Surathkal, for their inspiring guidance, encouragement, endless advice, fabulous support and invaluable suggestions throughout my research work.

I am forever grateful to my RPAC member and the former head of department Dr. Hari Mahalingam, for imparting his knowledge and providing continuous feedback and comments on this field of research work. I would also like to express my sincere gratitude to my RPAC member, Dr. H. D. Shashikala, Department of Physics, for her kind and encouraging support and suggestions for the enhancement of my research thesis.

I would like to express my heartfelt thanks and sincere gratitude to the past and the present HODs of Chemical Engineering, Prof. Vidya Shetty K, Prof. Raj Mohan B, Dr. Hari Mahalingam and Dr. Prasanna B. D., for their unstinted support at crucial occasions. I would like to thank all the faculty members of Chemical Engineering for the valuable support and encouragement.

I am also greatly indebted to Mrs. Shashikala, Mr. Sadashiva, Mrs. Thrithila Shetty, Mr. Mahadeva, Mr. Suresh, Mr. Harish, Mr. Sukesh, Mr. Ramesh, Mrs. Bhavya, Mrs. Sandhya, Mrs. Vijetha and all the technical and non-technical staffs of the Department of Chemical Engineering for their passionate and timely help during my research work.

I express my special thanks to Dr. Abhinav K. Nair, Dr. M. Shivananth, Dr. M. Rajashekara, Dr. K. Gopinath, Mr. K. S. Pragadeesh and Mr. Ajuy Sundar V. V. for their kind and wholehearted support.

I owe my deepest gratitude to my friends and my family members for giving their extended, tireless assistance and constant encouragement for the fulfillment of my research work.

MUGUNTHAN E.

ABSTRACT

Elimination of pharmaceutical compounds and their metabolites from the aquatic systems has been a tedious process. The various photocatalytic process using TiO_2 as semiconductor photocatalysts has enormous potential to cope with the challenges in the removal of pharmaceutical compounds. However, the TiO_2 -mediated photocatalytic water treatment suffers from the faster rate of recombination and wide bandgap energy corresponding to UV light. Coupling with other semiconductor oxides has reportedly reduced the recombination rate and drawbacks of the short excitation range. In the present work, the degradation of diclofenac in the photocatalytic system is carried out by using different mixed oxide catalysts prepared by hydrothermal method. The heterojunction mixed oxide catalysts can improve the photocatalytic activity by reducing the recombination rate of charge carriers and enhanced the excitation ability of the coupled catalysts in the visible light region. A series of mixed oxide catalysts were prepared with different molar concentrations of $\text{TiO}_2\text{-SnO}_2$, $\text{TiO}_2\text{-WO}_3$, ZnO-WO_3 and $\text{TiO}_2\text{-CdS}$ and were characterized by XRD, TEM, BET surface area and UV spectrophotometric analyses. Initially, the performance of a series of $\text{TiO}_2\text{-SnO}_2$ mixed oxide catalysts was studied. The photocatalytic efficiency was analyzed in the degradation of diclofenac and the degradation kinetics were extensively investigated. The influence of various parameters such as initial drug concentration, pH and catalyst loading was also studied. The $\text{TiO}_2\text{-WO}_3$ mixed oxide catalysts were tested for its photocatalytic efficiency and the results suggested that the series of prepared mixed oxide catalysts exhibited better catalytic activity than the pure TiO_2 under visible light irradiation.

The diclofenac degradation using ZnO-WO_3 heterojunction catalysts under visible light irradiation were evaluated and the synthesized ZnO-WO_3 mixed oxide catalyst produced better performance than the individual components of the photocatalyst. Degradation of diclofenac using $\text{TiO}_2\text{-CdS}$ mixed oxides shows that the presence of the optimum amount of CdS in the coupled heterostructure exhibited higher photocatalytic efficiency under visible light. Comparing the performance of all the mixed oxide catalysts, $\text{TiO}_2\text{-WO}_3$ mixed oxide catalysts displayed the best catalytic activity among others under optimum operating conditions. Degradation experiment data of all the mixed oxide catalysts well fitted to pseudo-first-order reaction and the rate constants were determined.

The photocatalytic degradation of diclofenac was greatly affected by initial pH, catalyst dosage and initial diclofenac concentration. The degradation was highly effective under the acidic condition for all the prepared coupled photocatalysts and the surface charge property of photocatalysts played an important role in the adsorption of drug diclofenac onto the catalyst surface. The degradation reaction mechanisms of the mixed oxide catalysts were studied and it must be noted that the hydroxyl radicals and photogenerated holes were the main active species in the diclofenac degradation process. The charge transfer between heterostructure photocatalysts has been confirmed by the photoluminescence studies. LCMS was used to analyze the various degradation products formed during the irradiation and it is revealed that several MS peaks corresponding to partially degraded products were observed during the course of photocatalytic degradation of diclofenac. Mainly these observed degradation products were preceded by the attack of $\cdot\text{OH}$ radicals and hydroxylation reactions which was further followed by decarboxylation, dechlorination and C-N cleavage reactions.

Keywords: Diclofenac, Photocatalytic activity, adsorption, hydroxyl radicals, holes, degradation products, hydroxylation, decarboxylation.

CONTENTS

S.NO.	TITLE	PAGE NO.
	LIST OF FIGURES	vi
	LIST OF TABLES	xi
	NOMENCLATURES	xiii
1	INTRODUCTION	1
1.1	Pharmaceuticals and their environmental concern	2
1.1.1	Diclofenac	3
1.2	Removal of Pharmaceuticals	5
1.3	Advanced Oxidation Process	6
1.4	Mechanism of Semiconductor Photocatalysis	7
1.5	Modifications of photocatalysts	8
1.6	Organisation of the thesis	9
2	LITERATURE REVIEW	11
2.1	Occurrence and fate of pharmaceuticals in the environment	11
2.2	Removal techniques used for pharmaceutical compounds	14
2.3	Advance treatment techniques for removal of pharmaceuticals	14
2.4	Photocatalysis	17
2.4.1	Choice of photocatalyst	18
2.5	Photocatalytic degradation of pharmaceutical compounds	21

2.6	Development of coupled photocatalysts	24
2.7	Inferences from the literature	28
2.8	Scope and Objectives of the work	30
3	MATERIALS AND METHODS	31
3.1	Catalysts preparation	31
3.1.1	Materials used	31
3.1.2	Preparation of TiO ₂ -SnO ₂ catalysts	31
3.1.3	Preparation of TiO ₂ -WO ₃ catalysts	32
3.1.4	ZnO-WO ₃ photocatalysts preparation	32
3.1.5	Preparation of TiO ₂ -CdS catalysts	33
3.2	Characterization of catalysts	33
3.3	Photocatalytic experiments	34
3.4	Analytical methods	35
3.5	Kinetics of photodegradation	36
4	PHOTOCATALYTIC DEGRADATION OF DICLOFENAC USING TiO ₂ -SnO ₂ CATALYSTS	37
4.1	RESULT AND DISCUSSION	37
4.1.1	Characterisation of TiO ₂ -SnO ₂ catalysts	37
4.1.2	Photocatalytic activity evaluation	42
4.1.2.1	Effect of molar composition of Ti-Sn	42
4.1.2.2	Effect of catalyst loading	45

4.1.2.3	Effect of initial pH	46
4.1.2.4	Effect of initial diclofenac concentration	47
4.1.3	Effect of scavengers and the role of active species	49
4.1.4	Reusability and stability	51
4.1.5	Identification of intermediate products	52
4.1.6	Cost analysis for TiO ₂ and TiO ₂ -SnO ₂ mixed oxides	54
4.2	CONCLUSION	55
5	PHOTOCATALYTIC DEGRADATION OF DICLOFENAC USING TiO ₂ -WO ₃ CATALYSTS	57
5.1	RESULT AND DISCUSSION	57
5.1.1	Characterisation of TiO ₂ -WO ₃ catalysts	57
5.1.2	Photocatalytic activity evaluation	62
5.1.2.1	Effect of molar composition of Ti-W	62
5.1.2.2	Effect of catalyst loading	64
5.1.2.3	Effect of initial pH	64
5.1.2.4	Effect of initial diclofenac concentration	65
5.1.3	Effect of radical scavengers and the role of active species	66
5.1.4	Catalyst stability	68
5.1.5	Identification of degradation products	68
5.1.6	Cost analysis for TiO ₂ and TiO ₂ -WO ₃ mixed oxides	71
5.2	CONCLUSION	71

6	PHOTOCATALYTIC DEGRADATION OF DICLOFENAC USING ZnO-WO ₃ CATALYSTS	73
6.1	RESULT AND DISCUSSION	73
6.1.1	Characterisation of prepared catalysts	73
6.1.2	Photocatalytic activity of mixed oxide catalysts	78
6.1.2.1	Effect of molar ratios of Zn and W	78
6.1.2.2	Effect of catalyst loading	80
6.1.2.3	Effect of initial pH	81
6.1.2.4	Effect of initial diclofenac concentration	82
6.1.3	Role of active species and reaction mechanism	83
6.1.4	Stability and reusability of the catalyst	85
6.1.5	Identification of degradation products	86
6.1.6	Cost analysis for ZnO and ZnO-WO ₃ mixed oxides	88
6.2	CONCLUSION	89
7	PHOTOCATALYTIC DEGRADATION OF DICLOFENAC USING TiO ₂ -CdS CATALYSTS	91
7.1	RESULT AND DISCUSSION	91
7.1.1	Characterisation of TiO ₂ -CdS catalysts	91
7.1.2	Photocatalytic activity evaluation	96
7.1.2.1	Effect of different molar ratios	96
7.1.2.2	Effect of catalyst dosage	98
7.1.2.3	Effect of initial pH	99

7.1.2.4	Effect of initial concentration	100
7.1.3	Effect of scavengers and the role of active species	101
7.1.4	Catalyst stability	102
7.1.5	Identification of degradation products	103
7.1.6	Cost analysis for TiO ₂ and TiO ₂ -CdS mixed oxides	105
7.2	CONCLUSION	106
8	SUMMARY AND CONCLUSION	109
8.1	Scope for future work	113
	REFERENCES	114
	LIST OF PUBLICATIONS	131
	APPENDIX	132
	BIODATA	133

LIST OF FIGURES

Figure No.	Title	Page No.
1.1	Sources and routes of pharmaceutical compounds into the aquatic environment	3
1.2	Chemical structure of diclofenac	4
1.3	A Schematic diagram of mechanism of semiconductor photocatalysis	7
2.1	Band positions of several semiconductor oxides and chalcogenides in contact with aqueous electrolyte at pH 1	20
2.2	Charge transfer mechanism in the coupled photocatalytic system	25
3.1	Schematic representation batch photocatalytic reactor	35
4.1	XRD patterns of the prepared TiO ₂ -SnO ₂ catalysts with different molar ratios	38
4.2	TEM images of (a) Pure TiO ₂ ; (b) T1S1; (c) T5S1; (d) T10S1; (e) T20S1; (f) T30S1 and HRTEM images of (g) T1S1; (h) T5S1; (i) T10S1; (j) T20S1; (k) T30S1.	39
4.3	EDS images of (a) Pure TiO ₂ ; (b) T1S1; (c) T5S1; (d) T10S1; (e) T20S1 and (f) T30S1	40
4.4	Tauc plot for calculation of band gap of all the prepared catalysts	42
4.5	Effect of molar ratios of Ti-Sn on photocatalytic degradation of diclofenac (Initial concentration = 20 mg/L, pH = 5 and catalyst loading = 0.8 g/L) (a) Plot of degradation % vs time; (b) Kinetics of diclofenac degradation and (c) TOC removal % vs time	45
4.6	Effect of catalyst concentration on photocatalytic degradation of diclofenac (pH = 5 and initial diclofenac concentration = 20 mg/L)	46
4.7	(a) The pH _{ZPC} of the pure TiO ₂ and T20S1 catalyst and (b) Effect of initial pH on photocatalytic degradation of diclofenac	47

	(Initial concentration = 20 mg/L and catalyst loading = 0.8 g/L)	
4.8	Effect of initial concentration on photocatalytic degradation of diclofenac (a) Diclofenac degradation over irradiation time; (b) Kinetics of diclofenac degradation with respect to initial concentration; (c) Plot of TOC removal % vs time and (d) plot of rate constants vs initial diclofenac concentration (pH = 5 and catalyst loading = 0.8 g/L).	49
4.9	(a) Effect of different scavengers and (b) PL spectra for $\cdot\text{OH}$ radical evaluation under UV irradiation (Initial concentration = 20 mg/L, pH = 5 and catalyst loading = 0.8 g/L)	50
4.10	Reusability and stability of the prepared catalysts (Initial concentration = 20 mg/L, pH = 5 and catalyst loading = 0.8 g/L)	51
4.11	The LCMS spectra of intermediates formed (Initial concentration = 20 mg/L, pH = 5 and catalyst loading = 0.8 g/L)	52
4.12	The probable degradation pathway of diclofenac using TiO_2 – SnO_2 mixed oxide catalysts	53
5.1	XRD patterns of the prepared TiO_2 - WO_3 catalysts	58
5.2	TEM images of (a) Pure TiO_2 ; (b) TW1; (c) TW5; (d) TW10 and (e) TW20 and HRTEM images of (f) TW1; (g) TW5; (h) TW10 and (i) TW20	59
5.3	EDS of (a) TW1; (b) TW5; (c) TW10 and (d) TW20	60
5.4	Tauc plot for calculation of band gap of all the prepared catalysts	61
5.5	Effect of molar ratios on TiO_2 - WO_3 catalyst for photocatalytic degradation of diclofenac (a) percentage degradation of diclofenac over the time (b) kinetics of photodegradation and (c) TOC removal efficiency for different mixed oxide catalysts (Initial concentration = 25 mg/L, pH = 5 and catalyst loading = 0.6 g/L).	63
5.6	Effect of catalyst loading on photocatalytic degradation of diclofenac (pH = 5 and initial diclofenac concentration = 25 mg/L)	64

5.7	(a) The pH_{ZPC} of the TiO_2 and TW10 catalyst and (b) Effect of initial pH on photocatalytic degradation of diclofenac (Initial concentration = 25 mg/L and catalyst loading = 0.6 g/L)	65
5.8	Effect of initial concentration on photocatalytic degradation of diclofenac (pH = 5 and catalyst loading = 0.6 g/L). (a) plot of percentage degradation vs time; (b) kinetics of degradation with respect to time; (c) TOC removal percentage for different initial concentrations; (d) plot of rate constant vs initial concentration.	66
5.9	(a) Effect of different scavengers on diclofenac degradation (b) PL spectra for $\cdot OH$ radical evaluation (Initial concentration = 25 mg/L, pH = 5 and catalyst loading = 0.6 g/L)	67
5.10	Reusability and stability of TiO_2-WO_3 photocatalysts (Initial concentration = 25 mg/L, pH = 5 and catalyst loading = 0.6 g/L)	68
5.11	LCMS spectra corresponding to degradation products formed (Initial concentration = 25 mg/L, pH = 5 and catalyst loading = 0.6 g/L)	69
5.12	Tentative degradation pathway for diclofenac degradation	70
6.1	X-ray diffraction patterns of $ZnO-WO_3$ mixed oxide catalysts	73
6.2	TEM and HR-TEM images of ZnW1 (a and e); ZnW10 (b and f); ZnW20 (c and g) and Bare ZnO (d)	75
6.3	EDS spectrum of (a) ZnW1; (b) ZnW10; (c) ZnW20 and (d) Bare ZnO	76
6.4	Tauc plot for all the prepared $ZnO-WO_3$ mixed oxide catalysts	77
6.5	Photocatalytic degradation of diclofenac using the $ZnO-WO_3$ catalysts prepared with different molar ratios (a) Degradation efficiency of all the prepared catalysts; (b) Kinetics of photodegradation and (c) TOC removal % for all the prepared catalysts (Catalyst loading = 0.8 g/L and Initial diclofenac concentration = 20 mg/L and at solution pH 6)	79
6.6	Effect of catalyst loading on photocatalytic degradation of diclofenac using the $ZnO-WO_3$ catalysts under constant initial diclofenac concentration = 20 mg/L and at pH 6	80
6.7	(a) pH of zero-point charge of bare ZnO and ZnW10 catalyst and (b) Effect of pH on photocatalytic degradation of	81

diclofenac using the ZnO-WO₃ catalysts under constant catalyst dosage = 0.8 g/L and Initial diclofenac concentration = 20 mg/L

6.8	Effect of initial diclofenac concentration on photocatalytic degradation of diclofenac using the ZnO-WO ₃ catalysts under visible light irradiation (a) Degradation percentage with respect to time; (b) Kinetics of degradation; (c) TOC removal efficiency under different initial concentration and (d) Rate constant with respect to different initial concentration (constant catalyst dosage = 0.8 g/L and at solution pH 6)	83
6.9	(a) Role of active species evaluation and (b) PL spectra for [•] OH radical evaluation of pure ZnO and ZnW10 irradiated samples	84
6.10	Stability and reusability of ZnO-WO ₃ photocatalysts under optimum reaction conditions (pH = 6, initial diclofenac concentration = 20 mg/L and catalyst dosage = 0.8 g/L)	86
6.11	LCMS peaks of intermediates formed during diclofenac degradation (pH = 6, initial diclofenac concentration = 20 mg/L and catalyst dosage = 0.8 g/L)	86
6.12	The probable degradation pathway for diclofenac degradation	87
7.1	XRD patterns of all the prepared TiO ₂ -CdS catalysts	92
7.2	TEM images of (a) Pure TiO ₂ ; (b) TC1; (c) TC5; (d) TC10 and HRTEM images of (e) TC1; (f) TC5 and (g) TC10	93
7.3	EDS of (a) TiO ₂ ; (b) TC1; (c) TC5 and (d) TC10	94
7.4	Tauc plot for calculation of bandgap of all the prepared catalysts	95
7.5	Effect of molar ratios on TiO ₂ -CdS catalyst for photocatalytic degradation of diclofenac (a) Degradation efficiency for all the mixed oxide catalysts; (b) Kinetics of photodegradation and (c) TOC removal efficiency for all the mixed oxide catalysts (Initial concentration = 20 mg/L, pH = 5 and catalyst loading = 0.6 g/L)	97
7.6	Effect of catalyst loading on photocatalytic degradation of diclofenac (pH = 5 and initial diclofenac concentration = 20 mg/L)	98

7.7	(a) The pH_{ZPC} of the TiO_2 and TC5 catalyst and (b) Effect of initial pH on photocatalytic degradation of diclofenac (Initial concentration = 20 mg/L and catalyst loading = 0.6 g/L)	99
7.8	Effect of initial concentration on photocatalytic degradation of diclofenac (a) Plot of degradation percentage vs time; (b) Kinetics of photodegradation; (c) TOC removal % for different initial concentration and (d) Rate constant values with respect to initial diclofenac concentration (pH = 5 and catalyst loading = 0.6 g/L)	100
7.9	(a) Effect of different scavengers on diclofenac degradation and (b) PL spectra for $\cdot OH$ radical evaluation of pure TiO_2 and TC5 irradiated samples	101
7.10	Reusability and stability of TiO_2 -CdS photocatalysts under optimum reaction conditions (Initial diclofenac concentration = 20 mg/L; pH = 5 and catalyst loading = 0.6 g/L)	103
7.11	LCMS spectra of intermediates formed during the visible light irradiation (Initial diclofenac concentration = 20 mg/L; pH = 5 and catalyst loading = 0.6 g/L)	104
7.12	Probable diclofenac degradation pathway	105

LIST OF TABLES

Table No.	Title	Page No.
1.1	Physico-chemical properties of diclofenac	5
2.1	Most frequently detected pharmaceutical compounds in WWTP Effluents and their concentrations	11
2.2	Diclofenac metabolites and their toxicity in living organisms	13
2.3	The bandgap of some common photocatalysts at pH 7	19
2.4	Degradation efficiency for diclofenac removal using different methods	29
4.1	Elemental composition and weight percentage of TiO ₂ -SnO ₂ catalysts	41
4.2	Surface area and Size of the catalysts prepared with different molar ratios of Ti-Sn	41
4.3	Apparent rate constant for all the prepared TiO ₂ -SnO ₂ catalysts	43
5.1	Elemental composition and weight percentage of TiO ₂ -WO ₃ catalysts	60
5.2	Surface area and size of the catalysts prepared with different molar composition	61
5.3	Apparent rate constants for all the prepared TiO ₂ -WO ₃ catalysts	62
6.1	Elemental composition and weight percentage of ZnO-WO ₃ catalyst	76
6.2	Surface area and pore volume of all the prepared photocatalysts	78
6.3	Apparent rate constant for all the prepared ZnO-WO ₃ catalysts	79
7.1	Elemental composition and weight percentage of TiO ₂ -CdS catalyst	94
7.2	Surface area and Size of all the prepared TiO ₂ -CdS photocatalysts	96

7.3	Apparent rate constant for all the prepared TiO ₂ -CdS catalysts	96
8.1	Performance of as-prepared catalysts in comparison with other researchers	110
8.2	Degradation efficiency for diclofenac removal using different methods and cost analysis comparison for the prepared mixed oxide catalysts	112

NOMENCLATURE

Symbol	Description
AC	Activated carbon
AOP	Advanced oxidation process
API	Active pharmaceutical ingredient
BDD	Boron doped diamonds
BET	Brunauer-Emmett-Teller
BOD	Biological oxygen demand
COD	Chemical oxygen demand
CB	Conduction band
DBP	Disinfection by-products
EDC	Endocrine disrupting compound
EDS	Energy dispersive X-ray spectroscopy
E _g	Bandgap energy
eV	Electron volt
HR-TEM	High-resolution transmission electron microscope
h _v	Photon energy
ICDD	International Centre for Diffraction Data

MWCNT	Multiwalled carbon nanotubes
NF	Nanofiltration
NHE	Normal hydrogen electrode
NSAID	Non-steroidal anti-inflammatory drug
PL	Photoluminescence
PPCP	Pharmaceuticals and personal care compound
RO	Reverse osmosis
TC	Total carbon
TEM	Transmission electron microscope
TIC	Total inorganic carbon
TOC	Total organic compound
UV	Ultraviolet
UV-Vis	Ultraviolet-visible
VB	Valence band
XRD	X-ray diffraction

CHAPTER 1

INTRODUCTION

Water pollution becomes an issue of increasing concern in most countries. There is an increasing necessity for clean water for all living things across the globe due to the depletion of natural water resources. Surface waters and groundwater are a significant source of easily accessible freshwater resources in many countries. Currently, there are more than 25 % of the earth's population suffer from inadequate water supply to meet standard water demand. This demand for safe drinking water bodies has been an increasing global risk over the past few years. The reduction in accessible freshwater resulted due to poor management and increased human consumption. Water scarcity and polluted water resources have become a serious threat to the sustainability of aquatic environments. The accumulation of certain toxic chemicals and recalcitrant organic and inorganic compounds due to various human activities polluted the fresh groundwater resources. Urbanization and industrialization have also resulted in a serious impact on freshwater resources. However, the major source of water pollution is mainly from industries, which use a huge amount of water for its manufacturing purposes. The impact of untreated industrial effluents depends on their collective characteristics including Biological oxygen demand (BOD), Chemical oxygen demand (COD) and the nature and quantity of suspended solids as well as the presence of some specific inorganic and organic substances. The industrial effluent and municipal sewage water encompass a great quantity of contaminated organic and inorganic compounds which include heavy metals, dyes, inorganic and organic chemicals, pesticides, pharmaceuticals, etc. Certainly, the complete removal of these toxic substances and their refractory residues are not possible by means of conventional wastewater treatment methods. Thus, the pollutants present in these untreated or partly treated domestic or industrial wastewater could accumulate into various drinking water resources could cause a serious risk of contagious water-borne diseases in most developing countries. In India, more than 21% of communicable diseases accounted for are due to unsafe and pollutant drinking water resources as estimated by the world bank. Thus, access to safe and clean freshwater resources is the basic necessity for the living population around the world.

1.1. Pharmaceuticals and their Environmental concern

Pharmaceutical compounds are largely designed for diagnosis, treatment and disease prevention in both humans and livestock by inducing a biological activity. This group of substances includes both, recalcitrant organic and inorganic compounds, moderately water-soluble and biologically active. Pharmaceutical compounds and their residues in the environment are now classified as evolving organic contaminants since they have been detected frequently in aquatic environments (Petrovic et al. 2011). Amongst the countless active pharmaceutical ingredients (APIs) available on the market, the significant groups of pharmaceutical compounds include Non-steroidal anti-inflammatory drugs (NSAIDs), antibiotics, antilipidemic, beta-blockers, antidiabetics, blood lipid-lowering agents, antidepressants, hormones and antihistamines. These group of substances have been prescribed and consumed in large quantities over the past 50 years.

Large scale industrial production of pharmaceutical compounds results in the release of refractory organic compounds and their residues into the aquatic resources, which makes them difficult to treat. There are various chemical and biological processes and their subprocess involved in the production of pharmaceutical products. Generally, pharmaceutical effluents diverge in content and concentration, and hence unique treatment procedures were not applied in the conventional wastewater treatment plants. So, removal of these pharmaceutical residues was not effective and hence receiving water bodies constitutes these pharmaceutical contaminants. Moreover, APIs being relatively hydrophilic in nature and non-biodegradable, conventional biological wastewater treatments were recognized ineffective, which lead to increased persistence of pharmaceutically active compounds and their metabolites in both aquatic and terrestrial environments. Another main pathway of the APIs reaching aquatic resources was due to human consumption in the households, and other prescription drugs used in both human and animal healthcare facilities. The excretion of these drugs reaching the sewer systems and most of the untreated pharmaceuticals along with their bioactive metabolites accumulates into aquatic environments. Several possible sources and routes which lead to the occurrence of pharmaceutical compounds and their metabolites in the aquatic environment are described in Figure 1.1.

The fate of pharmaceuticals depends on the following key factors: adsorption potential, biodegradability and photosensitivity. Studies on the elimination of pharmaceuticals has not always documented whether these compounds are completely

mineralized or simply chemically altered. Although the presence of these pharmaceuticals and their residues were regularly reported in trace amounts (ng/L to µg/L) across the globe, the continuous occurrence of trace amounts of pharmaceutical residues in environmental compartments leads to serious impacts on human and aquatic organisms (Kümmerer 2004). Pharmaceutical compounds are generally regarded as biologically active substances, and they could result in adverse biological effects on interaction with living organisms. Since the eco-toxicological effect of numerous compounds has yet to be recognized, they could cause serious threats to aquatic organisms and the whole ecosystem. Hence, pharmaceutical compounds have been recognized as a significant group of emerging contaminants, as removal of such persistent compounds requires new alternative and effective technologies to eliminate their cumulative concentration in the water resources.

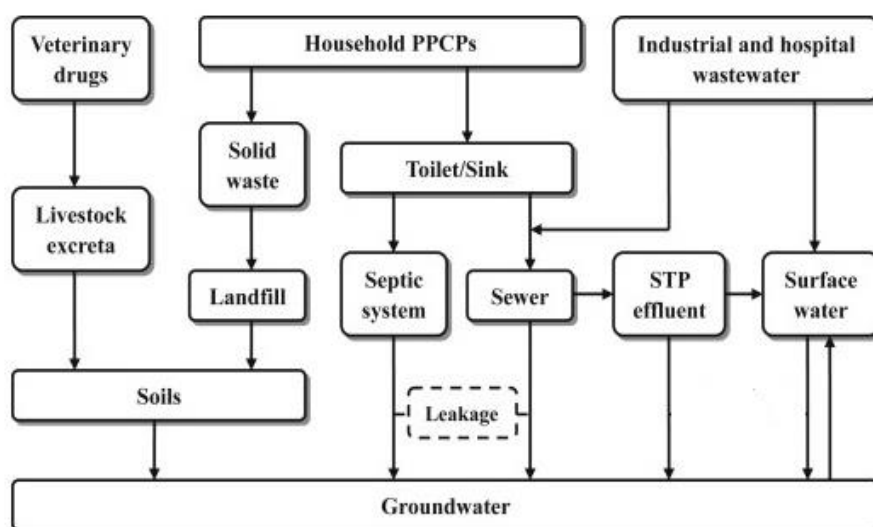


Figure 1.1. Sources and routes of pharmaceutical compounds into the aquatic environment (Source: (Sui et al. 2015)).

1.1.1. Diclofenac

Amid the many important classes of pharmaceuticals, non-steroidal anti-inflammatory drugs (NSAIDs) are of the most significant environmental interest owing to their extensive usability in hospitals and private households. Diclofenac is generally available in its sodium or potassium salt form. Diclofenac is one of the most consumed NSAIDs and diclofenac consumption is estimated and reported to be around 940 tons per year (Zhang et al. 2008b). Diclofenac is very prevalent in human medical care as an analgesic, anti-arthritic and anti-rheumatic agent. It is prescribed with other medication

combinations and also presented in various forms of medication, including oral tablets, capsules, topical gel, and powder forms. Several studies reported that diclofenac has the potential to bioaccumulate in the tissues of various organisms. Higher dosages of diclofenac intake could cause serious health risks to human beings such as stroke, cytotoxic to liver and kidney and various other problems (Haap et al. 2008). The more common side effects of diclofenac include indigestion, nausea, vomiting and stomach pain. Diclofenac is also lethal to other living creatures, as it was reported that diclofenac had been mainly attributed to the dramatic reduction of over 95 % vulture populations due to acute renal failure in the Indian subcontinent (Oaks et al. 2004). Also, the ingestion of 1 ppb of diclofenac possibly will mutilate liver and kidney cell functions in aquatic organisms (Hashim et al. 2014).

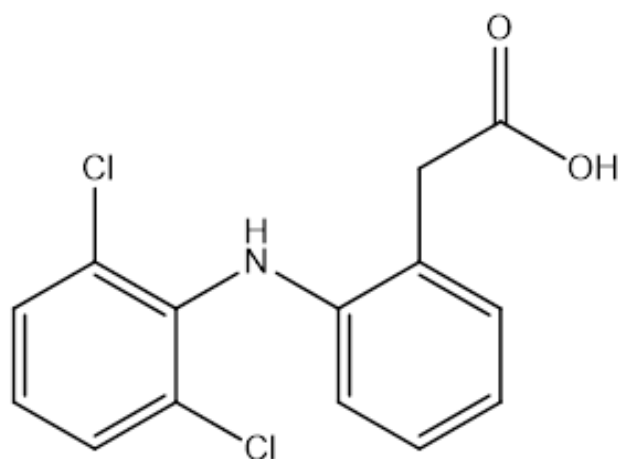


Figure 1.2. Chemical structure of diclofenac

Diclofenac, being resilient to biodegradation, is universally reported in detectable levels in surface waters and even in treated drinking waters (Loos et al. 2017; Sharma et al. 2019; Tröger et al. 2018; Zhang et al. 2008b). It is reported that the eco-toxicity of diclofenac is quite lower; however, in combination with other pharmaceutical metabolites accumulated in water, the toxic effects could increase considerably (Pérez-Estrada et al. 2005). The main cause behind the continuous presence of diclofenac residues in aquatic environments might be due to various factors such as higher consumption of diclofenac, incompetence of WWTPs, its stability and hydrophilicity (Bartels and Jr 2007; Madikizela et al. 2017; Sathishkumar et al. 2020). Even though the lower concentration of diclofenac and their residues in drinking water could not cause any adverse health effects on humans. There is still a need for precautionary measures to remove these pharmaceutical compounds from drinking water to minimize the risk of unforeseen long-term effects. Diclofenac is

regarded as a relentless pharmaceutical compound and their continuous accumulation into aquatic compartments has been a growing concern over the years. DCF is also known to harmfully affect several environmental species already at concentrations of $\leq 1 \mu\text{g/l}$. The removal of most pharmaceutical compounds in conventional WWTPs merely depends on the physical and chemical properties of the compound such as the chemical structure, volatility, acidity, hydrophilicity and sorption potential. The physicochemical properties of diclofenac are listed in table 1.1.

Table 1.1. Physico-chemical properties of diclofenac (Lonappan et al. 2016)

Common name	Diclofenac
Molecular formula	$\text{C}_{14}\text{H}_{11}\text{Cl}_2\text{NO}_2$
Molecular weight	296.149 g/mol
Monoisotopic Mass	295.017 g/mol
Solubility	2.37 mg/L
pKa Value	4.15 \pm 0.2
Melting point	156-158°C
Density	1.4 \pm 0.1 g/cm ³

1.2. Removal of Pharmaceuticals

In surface and groundwater resources, most pharmaceutically active compounds might transform into other products through various reactions which can be more toxic than the parent compound. The harmful effect of these transformed products could cause an undesirable biological effect on aquatic organisms. The conventional methods used for the treatment of these effluents include biological oxidation, physical and chemical treatment. Some of these active pharmaceutical compounds can be reduced or eliminated through biological wastewater treatment systems with the use of activated sludge treatment. Recent reports suggested that many pharmaceutical compounds were removed only to a certain extent in the conventional wastewater treatment methods. This resulted in a growing interest in various treatment technologies alternative to conventional processes to eliminate

these persistent pharmaceutical compounds and their residues from water. Moreover, advanced treatment techniques could be used along with the conventional biological treatment process as tertiary treatment to further stabilise the wastewater containing the recalcitrant organics.

Generally, advanced treatment techniques comprise ultrafiltration, adsorption with activated carbon, ion exchange, reverse osmosis and advanced oxidation process. The treatment techniques, such as adsorption by activated carbon, coagulation, and ion exchange simply transfer the pollutants from one phase to another instead of complete elimination from the wastewater resources, which leads to secondary pollution. Also, these techniques are non-selective and non-destructive processes, which require high-cost maintenance and energy costs. Among these treatment methods, advanced oxidation processes have been reported to be effective for the complete mineralization of recalcitrant organic pollutants from wastewaters.

1.3. Advanced Oxidation Process

Advanced oxidation processes (AOPs) generally rely on the generation of a sufficient amount of highly reactive oxidant species to affect water purification. These oxidant species react with a wide range of target pollutants and could effectively mineralize it to CO₂ and water. Over the years, the AOPs were effectively applied to eliminate numerous toxic recalcitrant chemicals without accumulating additional sludge, which necessitates further treatment. There are many oxidation processes or combinations of processes extensively applied to eliminate the low-biodegradable nature of various pharmaceutical contaminants in different countries.

AOPs are broadly classified into the homogeneous process and heterogeneous catalytic process. Homogeneous processes are further categorized into ozonation, wet oxidation, photo-Fenton, UV photolysis and Electrochemical process. The heterogeneous process involves reactions in which the reactants and the photocatalyst comprise two or more phases. Heterogeneous photocatalysis is a suitable alternative treatment technology, which attracted a lot of interest to cope with increasing challenges with wastewater treatment. The photocatalysis is fundamentally characterized as the acceleration of chemical reaction incited by light absorption by a suitable catalyst. The heterogeneous photocatalysts have been regarded as the potential process and are utilized in the

wastewater treatment process and hydrogen fuel production. As a result of redox reactions, organic contaminants in the effluents can be completely mineralized to a simpler form. Compared to traditional methods, the photocatalytic process has the capability to eliminate refractory organic compounds in the range of ppb, higher speed and lower cost. In recent years, the heterogeneous photocatalytic process has been broadly used for the degradation of various pharmaceutical compounds due to its wide range of benefits.

1.4. Mechanism of Semiconductor Photocatalysis

Semiconductor nanostructure materials with a proper electronic band structure have been used in semiconductor mediated photocatalysis. Generally, the semiconductor can be characterized by a unique electronic band structure, which consists of the highest occupied molecular orbitals, called valence band (VB) and the lowest unoccupied molecular orbitals, called conduction band (CB). The energy difference between the lower valence band and the upper conduction band is generally referred to as the Band Gap. In general, photocatalysis involves two major initial steps, absorption of photons and generation of the bulk electron (e^-) and hole (h^+) pairs.

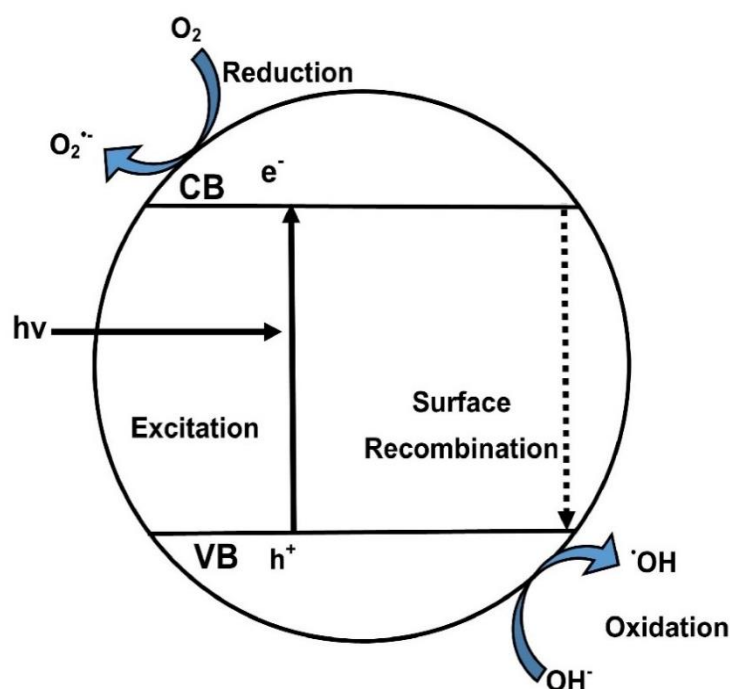
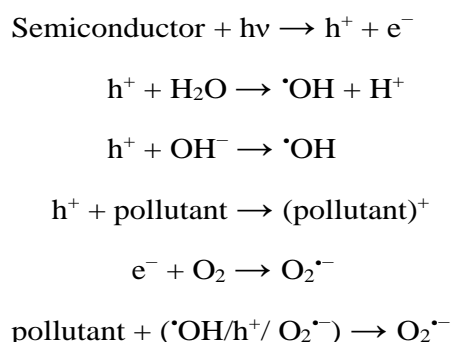


Figure 1.3. A schematic diagram of the mechanism of semiconductor photocatalytic process.

The semiconductor nanostructure materials become photoactivated by absorption of photons with an energy higher than materials bandgap energy, which results in the excitation of an electron from the valence band (VB) to the conduction band (CB) and leaving holes behind in the VB. The photogenerated electrons and holes will migrate to the semiconductor surface to undergo photochemical reactions.

In the presence of adsorbed water and oxygen at the semiconductor surface, electrons and holes could react with a water molecule to produce powerful oxidant species namely hydroxyl radicals ($\cdot\text{OH}$) and superoxide anions ($\text{O}_2^{\cdot-}$), and these reactive oxidant species reduces the refractory organic contaminants to produce CO_2 and water. Degradation of pollutants through semiconductor photocatalysis is catalyzed by the set of oxidation and reduction reaction and has been summarised below:



In certain cases, the photogenerated electrons and holes at the surface could recombine and releases heat energy. The surface recombination of electron and holes result in the reduction of degradation efficiency. In order to avoid this, the electron-hole pair recombination must be suppressed. Recently, various processes have been adapted to reduce recombination by trapping electron or the hole.

1.5. Modifications of photocatalysts

Initially, only TiO_2 had been exploited for photocatalytic purposes. However, various semiconductor nanostructures with proper physicochemical and optical properties can be successively used in the heterogeneous photocatalytic process for various environmental applications. The most important features of the semiconductor oxides to be used in the photocatalytic system are the wide bandgap, high surface area, stability and reusability. Recombination of holes and electrons is the major drawback in most of the photocatalytic system, which hinders its efficiency in the photocatalytic process. Also, the

active surface area will be a prime factor for the adsorption of pollutants onto the surface of the catalyst, thereby affects photocatalytic activity. Thus, it is important to increase the surface area of the catalyst and reduce recombination possibilities. This limitation is overcome by physical and chemical modification of catalysts to improve its performance. The advantages of modification result in improved particle surface area, the active sites and the extension of an optical property, thereby the high rate of reaction can be achieved. There are various improvements in catalyst modification in recent years. These include doping with transition metals, non-metal doping and coupled semiconductor photocatalysts. Doping with metals has been used to alter the electronic structure of semiconductors to efficiently utilize visible light. The presence of metals in semiconductor photocatalysts influences photo-reactivity and interfacial electron-transfer rates. Coupling semiconductor with other metals or semiconductor oxides improves charge separation, thereby reducing recombination rates. Coupling two semiconductors will be used to incorporate the charge transfer between materials of the different bandgap and to encompass the excitation wavelength for the photocatalytic system. Thus, lately, various approaches have been made to produce heterojunction nanostructures by coupling two or more semiconductors and successively applying them to various photocatalytic applications.

1.6. Organization of the thesis

The research study is presented and explained in five chapters, as given below:

Chapter 1 provides a brief overview of the pharmaceutical compounds and their environmental concerns and the use of the photocatalytic system to eliminate the persistent pharmaceutical compounds.

Chapter 2 presents a comprehensive literature review of different pharmaceuticals present in water resources and techniques used to eliminate them. The importance of different photocatalysts and coupled photocatalytic systems are also discussed. Moreover, the background study, the scope and objectives of the present study are also addressed.

Chapter 3 focuses on the materials and methods used for the synthesis of TiO₂-SnO₂ mixed oxide catalysts and its catalytic efficiency in photocatalytic degradation of diclofenac. The kinetic study and various parameters affecting the degradation efficiency are also discussed.

Chapter 4 discusses the photocatalytic degradation of diclofenac using the $\text{TiO}_2\text{-WO}_3$ mixed oxide catalysts under visible light irradiation. The various operating parameters affecting the degradation efficiency are also discussed.

Chapter 5 describes the synthesis and the photocatalytic degradation of diclofenac using ZnO-WO_3 mixed oxide catalysts under visible light irradiation and the effect of various operating parameters.

Chapter 6 deals with the degradation of diclofenac using $\text{TiO}_2\text{-CdS}$ mixed oxide catalysts and the analysis of optimum operating parameters under visible light irradiation.

Chapter 7 discusses the overall summary and conclusion of the present study and the scope for future work.

CHAPTER 2

LITERATURE REVIEW

2.1. Occurrence and fate of pharmaceuticals in the environment

Pharmaceutical industry produces a large and diverse group of human and veterinary medicines. This group of pharmaceutical compounds has been widely used in recent years. Their presence and fate in the aquatic resources pose a prospective threat to the living organisms which were stated in the various literature (Halling-Sorensen et al. 1998; Oaks et al. 2004). Out of the numerous available pharmaceuticals, Antibiotics, Antilipemic agents, NSAIDs, cytostatic drugs, steroids, antidepressants regulators, beta-blockers and endocrine-disrupting compounds (EDCs) were the compounds that were mostly detected in the environment in recent years. The most frequently detected pharmaceutical compounds and their concentration in wastewaters have been reported in Table 2.1.

Table 2.1. Most frequently detected pharmaceutical compounds in WWTP Effluents and their concentrations (Al-Rifai et al. 2007; Liu et al. 2009; Santos et al. 2007; Vieno et al. 2007)

Type of pharmaceuticals	Compound	Concentration
Antibiotics	Sulfamethoxazole	0.02–0.58 (µg/L)
	Ofloxacin	6–52 (ng/L)
	Ciprofloxacin	6–60 (ng/L)
	Trimethoprim	0.11–0.37 (µg/L)
Analgesics, Antipyretics	Acetaminophen	10–23.33 (µg/L)
	Diclofenac	0.01–410 (µg/L)
	Naproxen	0.5–7.84 (µg/L)
	Ibuprofen	0.49–390 (µg/L)
	Ketoprofen	0.13–3 (µg/L)
	Mefenamic acid	190–2390 (ng/L)
	Carbamazepine	0.1–1.68 (µg/L)

CNS Stimulant	Caffeine	3.2–11.44 (µg/L)
Antilipemic agents	Bezafibrate	1.55-7.6 (µg/L)
	Clofibric acid	0.47–170 (µg/L)
	Gemfibrozil	0.3–3 (µg/L)
Beta blockers	Propranolol	0.05 (µg/L)
	Atenolol	10–730 (ng/L)
	Metoprolol	10–390 (ng/L)
X-ray contrast media	Iopromide	0.026–7.5 (µg/L)
	Iomeprol	1.6 µg/L
Endocrine Disrupting Compounds (EDCs)	Estrone	15-96 ng/L
	17β-estradiol	19-118 ng/L
	Estriol	15-175 ng/L
	Tamoxifen	27-369 ng/L
	Bisphenol A	10-710 ng/L
	Nonylphenol	100-700 ng/L

NSAIDs are non-steroidal anti-inflammatory drugs that were extensively used to treat pain, feverish and inflammatory effects. Diclofenac, one of the widely used NSAIDs, has an average consumption of 0.33 ± 0.29 g/person/year globally and out of these, nearly 65 % of drugs has been indicatively used in Asian and European regions alone (Acuña et al. 2015). Diclofenac has been viewed as a concern of emerging contaminants and was counted in the emergency medical list (EML) of 74 nations (Lonappan et al. 2016). Diclofenac, along with certain antibiotics and natural hormones were listed in the previous watch list of EU Decision 2015/495 (Sousa et al. 2019). There are only a few studies that reported the occurrence of diclofenac and its metabolites in freshwater resources and effluents. The industrial production and excretion by patients lead to the recurrent detection of diclofenac in the influent and effluent streams of WWTPs (Kosma et al. 2014), surface water (Wang et al. 2010a), underground water and even drinking water (Rabiet et al. 2006), with a concentration level ranges from 13 ng/L to 7.1 µg/L. Various proportions of diclofenac have also been reported in some of the Indian rivers. The concentration of presence of diclofenac along the Kaveri river basin is reportedly up to 103 ng/L (Shanmugam et al. 2014) and also in the Ganges river up to 140 ng/L (Sharma et al. 2019). Some eco-toxicological studies demonstrated that trace levels of diclofenac could be

accumulated in aquatic organisms and are toxic to microorganisms (Ferrari et al. 2003) and fish (Schwaiger et al. 2004). The diclofenac has been found to undergo various hydroxylated and methoxylated metabolites through biotransformation in humans and other organisms. The major metabolites of diclofenac and their impact on humans and other organisms have been shown in table 2.2.

Table 2.2. Diclofenac metabolites and their toxicity in living organisms (Bonnefille et al. 2017; Sarkar et al. 2017; Sathishkumar et al. 2020)

S. No.	Diclofenac metabolites	Reported Source	Nature of toxicity
1.	3-hydroxydiclofenac	Humans	Prostaglandin synthesis inhibition
2.	4-hydroxydiclofenac & 5-hydroxydiclofenac	Humans, Bacteria and fungi, Mussels and Fish	Inhibition of ATP synthesis and acute toxicity
3.	Diclofenac glucuronide	Humans and mouse	Cytotoxicity and hepatotoxicity
4.	Dichlorobenzene	Bacteria	-
5.	4-hydroxydiclofenac acyl glucuronide	Mouse and Fish	Immune cytopenia

Moreover, the drinking water has been disinfected using various chemical disinfection treatment using chemicals such as chlorine, ozone chloramines and chlorine dioxide. Several works of literature reported that many pharmaceuticals were present in drinking water resources even after the disinfection process (Benotti et al. 2009; Kleywegt et al. 2011; Vulliet et al. 2011). Certain pharmaceuticals compounds present in drinking water resources could result in the formation of disinfection by-products (DBPs) on reacting with certain disinfection chemicals. Postigo and Richardson (2014) reviewed various DBPs formation during chemical disinfection treatment of drinking water using chemicals such as chlorine, ozone and chlorine dioxide. It is reported that pharmaceuticals containing amine and reduced sulfur functional groups have a high affinity to chlorine

reactivity. Similarly, pharmaceuticals having amine and phenol functional groups were highly expected to be transformed into different DPBs in the presence of ozone and chlorine dioxide. Diclofenac is reportedly transformed to chloro-diclofenac, decarboxy-diclofenac and chloro-decarboxy-diclofenac by-products with attack of chlorine on aromatic ring and amine groups. Correspondingly, diclofenac has also affinity towards ozone reactivity and results various hydroxylated and dechlorinated DBPs (Postigo and Richardson 2014; Soufan et al. 2012). The toxicity of these pharmaceutical DBPs on human and aquatic organisms was scarcely identified and reported and hence it is necessary to eliminate these pharmaceuticals and their by-products from aquatic resources.

2.2. Removal techniques used for pharmaceutical compounds

Some of the drugs consumed by humans can be metabolized completely inside the human body. But to the most extent, these compounds were incompletely metabolized and then defaecated and consequently end-up in the municipal wastewater treatment plants (Heberer 2002; Stackelberg et al. 2007). Pharmaceutical industries also contribute a large quantity of pharmaceutically active compounds in wastewater along with other organic and inorganic constituents. The active ingredients present in pharmaceutical effluents are resistant to organisms, such as bacteria and fungi, which makes pharmaceutical effluent extremely resistant to biological degradation. The pharmaceutical compounds like EDCs pose a potential threat to the reproductive system in humans, and antibiotics have the ability to cause long-term changes to the microorganism genome. For many other compounds, their effect on humans and other living organisms has not been understood completely (Halling-Sorensen et al. 1998). Since the pharmaceuticals are present as a mixture with other pollutants in the waste and surface waters, the synergistic or antagonistic effect can also occur (Cleuvers 2004; Jonker et al. 2005). But to the most extent, these compounds were partially metabolized and excreted in the urine and feces and then entered into municipal wastewater treatment plants (Heberer 2002; Stackelberg et al. 2007). Due to variations in composition and concentration of these recalcitrant pharmaceuticals in the wastewaters, conventional methods were not efficient to remove these compounds completely, which leads to accumulating in surface waters and groundwater (Giger et al. 2003; Tekin et al. 2006; Webb et al. 2003). Over the years, various advanced treatment methods like membrane technology, adsorption onto activated carbon, advanced oxidation processes (AOPs), etc., are used for the elimination of these refractory pharmaceutical compounds.

2.3. Advanced treatment technologies for removal pharmaceuticals

Various membrane technologies such as microfiltration, nanofiltration (NF), membrane bioreactors (MBR), reverse osmosis (RO) and ultrafiltration were also applied for the removal of recalcitrant organics from wastewater. Nanofiltration, a membrane filtration based process lately applied to the elimination of various pharmaceutical mixtures in the aqueous solutions. Shahtalebi et al. (2011) investigated the removal of pharmaceutical compound amoxicillin by using polyamide-based NF membrane from industrial wastewater. The various factors influencing the membrane efficiency was evaluated and they achieved high amoxicillin rejection with 97 % efficiency and with about 40 % of COD rejection. Cuhorka et al. (2020) studied the removal of ibuprofen and diclofenac using commercially available NF membranes such as AFC 80, AFC40 and AFC30 and it was reported that the removal of these pharmaceuticals was based on steric mechanism. Kimura et al. (2005) explored the removal of different pharmaceuticals including diclofenac, ibuprofen, clofibric acid, naproxen and ketoprofen using a membrane bioreactor equipped with microfiltration membranes. Better removal efficiency was achieved for naproxen and ibuprofen removal. Additionally, the study specified that the removal efficiency of pharmaceuticals was largely depended on their molecular structure. It is reported that compared to other membrane technologies, microfiltration and ultrafiltration very inefficient and were only able to reject a few pharmaceutical compounds (Snyder et al. 2007). The disadvantages of membrane techniques are flux decline and membrane fouling, necessitating frequent cleaning of the membranes. Another major problem was the disposal of retentate, which requires further treatment (Gadipelly et al. 2014).

Adsorption with activated carbon or other adsorbent materials can be used to remove various organic contaminants from wastewater, due to the following advantages; high surface area, higher pore volume and surface properties. The important parameters that define the effectiveness of adsorbents include adsorption capacity, thermodynamic criteria, pH of aqueous media, contact time, and reusability potential. Mestre et al. (2007) established the ability of activated carbon derived from cork waste for removal of ibuprofen and reported around 90 % removal efficiency. However, activated carbon adsorption was ineffective in eradicating certain refractory organic compounds which might be due to the fact that removal efficiency largely dependent on the pore-size of adsorbent and physical and chemical properties of each compound (Snyder et al. 2007). Also, the isolation of the

adsorbent material from the effluent requires a filtration unit and also it is a costly process. Recently, various adsorbents such as graphene, clay, porous silica, chitosan and zeolites were also reportedly used in the removal of recalcitrant pharmaceutical compounds and however, graphene and grafted chitosan showed better removal efficiency due to its high adsorption capacity. It is reported that the adsorption processes were strongly based on the chemical structure and functional groups of the target pharmaceuticals (Kyzas et al. 2015). The removal of many NSAIDs using the sorption process was ineffective due to its hydrophilic nature, as the pKa value of NSAIDs ranges from 4.1-4.9 (Nikolaou et al. 2007).

Advanced Oxidation Process involves the production of highly reactive oxidant species like hydroxyl radicals ($\cdot\text{OH}$), H_2O_2 , $\cdot\text{OOH}$, O_3 and superoxide anion radical ($\text{O}_2^{\cdot-}$), in reaction media. These strong oxidants provoke redox reactions with various toxic refractory organics such as dyes, aromatics, pharmaceuticals and pesticides to endure complete mineralization (Dalrymple et al. 2007). The AOP was found to be more attractive due to the variety of technologies encompassed and the widespread applicability. AOPs have been utilized to treat various recalcitrant compounds due to their ability to reduce the toxic non-biodegradable compounds. Some of the AOPs that were employed to treat pharmaceutical residues include ozonation, wet-oxidation, Fenton and photo-Fenton process, sonolysis, electrochemical oxidation and semiconductor photocatalysis.

Ozonation process involves two different reaction mechanisms in which ozone itself mediates the direct attack of certain functional groups of organic compounds or by inducing hydroxyl radical formation on decomposition in water. The formed hydroxyl radicals are stronger oxidizing species than ozone. Ozonation has been largely employed in the removal of antibiotics. Ozonation treatment for removal of various pharmaceutical compounds might result in a sequence of oxidation and some transformed pharmaceutical compounds. Dantas et al. (2008) disclosed the necessity for high ozone concentration to attain the complete mineralization of the intermediate products during the ozonation treatment of sulfamethoxazole, and the biodegradability factor increased from 0 to 0.28 under ozonation treatment. Addition of hydrogen peroxide with ozone could also enhance the biodegradation of compounds that were resistant to ozone. Chen et al. (2016a) reported the catalytic ozonation of diclofenac using the Fe-MCM-41 catalyst. The combination of both ozonation and the catalytic process proved to be efficient in mineralizing diclofenac as compared to a single ozonation system. Ahmed et al. (2017) revealed EDCs and pesticides were efficiently removed via ozonation treatment due to their high susceptibility

for ozone reactions. Nevertheless, ozone reactivity is limited to the treatment of certain pharmaceuticals and some compounds with amide functional groups are resistant to ozone.

Electrochemical oxidation is based on in situ production of hydroxyl radicals ($\cdot\text{OH}$) through direct or indirect electrochemistry reactions, thereby persistent organic pollutants in wastewater could be completely degraded. This method has shown great potential for the removal of various pharmaceutical products in recent years. Literature suggests that electrochemical treatment by using platinum and boron-doped diamond (BDD) electrodes exhibited as high as 97 % TOC removal for paracetamol and diclofenac spiked wastewater (Brillas et al. 2005, 2010). Domínguez et al. (2012) observed nearly 100 % TOC removal at optimum operating conditions such as current density and flow rate for pharmaceutical industry effluent by using corrosion stable BDD anode. The foremost downsides of using electrochemical oxidation for the treatment of pharmaceuticals are expensive BDD-electrodes, the energy consumption and the risk of several chlorinated by-products formation. Fernández-Aguirre et al. (2020) reported a cheaper and potential alternative to high-cost BDD-electrodes for electrochemical oxidation of diclofenac.

Fenton process is an advanced oxidation process that involves specific reactions of hydrogen peroxide (H_2O_2) with ferrous or ferric ions in the aqueous medium to yield hydroxyl radicals. The generated $\cdot\text{OH}$ radicals can reduce resistant organic compounds and convert them into benign end products. The photo-Fenton process is characteristically advanced with the help of UV or solar irradiation which results in a higher rate of degradation. Badawy et al. (2009) reported the use of the Fenton process as a pre-treatment for pharmaceutical wastewater containing paracetamol and chloramphenicol with higher COD load, and they achieved over 95 % of COD removal efficiency. Alalm et al. (2015) studied the removal of four different pharmaceuticals such as amoxicillin, ampicillin, diclofenac and paracetamol using the solar photo-Fenton process. It is reported that the removal of pharmaceuticals highly dependent on pH values and optimum dosage of Fenton reagent and the complete removal of all pharmaceuticals attained under acidic conditions. The major drawback of this treatment method is the generation of iron sludge and pH dependence (Gadipelly et al. 2014).

2.4. Photocatalysis

Photocatalysis is a type of catalytic process which involves the light-induced transformation of chemical species in the presence of a catalyst. Fujishima and Honda

(1972) discovered the photosensitization effect of TiO₂ electrodes on the electrolysis of water into H₂ and O₂. Hoffmann et al. (1995) documented the utilization of illuminated semiconductors for the elimination of recalcitrant organics dissolved in air or water and proven to be effective for the degradation of such recalcitrant organic compounds. The photocatalytic degradation process is regarded as the most promising destructive AOPs owing to their ability to eradicate the toxic or non-biodegradable refractory pollutants from the environment. Photocatalytic water treatment has been applied to treat various groups of pharmaceutical compounds (Kanakaraju et al. 2014). The major factors which influence the photocatalytic efficiency include catalyst concentration, initial pH of the solution, adsorption, light source and intensity (Akpan and Hameed 2009).

2.4.1. Choice of Photocatalyst

An ideal photocatalyst must satisfy certain characteristics such as low-cost, appropriate bandgap energy, photoactivity, large specific surface area, non-toxicity and chemically stable. Another important factor to be considered for the use of photocatalyst in the degradation of organic compounds is that the redox potential of H₂O/*OH couple lies within the band edge positions of the semiconductor (Hoffmann et al. 1995). The band edge potentials of various semiconductor materials are listed in table 2.3. Amongst the likely semiconductor materials that can be used in heterogeneous photocatalysis, TiO₂ is extensively used and the most promising photocatalyst for the degradation of various refractory pollutants. TiO₂ has been widely exploited in the photocatalytic water treatment process owing to its superior characteristics such as non-toxic nature, water insolubility, low cost, chemical stability, photoreactive, environmental friendliness and corrosion-resistance (Hassani et al. 2015). ZnO is also a promising catalyst because of the reasons that include exceptional physical and chemical stability, inexpensive, rapid photoresponse, faster electron transport and improved light absorptivity than TiO₂ (Sun et al. 2009). However, it dissolves in acidic solutions and the photoelectron recombination rate is also high, which significantly lessens its quantum efficiency and thus limiting its applicability in photocatalysis (Lv et al. 2016; Di Paola et al. 2012).

Table 2.3. The bandgap of some common photocatalysts at pH 7 (Hu et al. 2016; Xie et al. 2014; Zhang et al. 2019a)

Semiconductor	CB edge potential	VB edge potential	Bandgap energy
Fe ₂ O ₃	0.28	2.48	2.2
CdS	-0.55	1.85	2.4
WO ₃	0.25	2.85	2.6
g-C ₃ N ₄	-1.3	1.4	2.7
TiO ₂	-0.4	2.8	3.2
ZnO	-0.31	2.89	3.2
CeO ₂	-0.35	2.85	3.3
SnO ₂	-0.05	3.55	3.6
ZnS	-1.04	2.56	3.6

Over the years, the photocatalytic activity of different semiconductor materials such as SnO₂, ZrO₂, CdS, CdSe, CeO₂, g-C₃N₄, Fe₂O₃ and WO₃, have been evaluated. These semiconductor nanostructures possess excellent physicochemical properties that could meet the requirement of ideal photocatalyst materials. Band energies of various semiconductor materials are depicted in Figure 2.1. WO₃ is one of the metal oxides which displayed predominant photocatalytic properties such as large specific surface area, good absorption capability and suitable bandgap energy (2.8 eV) for visible light absorption. However, the lower CB edge value of WO₃ (+0.2 to 0.5 V NHE) was more positive than the reduction potential to reduce O₂, thereby, makes it less favorable in the photocatalytic process (Kim et al. 2010). Semiconductor metal sulfides and selenides such as CdS and CdSe could engross greater portions of the solar spectrum due to their narrow bandgap energy of 2.4 eV and 1.75 eV, respectively. Both with a maximum absorption wavelength of over 500 nm, makes them favorable for application in visible light photocatalytic process.

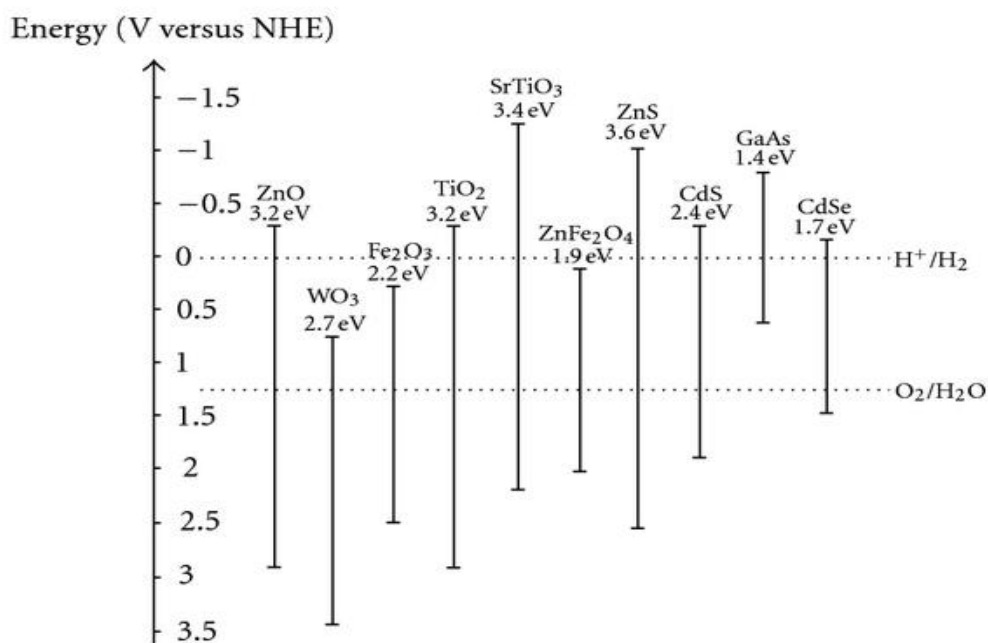


Figure 2.1. Band positions of several semiconductor oxides and chalcogenides in contact with aqueous electrolyte at pH 1 (Source:(Artero and Fontecave 2011)).

However, these catalytic materials were susceptible to photo corrosion and dissociates more toxic Cd^{2+} ions into the solution which limits its practical application in the photocatalytic water treatment process (Li et al. 2015; Wang et al. 2010b). This downside can be resolved by using a coupled semiconductor system or ion doping method. SnO_2 is an n-type semiconductor whose electronic properties, ionic radius, and chemical stability were similar to those of TiO_2 and their electron mobility was reported to be higher than nanocrystalline TiO_2 (Elakhya et al. 2017; Huang et al. 2015). But the photocatalytic performance of SnO_2 in the presence of visible light irradiation is ineffective owing to its wide bandgap and intrinsic defects (Hu et al. 2016). CeO_2 is one of the rare earth metal oxides which were widely used in the photocatalytic process and fuel cell technologies due to its unique optical properties, redox potential, UV absorption ability and catalytic property (Mingyan et al. 2014; Pouretedal et al. 2012). have a high specific surface area and can promote electron transfer reactions at a lower potential. Over the last few years, CeO_2 nanoparticles have been used in photocatalytic applications due to thermal stability, high specific surface area, faster electron transfer reactions, high hardness and reactivity (Phoka et al. 2009). CeO_2 has large oxygen storage capacity which is helpful for electrochemical activity. The large bandgap of CeO_2 ($E_g = 3.4 \text{ eV}$) hinders the visible light utilization, which reduces its applicability in photocatalytic degradation.

Fe₂O₃ is an extensively studied iron oxide for its high photocatalytic activity in the visible light region. The low-cost, chemically stable and non-toxic nature of Fe₂O₃ was the foremost advantage for its application in photocatalytic water treatment (Mishra and Chun 2015). Moreover, there are various oxides such as V₂O₅, Bi₂O₃, ZrO₂, and Cu₂O and other non-metallic polymer-based semiconductors such as g-C₃N₄ and some chalcogenide-based semiconductors such as MoS₂, ZnS, CuS, CdTe were also explore in the photocatalytic applications in the recent years (Di Paola et al. 2012; Rao et al. 2019; Zhang et al. 2019a). Most of these photocatalysts were also suffers drawbacks of recombination of charge carriers and insufficient reduction or oxidation potential. Nevertheless, these catalysts have been modified and synthesized with different preparation methods, through which these catalysts could be used efficiently in photocatalytic water treatment or hydrogen production (Di Paola et al. 2012).

2.5. Photocatalytic degradation of pharmaceutical compounds

The effluents from the pharmaceutical industry contained refractory toxic compounds and their active metabolites generally rendered it non-biodegradable. Hence various advanced treatment technologies like photocatalysts were used to treat pharmaceutical compounds owing to its ability to mineralize toxic pollutants. In the last decades, various researchers successfully applied the photocatalytic process for the degradation of various active pharmaceutical compounds using the commercially available TiO₂ catalysts (Kanakaraju et al. 2014). The high photoreactivity of commercial TiO₂ materials such as anatase TiO₂ and Degussa P25 has gained a lot of interest in photocatalytic water treatment of a wide variety of pharmaceutical compounds.

Calza et al. (2006) studied the photocatalytic degradation of anti-inflammatory drug diclofenac using Degussa P25 under solar irradiation. The optimal parameters for pollutant degradation were evaluated and fitted using response surface methodology. The study reported that increased TiO₂ concentrations had a negative effect on degradation efficiency due to the light scattering phenomenon. The experimental results were fitted with the Langmuir-Hinshelwood model. During the irradiation, several hydroxy- and dihydroxy-diclofenac derivatives were observed during the process. Complete mineralization was reached after 2 h of irradiation and residual diclofenac was reduced to less than 1%.

Hu et al. (2007) inspected the mineralization of sulfamethoxazole and sulfonamide antimicrobial agents using TiO₂ photocatalytic degradation process under UV irradiation. The results suggested that the degradation rate depended on several operational variables, including initial concentration and catalyst concentration. It is observed that initial pH has a negligible effect on reaction rates. It is revealed that the degradation paths of sulfamethoxazole and sulfonamide agents are instigated by [•]OH radical attack on the aromatic or heterocyclic ring or the sulfonamide bond.

Yurdakal et al. (2007) studied the photocatalytic degradation of two drugs Tamoxifen and Gemfibrozil by using commercially available polycrystalline TiO₂ catalysts. The photocatalysis had a minor role in Tamoxifen mineralization, while faster degradation and mineralization of Gemfibrozil is observed. The photodegradation kinetics of Gemfibrozil has been demonstrated by using the Langmuir-Hinshelwood model.

Zhang et al. (2008a) investigated the effect of operational parameters such as initial concentration, initial pH value and catalyst dosage for the acetaminophen photocatalysis using commercial TiO₂ under irradiation of 250W metal halide lamp. The results showed that 95 % of acetaminophen was degraded using the TiO₂ dosage of 1.0 g/L with an initial concentration of 100 μmol/L within 100 min of irradiation time. And it was concluded that acetaminophen adsorption and degradation rate were faster at pH 3.5. Moreover, the effect of catalyst concentration and initial acetaminophen concentration has a significant influence on their degradation efficiency.

Méndez-Arriaga et al. (2008) investigated the TiO₂ mediated photocatalytic degradation of naproxen, diclofenac and ibuprofen in Milli-Q water with the initial concentration of 200mg/L. The study reported that the maximum degradation efficiency of naproxen was accomplished at an optimal TiO₂ concentration of 1 g/L. But in the case of diclofenac or naproxen degradation, the optimum TiO₂ dosage was 0.1 g/L. Effect of temperature has a significant influence only for naproxen, at 40°C 99% naproxen of degraded during the 2 h of irradiation time. It is reported that optimum dissolved oxygen concentration led to the enhanced degradation rate of naproxen and ibuprofen. However, it had no positive effect on the mineralization rate. Only ibuprofen showed improvement in biodegradability factor after photocatalysis.

Rizzo et al. (2009a) analyzed the effect of diclofenac degradation as a single compound and as a mixture with other pharmaceuticals, such as amoxicillin and

carbamazepine using Degussa P25. The study also reported the degradation rate in the distilled water matrix as well as the urban wastewater effluent. The results showed that the mineralization rate from the sample mixture prepared using distilled water was higher when compared to that in wastewater effluent during 30 min of irradiation, which indicated the presence of other oxidizing species and alkaline substances in wastewater affected the degradation rate.

Abellán et al. (2009) evaluated photocatalytic degradation of two antibiotics, sulfamethoxazole and trimethoprim using TiO_2 catalyst. The study indicated that both sulfamethoxazole and trimethoprim are susceptible to endure photolysis beneath the wavelength of 310 nm. The catalyst loading had a significant effect on the degradation rate and rate enhanced with the increase in the catalyst loading. But at higher catalyst concentration degradation rate reduced owing to the scattering effect.

El-Kemary et al. (2010) prepared ZnO semiconductor photocatalyst using the precipitation method and investigated its photocatalytic activity for the photocatalytic degradation of ciprofloxacin drug. The effect of pH on the degradation efficiency was studied and results disclosed that the photocatalytic degradation efficiency was maximum at pH 7 and 10 than at acidic medium. Higher degradation efficiency (50%) was exhibited at pH 10 during 1 h of irradiation. It is reported that at low pH values (pH 4) the formation of hydroxyl radicals was prevented, thereby reducing its photodegradation efficiency.

Martinez et al. (2011) analyzed the effect of various factors on the photodegradation kinetics of diclofenac using the different nanostructured materials. The photocatalytic efficiency of synthesized TiO_2 and modified TiO_2 multi-walled carbon nanotube ($\text{TiO}_2/\text{MWCNT}$) catalysts. The degradation efficiency is enhanced using UV irradiation compared to near UV-visible light irradiation. Also, the supply of dissolved oxygen could enhance the rate of the photocatalytic degradation process.

Sturini et al. (2012) investigated the efficacy of the TiO_2 mediated photocatalytic process for the degradation of six fluoroquinolones in surface water under natural sunlight. The results showed that the degradation rates were 2-5 times greater than that of direct photolysis. All the drugs underwent faster degradation except ciprofloxacin in the presence of 0.5g/L TiO_2 loading. The results indicated that TiO_2 photocatalysis was effective in the degradation of fluoroquinolones from untreated surface water, in spite of the presence of other non-target matrix interferences such as dissolved organic matter.

Lin and Lin (2014) studied photocatalytic oxidation 5-fluorouracil and cyclophosphamide using two types of commercially available TiO_2 and ZnO . The commercial catalyst Degussa P25 displayed a higher mineralization efficiency for both 5-fluorouracil and cyclophosphamide as compared to Aldrich TiO_2 and ZnO catalysts, due to its larger active surface area. It was observed that complete mineralization of 5-fluorouracil accomplished with 24 h of irradiation time, but in the case of cyclophosphamide, complete mineralization required extended operation time. The toxicity results showed that the degradation products were even more toxic than the parental drug.

Basha et al. (2014) investigated the adsorption characteristics and kinetics of photodegradation of acetaminophen using the bifunctional TiO_2/AC composite catalysts. They reported that the photocatalytic degradation kinetics followed the Langmuir-Hinshelwood model and the rate constants were reliant on the dosage of TiO_2 .

Gou et al. (2017) analyzed the efficacy of photocatalytic diclofenac degradation using the visible light active Ag_3PO_4 photocatalysts. It is reported that the prepared catalysts exhibited complete diclofenac removal and the catalyst load and initial pH had a significant effect on photocatalytic degradation of diclofenac. Nearly 8 intermediates were formed during the degradation process, and three major degradation paths were reported including OH radical attack on the aromatic ring, direct oxidation by holes and decarboxylation of the side chain.

2.6. Development of coupled photocatalysts

As already mentioned, TiO_2 is the most extensively used semiconductor photocatalyst to date. However, the main drawback of TiO_2 is its restricted light absorption in the solar spectrum and high recombination rate of charge carriers. Also, most of the other semiconductors suffer from the same drawbacks. To overcome these downsides, various alternative modification methods have been applied to photocatalysts in recent years. One of the important methods includes the coupling of two or more nanosized semiconductor materials for the design of heterostructure nanocomposites which were conceivably efficient in photocatalytic water splitting and water treatment process. These heterojunction photocatalysts are characteristically comprised of two different semiconductors, a wide bandgap semiconductor oxide and the other narrow bandgap semiconductor oxide. The coupling of one semiconductor with the narrow bandgap semiconductor could incorporate the large fraction of visible light absorption in the heterojunction system. The photoinduced

charge transfer amongst the heterojunction system could also enhance the efficient charge separation and thereby reduces the surface recombination of charge carriers (Zhang et al. 2019a). The mechanism of charge transfer between the coupled heterojunction is shown in figure 2.2.

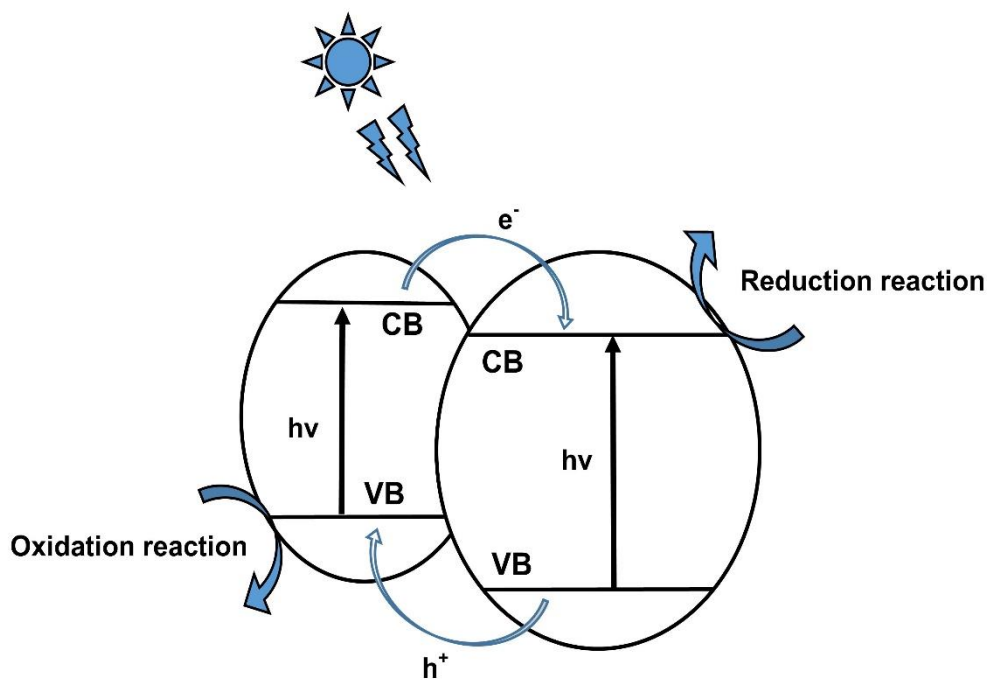


Figure 2.2. Charge transfer in the coupled photocatalytic system

The charge transfer mechanism in a coupled photocatalytic system involves two different charge transfer mechanism. One is the traditional type II heterojunction and the other is the direct Z-Scheme heterojunction. The traditional type II heterojunction involves the exciting electron transfer from the material with higher CB potential to the material with lower CB potential. The transferred electron undergoes reduction reactions to produce powerful radicals and the holes excited in the VB could directly oxidize pollutants or to yield $\cdot\text{OH}$ on reaction with adsorbed water molecules. Thus, the charge transfer between these heterojunctions forbids the recombination of electron-hole pairs. However, in the direct Z-scheme mechanism, initially the photogenerated electrons and holes in the inferior band energy recombine via intimate contact interface and the electrons and holes in the higher band potential undergoes redox reactions. Thus, the recombination of electrons and holes suppressed and also the Z-scheme mechanism facilitates enhanced charge transfer between the coupled heterojunction system (Ahmed et al. 2020; Meng et al. 2017).

Pouretedal et al. (2012) investigated the photocatalytic efficiency of $\text{ZrO}_2/\text{SnO}_2$, $\text{ZrO}_2/\text{CeO}_2$ and $\text{SnO}_2/\text{CeO}_2$ nanocomposites prepared using sol-gel method. It was observed that the coupled photocatalytic system enhanced the degradation efficiency of individual catalysts and the reaction rate of photocatalytic degradation of 2-nitrophenol. The results showed that $\text{ZrO}_2/\text{SnO}_2$ has the highest photocatalytic activity compared to others. High photocatalytic activity is attributed to the increased charge separation and reduced recombination rate. The catalyst reactivity is highly influenced by the molar composition of nanocomposites and the initial pH of the solution.

Subash et al. (2013) prepared WO_3 loaded Ag-ZnO nanocomposite by precipitation-decomposition method. It is reported that the prepared WO_3 -Ag-ZnO composite exhibited excellent photocatalytic efficiency compared to other prepared catalyst combinations such as Ag-ZnO, WO_3 -ZnO, Ag- WO_3 , pure ZnO, commercial ZnO, and TiO_2 -P25 for photocatalytic removal of Naphthol Blue Black under solar light irradiation. It was reported that the presence of WO_3 resulted in efficient charge separation and the presence of Ag suppressed the recombination of electrons and holes.

Liu et al. (2014) prepared TiO_2 - WO_3 composite crystallites by a one-pot hydrothermal method. It is observed that the WO_3 particles dispersed homogeneously on the surface of TiO_2 particles. The prepared composite showed better degradation efficiency than pure TiO_2 for the photocatalytic degradation of Rhodamine B. It is reported that the introduction of a certain amount WO_3 has improved the photocatalytic activity of composites, however excess WO_3 could force reduce the efficiency of charge separation between TiO_2 and WO_3 . It was revealed that high acid sites formed on WO_3 surface resulted in stronger adsorption between the composite particle and Rhodamine B molecule.

Huang et al. (2015) analyzed the photocatalytic degradation of methylene blue using the TiO_2 - SnO_2 composite catalysts prepared by the sol-hydrothermal method. It is revealed that the addition of a small quantity of SnO_2 into the TiO_2 surface greatly enhanced the catalytic activity of composite catalysts since Sn substitution acted as the sink for electrons and thereby reduced the rate of recombination of charge carriers. It is reported that the higher photocatalytic activity might be due to the solid-solid interfacial effect between anatase and rutile-type TiO_2 phases. High photocatalytic activity observed is also attributed to the increased specific surface area of TiO_2 - SnO_2 photocatalysts.

Daya Mani et al. (2015) synthesized different CdS/CeO₂ nanocomposites by varying compositions using the one-pot synthesis method and studied the removal of phenol and Cr (VI) from aqueous streams. It was observed that CdS/CeO₂ with molar ratio 1:1 had shown superior catalytic activity, due to the enhanced electron transfer from CdS to CeO₂.

Lamba et al. (2015) investigated the catalytic activity of ZnO-SnO₂ for photocatalytic removal of methylene blue. The results stated that the ZnO-SnO₂ heterostructures exhibited superior photocatalytic performance when compared with commercial TiO₂ (PC-50), TiO₂ (PC-500) and bare SnO₂ photocatalysts.

Gar Alalm et al. (2016) investigated the catalytic efficiency of prepared WO₃/ZrO₂ nanoparticles for the removal of carbofuran and ampicillin under simulated solar light. The results showed that the degradation of carbofuran and ampicillin using as-prepared WO₃/ZrO₂ photocatalysts showed improved photocatalytic efficiency than individual photocatalysts. Also, the addition of Ru to the WO₃/ZrO₂ composite catalyst unveiled a faster degradation rate than the coupled WO₃/ZrO₂. The stability analysis of the composite catalyst revealed that better stability with 92% of its efficiency during the first cycle.

Zhang et al. (2017) studied the photocatalytic activities of AgI/g-C₃N₄ composite catalysts for diclofenac degradation under visible light irradiation. All the prepared coupled catalysts displayed superior catalytic activities than those of the individual AgI and g-C₃N₄ photocatalysts. The catalysts with 45 % of the mass ratio of AgI in AgI/g-C₃N₄ composite catalysts exhibited a higher degradation rate with a higher rate constant of 0.561 min⁻¹. It is reported that the main reactive species in photocatalytic removal of diclofenac is the h⁺ and O₂^{•-}. The prepared photocatalysts also exhibited exceptional stability and durability for over successive reaction cycles. The toxicity assay showed that the chloro-derivatives and carbazole byproducts were formed during the reaction.

Rohani Bastami et al. (2017) synthesized Fe₃O₄/Bi₂WO₆ nano heterostructures and tested its catalytic efficiency for the photocatalytic removal of ibuprofen. The results revealed that the prepared heterojunction catalysts showed higher photocatalytic efficiency for Ibuprofen removal under solar light irradiation. It is reported that the initial pH and surface charge property of the catalysts played a significant role in the adsorption and degradation of ibuprofen under sunlight. It is stated that the Ibuprofen degradation efficiency was higher in an acidic medium which might be due to electrostatic attraction

between protonated catalyst surface and carboxylic anions of ibuprofen. Photogenerated holes were reportedly the main active species in the degradation reaction of ibuprofen.

Kaur et al. (2018) hydrothermally synthesized CdS/TiO₂ photocatalysts and studied its catalytic efficiency for removal of ofloxacin using visible light illumination. The nanoparticle characterization documented that the catalysts show high crystallinity, purity and excellent optical properties. The photocatalytic degradation experiments for removal of ofloxacin suggested catalytic activity of the prepared showed higher degradation efficiency of 86 % ofloxacin within 180 min of visible irradiation.

Zhang et al. (2019b) reported the high stability CdS/ZnS heterojunction catalysts for photocatalytic removal of rhodamine B and methylene blue under sunlight irradiation. Among the series of CdS/ZnS heterojunction catalysts, the catalyst with 7:1 molar ratio of CdS/ZnS displayed superior photocatalytic efficiency as compared with other reported CdS/ZnS catalysts. The stability tests suggest that the prepared photocatalysts were highly stable with retaining catalytic efficiency of around 96 % over the next 10 reaction cycles.

2.7. Inferences from literature

It is reported that the removal of pharmaceutical compounds is the most complicated task as many of these technologies result in the transformation of drugs into another intermediate form which could be more lethal than the targeted drugs. There are different treatment methods used to remove the pharmaceutical pollutant diclofenac. But the complete degradation and mineralization of diclofenac drug has not been achieved. It is necessary to develop various advanced treatment process to completely mineralize the diclofenac with an easier and chaper techniques. The use of a proper photocatalytic system needed to achieve complete mineralization of pharmaceutical compound diclofenac has received a greater interest. Photocatalytic degradation studies of pharmaceutical compounds were mostly restricted to the use of commercial TiO₂. It is revealed that the physio-chemical and optical properties of some semiconductors such as SnO₂, WO₃, CdS, and ZnO shows a favorable option for the photocatalytic process, but its practical application is limited. To synthesize different efficient semiconductor nanomaterials and their application in the photocatalytic process under visible-light irradiation, several efforts have been made in the last decade. Coupled semiconductor oxides and metal-doped semiconductors have been reported to improve visible light absorption and the catalytic activity in the photocatalytic process for target pollutants. Especially coupling between

different semiconductors may induce vectorial transfer of photogenerated charge carriers between the conduction band and valence band edges. Use of coupled photocatalytic system with higher catalytic efficiency for degradation various pharmaceutical is possibly achieved through proper methods. From the literature review, the degradation/removal of diclofenac through different treatment techniques and their treatment efficiency were compiled and reported in the table 2.4.

Table 2.4. Degradation efficiency for diclofenac removal using different methods

Initial diclofenac concentration	Degradation/Removal method	Degradation efficiency	References
100 mg/L	Membrane bioreactor (Microfiltration membranes)	50 % rejection	Kimura et al. (2005)
100 mg/L	Photo-Fenton process	94 %	Alalm et al. (2015)
20 mg/L	Catalyst Ozonation	76 %	Chen et al. (2016b)
1 mg/L	Photocatalysis (AgI/g-C ₃ N ₄ Composite)	100 %	Zhang et al. (2017)
6 mg/L	Photocatalysis (Ag ₃ PO ₄)	92 %	Gou et al. (2017)
10 mg/L	Photocatalysis C doped WO ₃ /TiO ₂	100 %	(Cordero-García et al. 2016)
200 mg/L	Electrochemical Oxidation	91 %	Fernández-Aguirre et al. (2020)
20 mg/L	Nanofiltration	99 %	Cuhorka et al. (2020)

2.8. Scope and Objectives of the work

Based on the inferences from the literature, it is identified that the photocatalytic degradation of pharmaceutical compounds has been primarily performed using commercial TiO_2 only. The scope of the present work focuses on the application of different semiconductor oxides such as TiO_2 , ZnO , SnO_2 , WO_3 , and CdS in the photocatalytic degradation process and to improve the catalytic efficiency. In order to analyze the effect of individual photocatalysts and mixed oxide catalysts in the photocatalytic process, the present study aims to synthesize various mixed oxide catalysts such as $\text{TiO}_2/\text{SnO}_2$, TiO_2/WO_3 , TiO_2/CdS , and ZnO/WO_3 , through the hydrothermal method and to investigate the effect of molar ratios on the synthesis of mixed oxide catalysts. Moreover, the effect of operating variables like pH, catalyst dosage and initial drug concentration were analyzed in detail. Furthermore, the role of major active species and the evaluation of different degradation products along with the possible degradation pathway of diclofenac will be discussed in detail.

1. To achieve the above scope, the following objectives are formulated
2. To synthesize various mixed oxide catalysts through the hydrothermal method.
3. To characterize the coupled semiconductor oxides using Scanning Electron Microscopy (SEM), X-ray Diffraction (XRD) and Transmission Electron Microscope(TEM).
4. To evaluate the photocatalytic activity of coupled semiconductor oxides using diclofenac and optimization of operating parameters using UV or Visible light irradiation based on the catalytic property.
5. To study the degradation kinetics and to evaluate the degradation products formed during irradiation.

CHAPTER 3

MATERIALS AND METHODS

3.1. CATALYSTS PREPARATION

3.1.1. Materials used

Titanium isopropoxide, sodium tungstate dihydrate, tin (IV) chloride pentahydrate, cadmium acetate and thiourea were purchased from Sigma-Aldrich and used as the precursor of TiO_2 , WO_3 , SnO_2 and CdS respectively. Zinc nitrate hexahydrate was purchased from Loba Chemicals Pvt. Ltd. and used as the precursor of ZnO. and other reagents used in the study were purchased from Merck. Ammonium hydroxide and diclofenac sodium salt were obtained from Sigma-Aldrich. Ethylene glycol, Isopropyl alcohol, acetic acid, sodium chloride, ethanol, HCl and other reagents used in the study were purchased from Merck. All the experiments in the study were performed using deionized water.

3.1.2. Preparation of TiO_2 - SnO_2 Catalysts

Catalysts with various molar ratios of TiO_2 - SnO_2 (1:1, 5:1, 10:1, 20:1 and 30:1) were prepared using the hydrothermal method. In the typical procedure, 4 ml of TTIP were added to a mixed solution of isopropyl alcohol (15 ml) and glacial acetic acid (4 ml) under continuous stirring for about 30 min. Then, 5 ml of de-ionized water was slowly added to the solution for hydrolysis under vigorous stirring and the solution was aged for 30 min to form a transparent sol. The calculated amount of $\text{SnCl}_4 \cdot 5\text{H}_2\text{O}$ (based on the Ti-Sn molar ratio 1:1 to 30:1) was added to the above solution under vigorous stirring and ultrasonicated for about 10 min. The ultrasonicated mixture was then stirred continuously for 1 h. Then the above solution was transferred to a Teflon-lined stainless steel autoclave and heated at 200°C for 24 h. Later, the solution was cooled to room temperature, centrifuged and the precipitate was washed three times with deionized water and ethanol and dried at 80°C overnight in an oven. The series of mixed oxide catalyst prepared with TiO_2 - SnO_2 molar ratios of 1:1, 5:1, 10:1, 20:1 and 30:1 were coded as T1S1, T5S1, T10S1, T20S1 and T30S1

respectively. The pure TiO₂ was prepared by a similar method without the addition of SnO₂ precursor.

3.1.3. Preparation of TiO₂-WO₃ Catalysts

TiO₂-WO₃ coupled semiconductor photocatalyst was synthesized by the hydrothermal method with different molar ratios of titanium (Ti) and tungsten (W). The TiO₂-WO₃ (molar ratio 1:1) photocatalyst is synthesized as follows: 4 ml of titanium isopropoxide was dissolved in 15 ml of isopropanol under dynamic stirring. 4 ml of acetic acid and 5 ml of distilled water was added to the above-mentioned reaction mixture and stirred for 10 min. Then, 2.214 g of sodium tungstate dihydrate was dissolved in the above mixture under constant stirring. The mixture was then sonicated in an ultra-sonicator for 10 min, in order to ease the precipitate reaction. Then the sonicated reaction mixture was poured into a Teflon-lined autoclave and heated at a temperature of 160°C in an oven for 24 h. After the completion of the hydrothermal reaction, the mixture was then collected and washed several times with distilled water and sequentially with ethanol and dried in an oven overnight. The molar ratio of TiO₂-WO₃ was varied as 1:1, 5:1, 10:1 and 20:1. The as-prepared catalysts were designated as TW1, TW5, TW10 and TW20 respectively. The pure TiO₂ was also prepared using a similar protocol without the addition of tungstate precursor.

3.1.4. ZnO-WO₃ photocatalysts preparation

Zinc nitrate hexahydrate was purchased from Loba Chemicals Pvt. Ltd. and used as the precursor of ZnO. Sodium chloride, ethanol, HCl and other reagents used in the study were purchased from Merck. The ZnO-WO₃ mixed oxide catalysts were synthesized using the hydrothermal method. Initially, 1 g of Zn(NO₃)₂·6H₂O was dissolved in 30 ml of distilled water under constant stirring, and then NH₄OH was added slowly until the solution pH reaches 8. Then 0.02 g of NaCl was added under vigorous stirring, and the calculated amount of Na₂WO₄·2H₂O was added to the above solution in order to attain the required molar ratios of Zn:W like 1:1, 10:1 and 20:1 and labeled as ZnW1, ZnW10, and ZnW20 respectively. The above solution was ultrasonicated for 30 min and then transferred to 50 ml Teflon-lined stainless-steel autoclave and heat-treated in an oven at 140 °C for about 24 h. The resulted product was then collected and centrifugally washed with distilled water and absolute ethanol, and then the washed material was dried at 60 °C overnight. The bare

ZnO particles were prepared using the procedure mentioned above without the addition of tungstate precursor.

3.1.5. Preparation of TiO₂-CdS catalysts

TiO₂-CdS coupled photocatalysts were prepared using a two-step hydrothermal process. Firstly, 150 ml of isopropanol was taken in a beaker and then 40 ml of titanium isopropoxide was gradually added to the solvent under vigorous stirring and continued for 1 h. Then, 20 ml of acetic acid was added dropwise and stirred continuously for 30 min. After 30 min, the solution was transferred to a Teflon-lined stainless-steel autoclave and placed inside a preheated oven at 160°C for 24 h. The autoclave was then cooled down to room temperature, and then the sedimented particles were collected and washed with distilled water and ethanol several times and dried at 60°C overnight. Then the particle was collected and grounded to a fine powder.

Different molar ratios of TiO₂-CdS mixed oxide catalyst were prepared as follows, 1 g of TiO₂ powder was dispersed in 50 mL distilled water under ultrasonication. To the above solution, 1.5 g of pluronic was added. Then, 2.87 g of cadmium acetate and 0.95 g of thiourea, were added to a mixed solution of ethylene glycol and distilled water. After that, solutions containing Ti and Cd precursors were mixed together and the mixed solution was ultrasonicated for 30 min and stirred for 1 hour. Later, the entire mixture was transferred to an autoclave and heated at 190 °C for 20 hours. After hydrothermal treatment, the obtained precipitates were washed again using water and ethanol successively to remove the impurities and then dried in an oven at 60 °C. The molar ratio of TiO₂-CdS mixed oxide catalyst was varied as 1:1, 5:1 and 10:1, which was designated as TC1, TC5 and TC10, respectively.

3.2. Characterization of catalysts

X-ray diffraction patterns of all the prepared catalysts were analyzed with the help of JEOL DX-GE-2P Goniometer operated at room temperature, at an accelerating voltage of 30 KV using CuK α radiation ($\lambda = 0.15406$ nm), with scattering angle from 20-80°.

The morphology of the catalyst, the size distribution, and the average diameter of the prepared catalysts were analyzed by using a JOEL JEM-2100 Transmission electron microscope (TEM), USA. Before observing in TEM, samples were dispersed

in ethanol by ultrasonication and dropped on to the carbon-coated copper grid. Energy-Dispersive X-ray spectroscopy (EDS) analysis was used to investigate the elemental composition of the prepared catalysts. The specific surface area of the prepared sample was calculated by the Brunauer-Emmett-Teller (BET) procedure.

Hitachi U-2900 Spectrophotometer was used to analyze the bandgap energy of the prepared catalysts. The known amount of prepared catalysts were dissolved in water and ultrasonicated for 30 min to achieve proper dispersion in the solvent. The sample was then subjected to a spectral analysis from 200 nm to 800 nm wavelength range.

The zero point charge of the prepared catalysts were analyzed by dissolving 30 mg of the catalyst in 50 ml of 0.1 M potassium nitrate (KNO_3) solutions of different pH values (2-10) and the pH was measured after agitated for 24 h, as reported in the literature (Hiew et al. 2018).

Photoluminescence (PL) study was conducted to analyze the evaluation of $\cdot\text{OH}$ radicals for the prepared photocatalysts using the spectrofluorometer, Fluoromax-4, Horiba Scientific, Japan. The solution containing the prepared mixed oxide catalysts were irradiated and analyzed over the wavelength range 300-600 nm to obtain the photoluminescent spectra.

3.3. Photocatalytic experiments

The photocatalytic degradation study was carried out using a laboratory-scale batch photoreactor as shown in figure 3.1. The setup consisted of a reactor vessel made up of 250 ml borosilicate glass which was placed on a magnetic stirrer. Degradation experiments were performed using 100 ml of aqueous diclofenac solution with different initial concentrations, under different catalyst loading and different initial pH. The reaction mixture was continuously stirred and was irradiated using a UV (UV-A lamp) or Visible light irradiation (400 W metal halide lamp). Before irradiation, the suspensions were stirred in the dark for 30 min to reach the adsorption-desorption equilibrium between the catalyst and drug molecule.

At different irradiation time intervals, aliquots were withdrawn and filtered through a 0.22 μm nylon membrane filter, to remove the catalyst from the sample and were further analyzed by appropriate analytical techniques. Each experiment was performed in triplicates and the results are presented as a mean and standard deviation of three analyses.

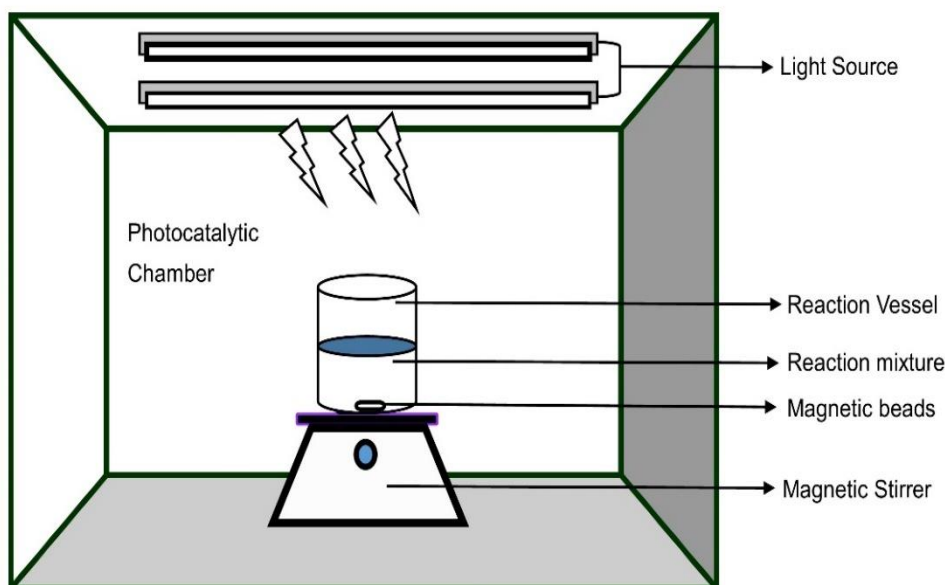


Figure 3.1. Schematic representation batch photocatalytic reactor

The photocatalytic degradation study was repeated for several cycles with the same catalyst to further analyzed for its stability and reusability. After each reaction cycle, the catalyst was separated by centrifugation and washed with ethanol and distilled water to eradicate the presence of any diclofenac molecule. Then the catalyst was dried at 80°C in an oven and used for the next reaction cycle. Fresh diclofenac solutions were used for each reaction cycle under the same reaction condition.

3.4. Analytical Methods

Diclofenac concentration was analyzed using a UV-Vis spectrophotometer at 276 nm (Rizzo et al. 2009b). The total organic carbon (TOC) is measured by a TOC analyzer (Shimadzu TOC-V-CSN, Shimadzu, Osaka, Japan).

In order to make 1000 mg/L of total carbon (TC) stock solution, 2.12 g of anhydrous potassium hydrogen phthalate was dissolved in 1000 ml of de-ionized water. This solution can be further diluted to get a desired concentration of TC. Similarly, 4.41 g of anhydrous sodium carbonate and 3.49 g of sodium hydrogen carbonate was dissolved in 1000 ml de-ionized water to make the stock solution of 1000 mg/L of total inorganic carbon (TIC), which can be further diluted accordingly to the desired TIC concentration.

The degradation products of diclofenac were analyzed using Liquid Chromatograph Mass Spectrometer (LC-MS-2020, Shimadzu, USA). The filtered samples were run in a reverse phase LC-MS C18 column, equipped with a UV detector. 20 μ L of the sample was

used as an injection volume and the total run time of each sample was 20 min. The mobile phase consisted of a mixture of acetonitrile and water with 0.3 % formic acid (80:20 %, v/v) at a flow rate of 0.5 mL/min.

3.5. Kinetics of photodegradation

The kinetic mechanism of diclofenac degradation using TiO₂-SnO₂ mixed oxide catalyst was also studied under different reaction conditions. Langmuir-Hinshelwood model is predominantly used to quantify the photocatalytic degradation kinetics of various organic compounds (Gar Alalm et al. 2016). The model developed by Turchi and Ollis (1990) was used to study the degradation kinetics of diclofenac and expressed as the following equation (3.1):

$$R = -\frac{dC}{dt} = \frac{k_{cat}K.C}{1+K.C} \quad (3.1)$$

where R is the rate of the reaction, K and k_{cat} are the thermodynamic adsorption constant and degradation rate constant of the pollutant over the catalyst, respectively. During dilute the concentration of pollutants (where C < 10⁻³ mol dm⁻³), adsorption-desorption equilibrium reached in 30 min, and adsorption was merely negligible, and (1+K.C) was found to be ≈ 1, and k_{cat}.K ≈ k_{app}, and the rate of reaction is simplified to the linear form of pseudo-first-order models as expressed by Eq. (3.2). Similarly at a higher concentration of pollutants (K.C+1) ≈ K.C, then the above equation will be reduced to the zero-order reaction as in Eq. (3.3) (Gar Alalm et al. 2016):

$$\ln \frac{C_0}{C} = k_{app} \cdot t \quad (3.2)$$

$$C = C_0 - k_{app} \cdot t \quad (3.3)$$

where k_{app} is the apparent rate constant; C₀= initial diclofenac concentration at the start of the photocatalytic reaction and C = concentration of diclofenac at reaction time t.

CHAPTER 4

PHOTOCATALYTIC DEGRADATION OF DICLOFENAC USING TiO₂-SnO₂ CATALYSTS

4.1. RESULTS AND DISCUSSION

4.1.1. Characterization of TiO₂-SnO₂ catalysts

Figure 4.1 shows the X-ray diffraction patterns of TiO₂-SnO₂ catalyst synthesized by varying molar ratios. No stronger peak of SnO₂ was observed in XRD patterns of all the prepared catalysts. Also, the use of higher moles of Sn leads to the transformation of anatase phase TiO₂ to rutile phase TiO₂ (Zhang et al. 2011). The major peaks observed in the T1S1 catalyst are at 27.2° and at 35.5°, which has good agreement with ICDD data (ICDD no. 21-1276) for TiO₂ rutile phase. The diffraction peaks showed at 26.6 and 34.8 are referred to cassiterite phase (ICDD no. 41-1445). On the other hand, XRD patterns of the catalyst T5S1 show both anatase and rutile phase peaks at 25.6° and 27.2°. The cassiterite phase SnO₂ peaks have existed only in T1S1 and T5S1 catalyst as seen in figure 4.1, however, other catalysts didn't show any SnO₂ peaks. This could be due to the low amount of Sn in their mixed oxides and these low Sn content might be incorporated into the crystal lattice of TiO₂ (Huang et al. 2015). But in the case of the catalysts T10S1, T20S1 and T30S1, the strong diffraction peaks of anatase phase TiO₂ were identified at 25.2°, 37.9° and 53.8° (ICDD no. 01-071-1166). However, weak rutile phase TiO₂ peaks were observed at 27.2°, 35.5° and 53.5°, which suggests that the small amount of Sn present in the mixed oxide catalysts has possibly resulted in the transformation of anatase phase TiO₂ to weaker rutile phase TiO₂ as compared with pure TiO₂. Also, the variation in the intensity of the rutile phase TiO₂ peaks was proportional to the amount of Sn loading in the mixed oxide catalysts.

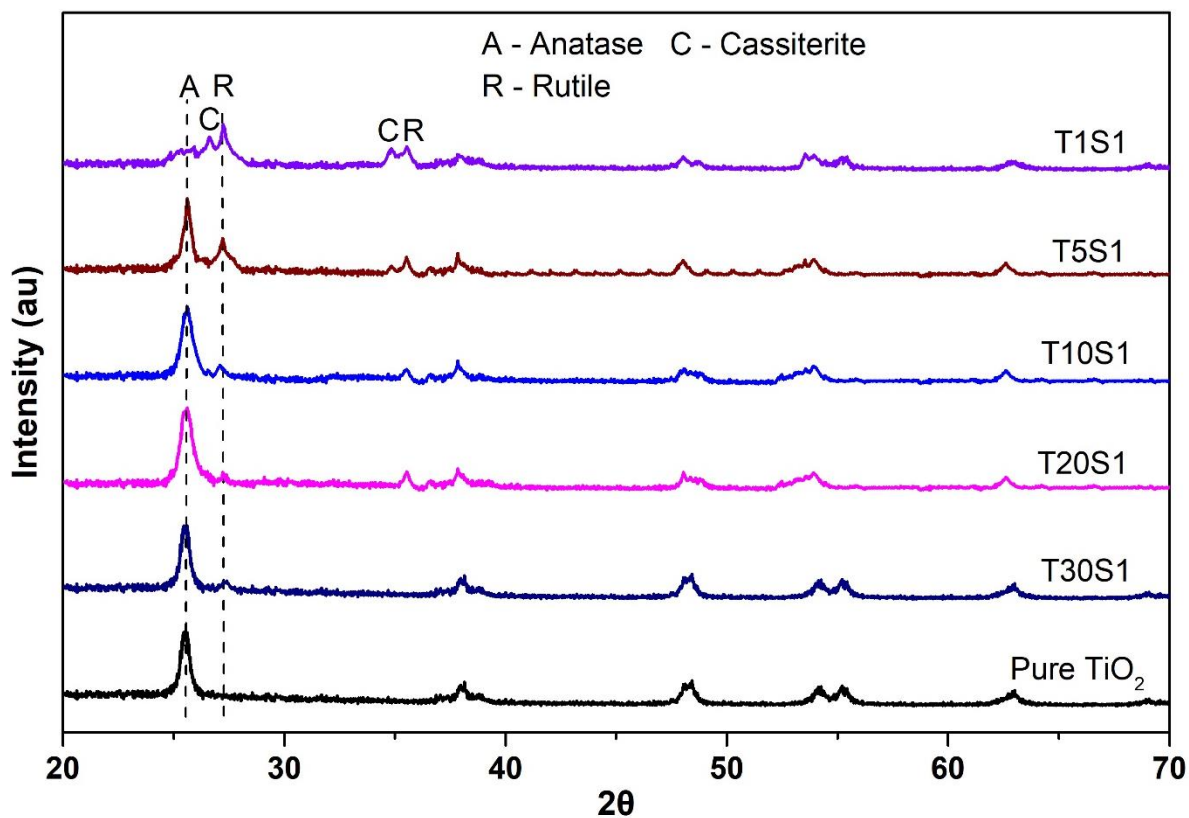


Figure 4.1. XRD patterns of the prepared $\text{TiO}_2\text{-SnO}_2$ catalysts with different molar ratios

The surface morphologies of the $\text{TiO}_2\text{-SnO}_2$ catalysts were analyzed by TEM, which is shown in figure 4.2. The TEM observations of the prepared catalysts revealed that the prepared nanoparticles were of different grain sizes. The increase in tin content resulted in disordered spherical-shaped nanoparticles and increased particle size. The morphologies of the catalyst T30S1, T20S1, T10S1 and T5S1 were found to be disordered spherical-shaped nanoparticles, but on the other hand, the T1S1 catalyst was found to be agglomerated with uneven size. The particle size of the catalysts T30S1, T20S1, T10S1 and T5S1 were found to be in the range of 9–30 nm. However, the particle size of the catalyst T1S1 was larger than pure TiO_2 . HRTEM images revealed that the presence of both anatase and rutile phase TiO_2 in T1S1 catalyst along with SnO_2 catalyst, as seen in figure 4.2 (g). The lattice fringes of 0.35 nm, 0.24 nm and 0.27 nm correspond to (101), (101) and (101) planes of anatase phase TiO_2 , rutile phase TiO_2 and cassiterite phase SnO_2 respectively. The lattice fringes of 0.34 nm as seen in figure 4.2 (h), attributed to (110) plane of cassiterite SnO_2 . The catalyst T20S1 and T30S1 didn't show any clear indication of SnO_2 lattice fringes as Sn content is very low in their mixed oxides. HRTEM results were well corresponding with the XRD results.

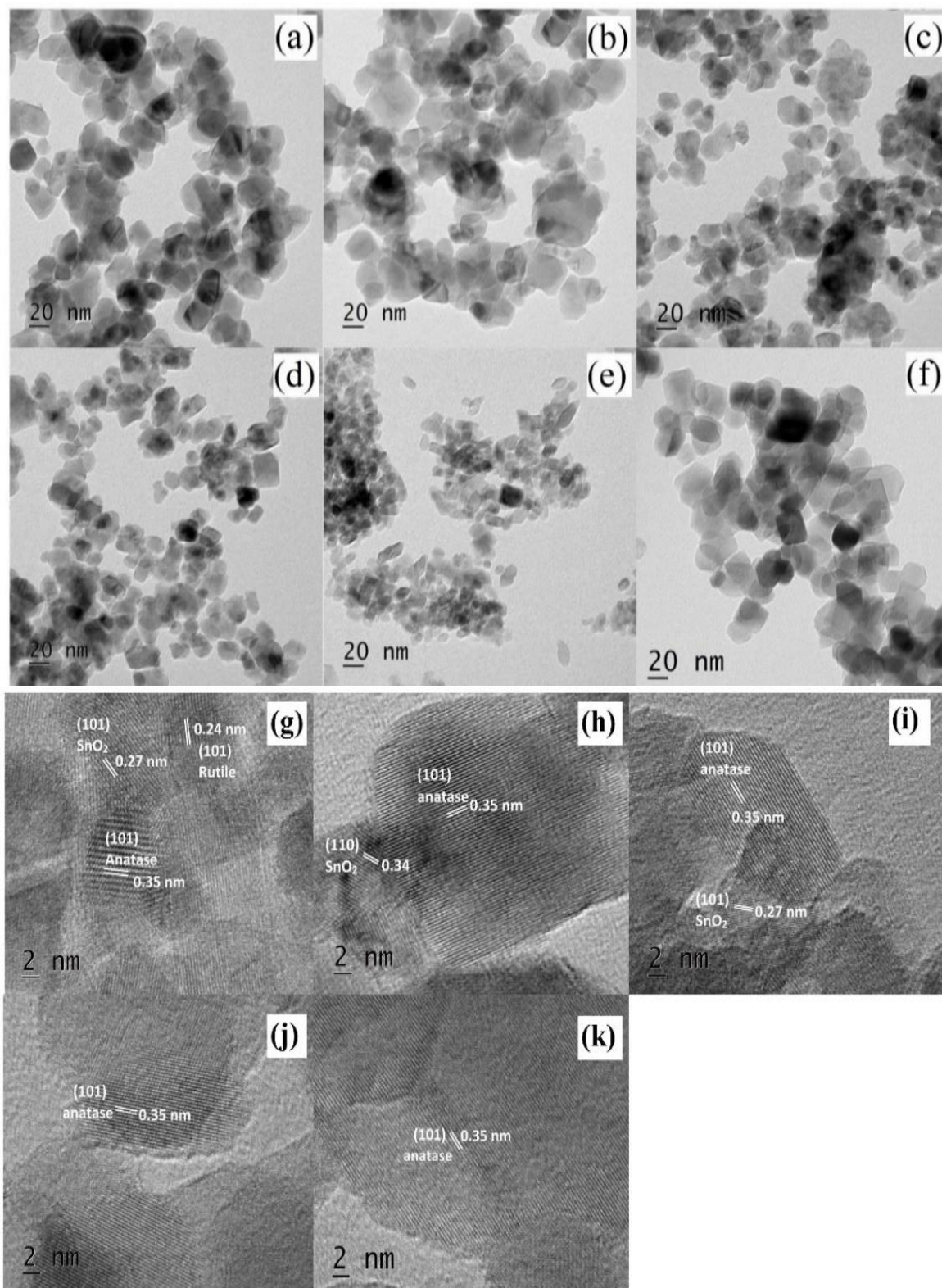


Figure 4.2. TEM images (scale = 20 nm) (of (a) Pure TiO₂; (b) T1S1; (c) T5S1; (d) T10S1; (e) T20S1; (f) T30S1 and HRTEM images (scale = 2 nm) of (g) T1S1; (h) T5S1; (i) T10S1; (j) T20S1; (k) T30S1.

Further, EDS analysis was performed to identify the elemental composition of the prepared catalysts. Figure 4.3 demonstrates the typical EDS analysis of all the $\text{TiO}_2\text{-SnO}_2$ catalysts. The results confirm the presence of elements Ti, Sn and O, on the surface of the prepared catalyst. The peak for C observed in the EDS image might be due to the carbon tape used in the analysis. Except for Ti, Sn and O, no other peak for any other element has been found in the spectrum. This confirms the prepared catalysts were in the pure state. The molar ratios of Ti and Sn in the prepared catalysts were also equivalent to the weight percentage observed in the EDS analysis. The elemental weight percentage of all the mixed oxide catalysts with different molar ratios were tabulated in table 4.1.

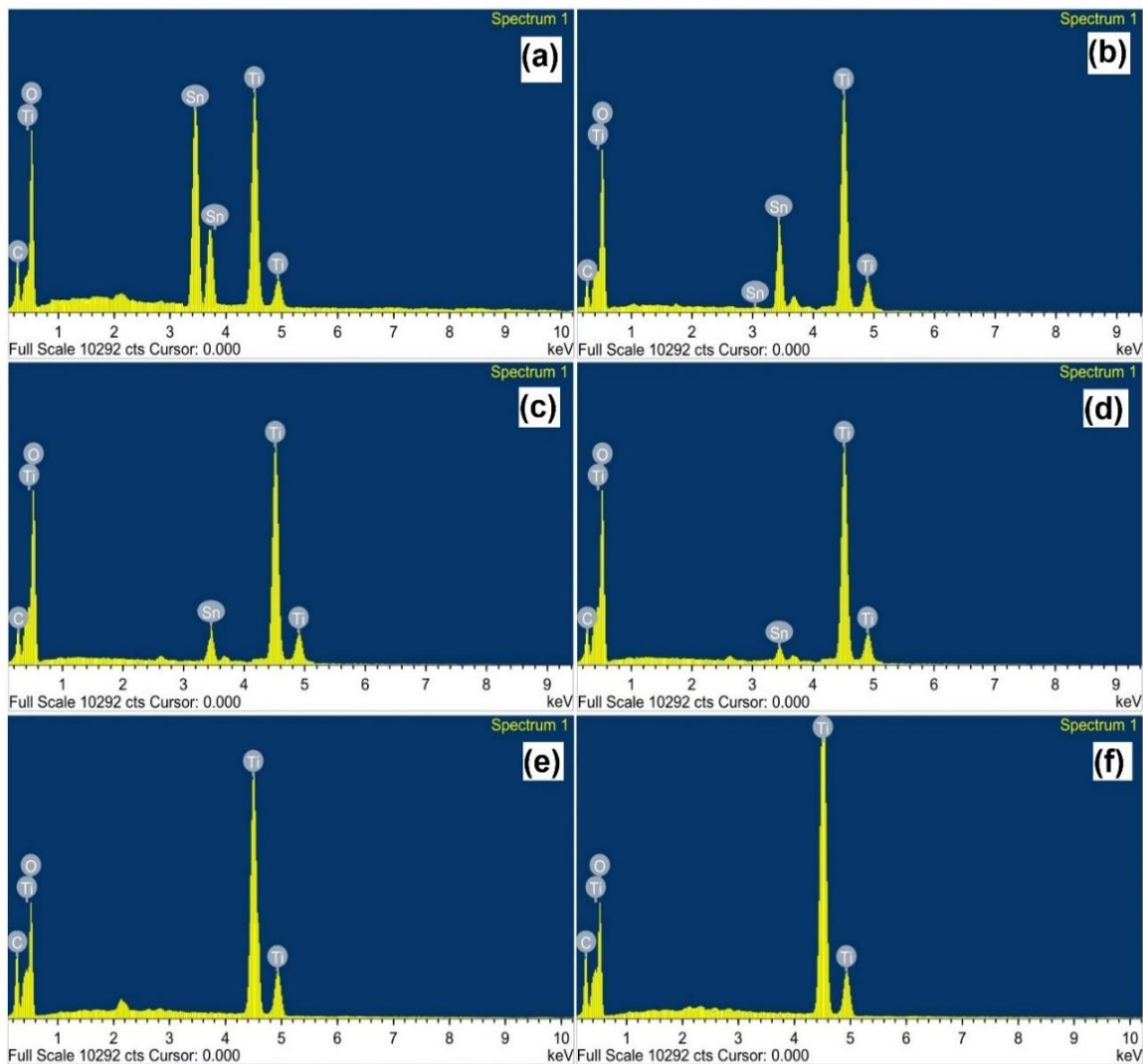


Figure 4.3. EDS images of (a) Pure TiO_2 ; (b) T1S1; (c) T5S1; (d) T10S1; (e) T20S1 and (f) T30S1

Table 4.1. Elemental composition and weight percentage of TiO₂-SnO₂ catalysts

Catalyst	Elements and their weight %		
	Ti	O	Sn
Pure TiO ₂	40.21	58.79	-
T1S1	16.65	65.76	17.28
T5S1	24.99.	67.57	5.22
T10S1	28.39	63.87	2.94
T20S1	32.45	61.97	1.66
T30S1	36.79	59.74	1.27

Photocatalytic activity is usually correlated to the active surface area available for the adsorption and desorption of organic pollutants (Bellardita et al. 2007). Table 4.2 shows the surface area of all the prepared mixed oxide catalysts. Among them, the T20S1 catalyst has the highest surface area of 113 m²/g and the T1S1 catalyst has the smallest surface area of 59 m²/g. The surface area of the T1S1 catalyst was much lower than the pure TiO₂, which might be due to the presence of rutile phase TiO₂, as the surface area of rutile phase TiO₂ is very small (Huang et al. 2015).

Table 4.2. Surface area and the average size of the TiO₂-SnO₂ catalysts

Catalyst with different molar ratios	BET surface area (m²/g)	Average size of nanoparticles (nm)
T30S1	84.4	25 ± 7
T20S1	113.5	12 ± 8.2
T10S1	87.6	19 ± 9.5
T5S1	79.05	27 ± 10.25
T1S1	59.14	52 ± 20
Pure TiO₂	68.33	38 ± 15.5

The energy bandgap of the prepared catalyst was analyzed by the Tauc plot, which is shown in figure 4.4. For comparison, the energy band gap of pure TiO_2 prepared through the hydrothermal method is also plotted. It has been found that the bandgap energy of the catalysts T30S1, T20S1, T10S1 and T5S1 were in the range of 3.3–3.5 eV. Similarly, the T1S1 catalyst has a higher energy bandgap ($E_g = 3.6$ eV) which is almost equal to SnO_2 . As the Sn content in the catalyst increases, the energy bandgap of the catalyst increases linearly, which indicates that the change in Sn content affects the light absorption of the prepared catalyst. The strong and broad absorption limits of the prepared catalysts were in the range of 340–380 nm.

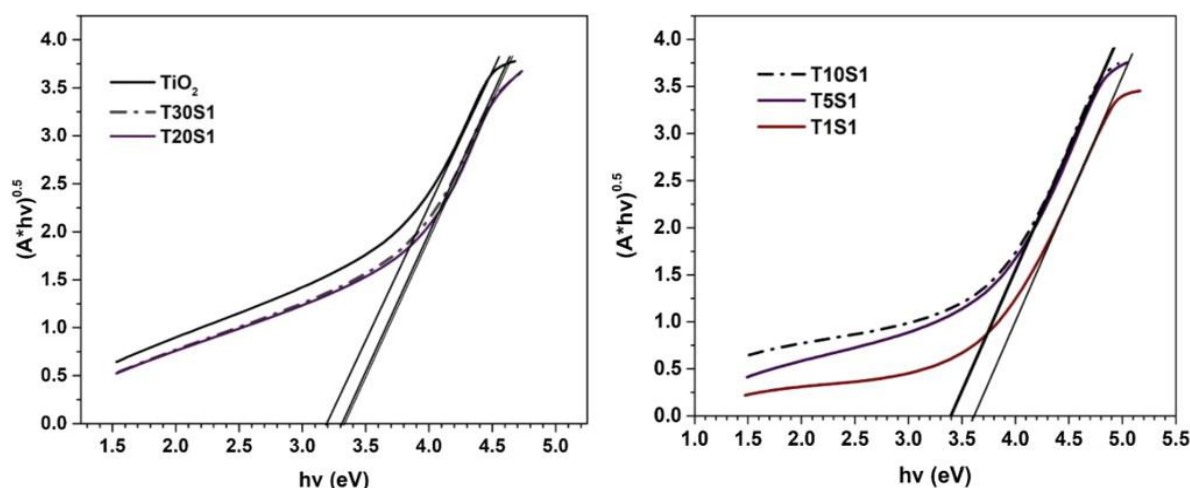


Figure 4.4. Tauc plot for calculation of band gap of all the prepared catalysts

4.1.2. Photocatalytic Activity Evaluation

The photocatalytic activity of all the prepared mixed oxide catalysts was assessed using diclofenac solutions of different initial concentrations, catalyst loading, and different pH values under UV irradiation.

4.1.2.1. Effect of molar composition of Ti-Sn

The photocatalytic activity of different $\text{TiO}_2\text{-SnO}_2$ catalysts is depicted in figure 4.5. The effect of photolysis was also evaluated by experimenting without the addition of a catalyst since it has been reported in the literature that diclofenac has partial absorption in the 300–400 nm range (Rizzo et al. 2009b). From figure 4.5, it is found that photolysis has a negligible effect on the degradation of diclofenac under UV-A irradiation (315–400 nm) and similar results were reported in the literature (Calza et al. 2006; Rizzo et al. 2009b). The apparent reaction rate constants for photocatalytic degradation of diclofenac were

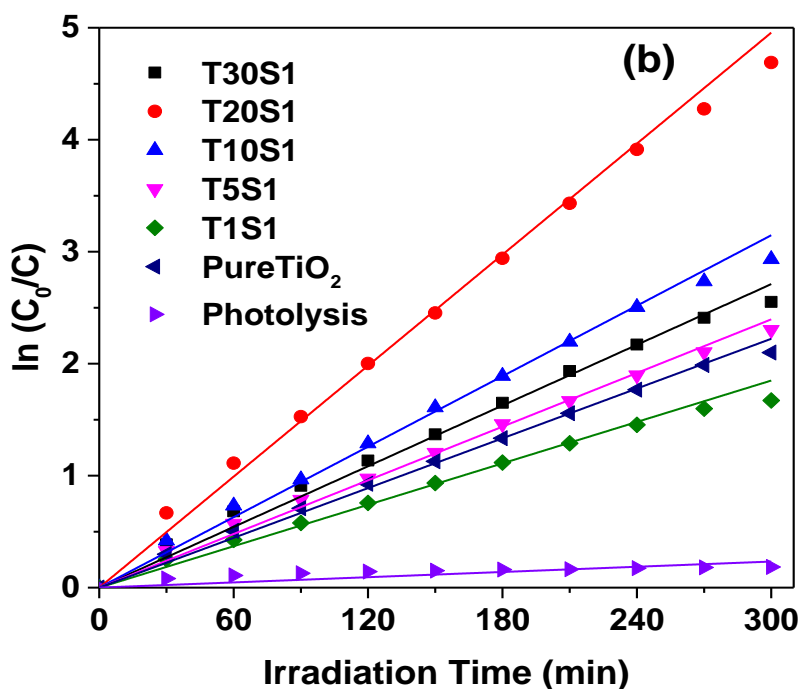
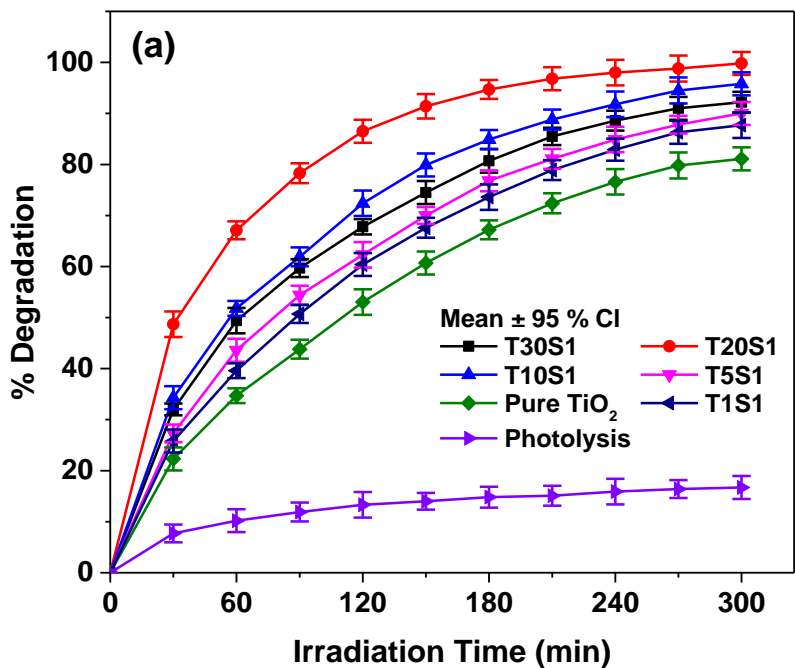
evaluated from experimental data using linear regression. The experimental data resulted that R^2 values for the pseudo-first-order reaction were ≥ 0.91 as compared to that of the zeroth-order reaction ($R^2 \geq 0.59$). Thus, degradation kinetics was best fitted to the pseudo-first-order kinetic model and the apparent rate constants for all the prepared catalysts were presented in table 4.3.

Table 4.3. Apparent rate constant for all the prepared TiO₂-SnO₂ catalysts.

Catalyst	Rate constant k_{app} (min⁻¹)	R²	Zeroth Order R²
T30S1	0.0090 ± 2.7E-4	0.9899	0.8262
T20S1	0.0165 ± 4.8E-4	0.9906	0.5937
T10S1	0.0105 ± 2.7E-4	0.9924	0.7773
T5S1	0.0079 ± 2.9E-4	0.9849	0.8689
T1S1	0.0062 ± 2.5E-4	0.9870	0.8562
TiO₂	0.0074 ± 2.9E-4	0.9126	0.8187

The catalyst T30S1, T20S1, T10S1 and T5S1 showed higher degradation efficiency compared to pure TiO₂. The catalyst T20S1 showed excellent photocatalytic activity for degradation of diclofenac when compared to others, which could be elucidated by the surface area of the catalyst. However, the photocatalytic efficiency of the catalyst T1S1 was lower than that of pure TiO₂. This might be due to increased Sn ions in the prepared catalyst, which has increased the amount of rutile phase and thereby limits the amount of light absorption in the UV-A region. Thus, the addition of a small quantity of Sn could enhance the efficiency of charge separation and thereby provide enhanced photocatalytic activity (Zhang et al. 2011). Correspondingly, the catalyst T30S1 has relatively lower photocatalytic efficiency compared to T20S1 and T10S1 catalysts. This may be due to the less amount of doped Sn content in the T30S1 catalyst to reduce recombination of electron and hole, resulting in a considerable reduction of photocatalytic activity (Huang et al.

2015). Also, the surface area of the catalyst T30S1 was lower than that of T20S1 and T10S1, which could be correlated to lower degradation efficiency.



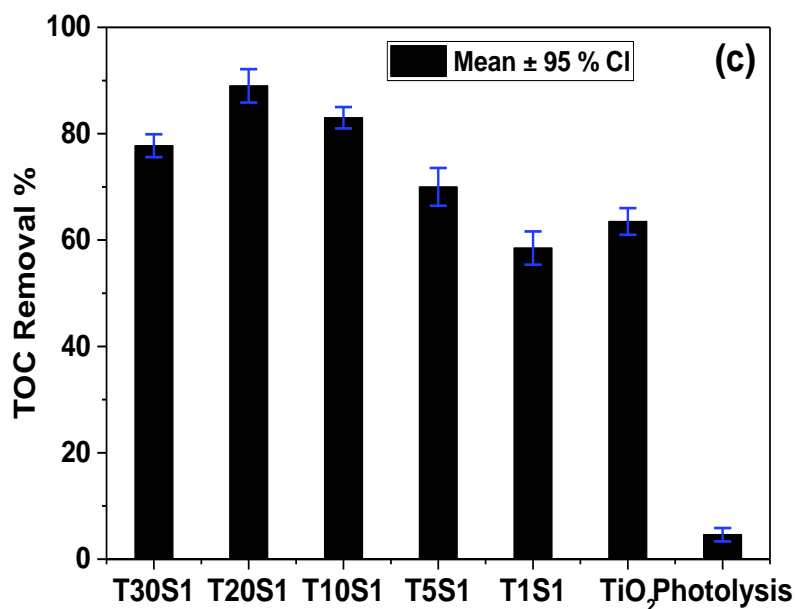


Figure 4.5. Effect of molar ratios of Ti-Sn on photocatalytic degradation of diclofenac (Initial concentration = 20 mg/L, pH = 5 and catalyst loading = 0.8 g/L) (a) Plot of degradation % vs time; (b) Kinetics of diclofenac degradation and (c) TOC removal % vs time.

It can be inferred from figure 4.5 that the catalyst T20S1 was the most efficient catalyst among all the prepared catalysts. Thus, all the other optimization experiments were carried out using the catalyst T20S1.

4.1.2.2. Effect of catalyst loading

To study the effect of catalyst loadings on photocatalytic degradation of diclofenac, different amounts of catalyst (0.4–1 g/L) were used. The reactions were performed under optimum conditions of initial concentration (20 mg/L) and at pH 5. The results are depicted in figure 4.6. It is observed that the photocatalytic efficiency increased with an increase in catalyst loading till catalyst loading of 0.8 g/L and then it decreased to a larger extent, which might be due to light scattering and screening effects, which reduces the specific activity of catalyst (Achilleos et al. 2010; Herrmann 1999). Thus, photocatalytic degradation efficiency decreases beyond 0.8 g/L. The maximum TOC removal of 90% was achieved during the irradiation time of 5 h.

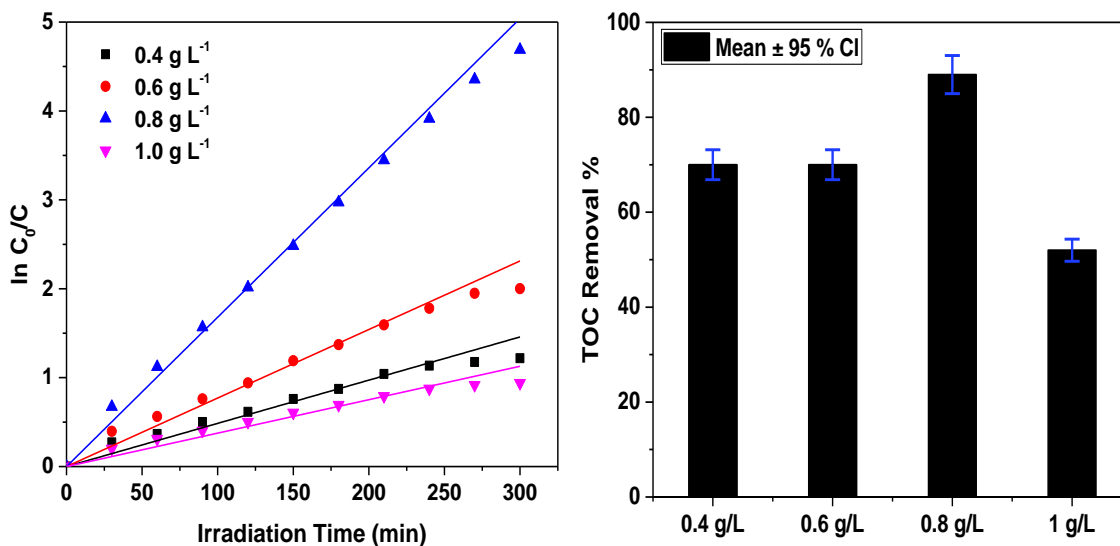


Figure 4.6. Effect of catalyst concentration on photocatalytic degradation of diclofenac (pH = 5 and initial diclofenac concentration = 20 mg/L).

4.1.2.3. Effect of initial pH

The pH of zero-point charge (pH_{ZPC}) is the pH at which the catalyst surface acquired a net zero charge. To understand the influence of pH on photocatalytic degradation of diclofenac, identification of pH_{ZPC} of the photocatalyst is very important. The pH_{ZPC} of the pure TiO_2 and T20S1 catalyst are shown in figure 4.7(a). The pH_{ZPC} of TiO_2 and T20S1 was found to be 6.3 and 6 respectively. This implies that the surface charge of the T20S1 catalyst would be positively charged when the solution pH is < 6 . The effect of initial pH on the degradation of diclofenac was carried out using the catalyst T20S1 and the results are presented in figure 4.7(b). The experiments were conducted at various initial pH values ranging from 4 to 7 with an initial diclofenac concentration of 20 mg/L and catalyst loading of 0.8 g/L. It is evident in Figure 4.7(b) that complete diclofenac degradation was observed at pH 5. This can be explained by the following observations. The pK_a value of diclofenac was reported to be 4.2, as it is a weak acid (Hiew et al. 2018). At $\text{pH} > \text{pK}_a$, diclofenac exists as a negatively charged ion due to dissociation of the diclofenac molecule. Hence, between pH 4.2 to 6, negatively charged diclofenac would be adsorbed more likely on to surface of positively charged T20S1 catalyst due to electrostatic attraction between catalyst and drug. Thus, photocatalytic degradation was higher at pH 5 compared to the efficiency at other pH ranges.

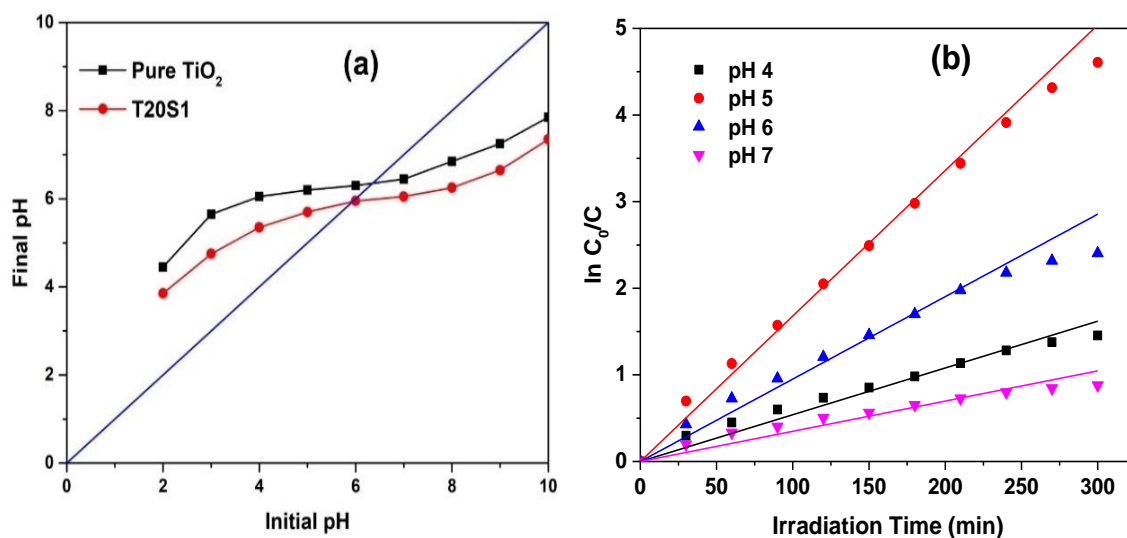
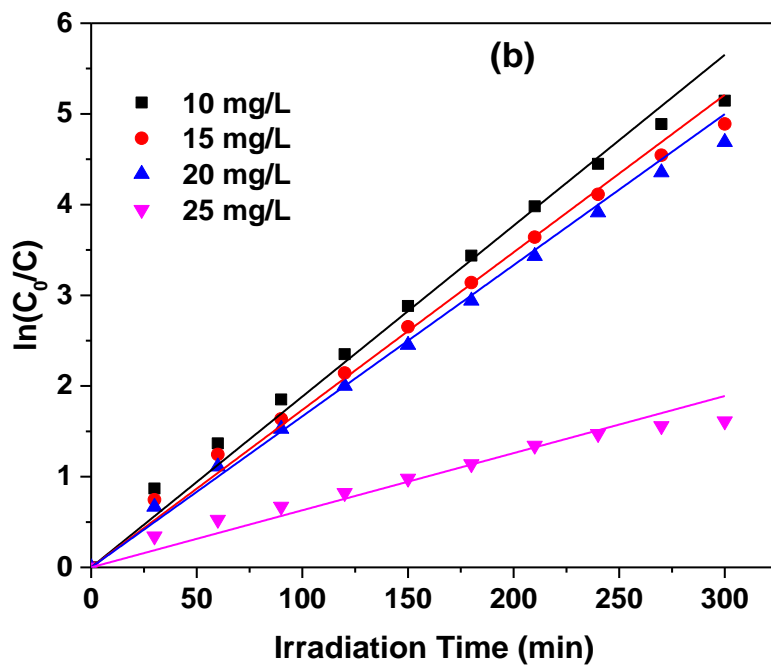
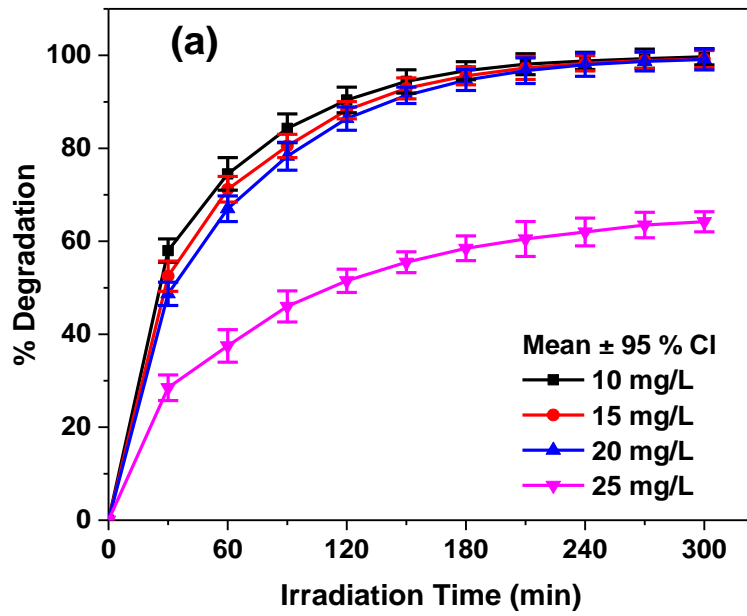


Figure 4.7. (a) The pH_{ZPC} of the pure TiO_2 and T20S1 catalyst and (b) Effect of initial pH on photocatalytic degradation of diclofenac (Initial concentration = 20 mg/L and catalyst loading = 0.8 g/L).

4.1.2.4. Effect of initial diclofenac concentration

Photocatalytic degradation of diclofenac was carried out using the catalyst T20S1 with varying initial concentrations (10–25 mg/L). The study was performed at an irradiation time of 5 h, at an initial of pH 5 and catalyst loading of 0.8 g/L. The results are presented in figure 4.8 in terms of diclofenac degradation efficiency, the rate constant with respect to initial concentration and TOC removal percentage. All the experimental data for different initial concentrations were best suited to the pseudo-first-order reaction. Degradation efficiency was found to be constant up to an initial diclofenac concentration of 20 mg/L and then decreased considerably. The rate constant values were also decreased with the increase in the initial diclofenac concentration as seen in figure 4.8 (d). This is due to the fact that at a higher concentration, amount of drug molecules adsorbed on the photocatalyst surface will be more, resulting in a reduced number of active sites of the catalyst. Therefore, the generation of hydroxyl radicals is reduced and hence leads to poor photocatalytic efficiency (Akpan and Hameed 2009). It is evident from figure 4.8 (c) that diclofenac was completely removed after an irradiation time of 5 h and 89 % TOC removal was obtained during the course of irradiation.



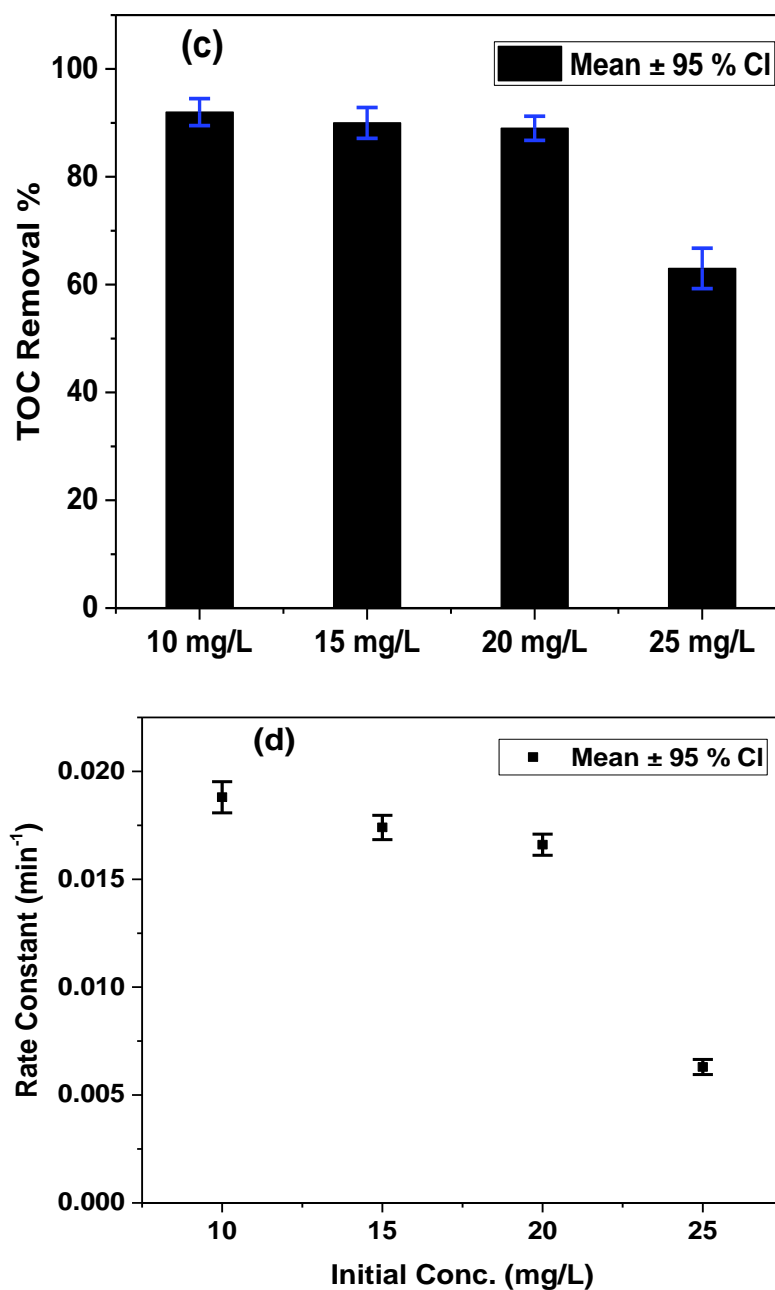


Figure 4.8. Effect of initial concentration on photocatalytic degradation of diclofenac (a) Diclofenac degradation over irradiation time; (b) Kinetics of diclofenac degradation with respect to initial concentration; (c) Plot of TOC removal % vs time and (d) plot of rate constants vs initial diclofenac concentration (pH = 5 and catalyst loading = 0.8 g/L).

4.1.3. Effect of scavengers and the role of active species

Different scavengers such as KI (0.01 M), 10 % methanol and NaN₃ (0.01 M) was introduced to the drug solution prior to illumination and addition of the catalyst. It can be seen from figure 4.9(a) that the photocatalytic degradation efficiency of diclofenac was

decreased to 34.5 %, 61.5 % and 69.5 % noticeably in the presence of KI, 10 % methanol and NaN₃ respectively. The degradation efficiency of diclofenac was greatly suppressed with the addition of KI (scavenger for both h⁺ and [•]OH radicals) suggesting that hydroxyl radicals are the prime active species in photocatalytic degradation of diclofenac. The transfer of charge carriers can be confirmed by [•]OH radical measurement as reported in the literature (Huang et al. 2009; Yuan et al. 2014). Figure 4.9(b) reveals the increased fluorescence intensity as compared to the bare pure TiO₂, which suggests that efficient charge transfer between coupled oxide systems and enhanced [•]OH radical generation. Also, h⁺ and O₂^{•-} were found to play a notable role in photocatalytic degradation system. Thus, h⁺, O₂^{•-} and [•]OH radicals were the active species responsible for the degradation of diclofenac in an aqueous solution under UV irradiation.

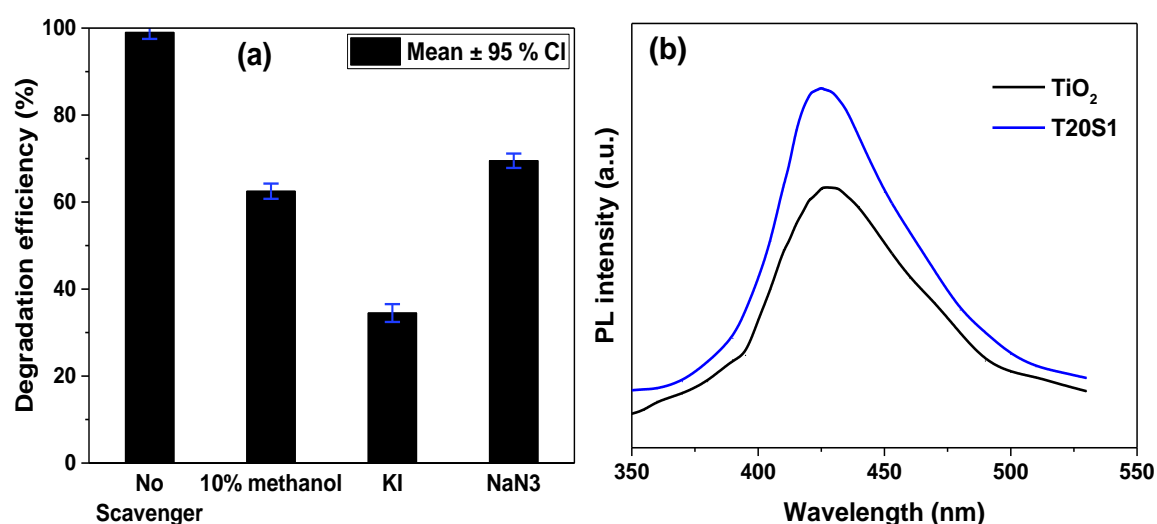
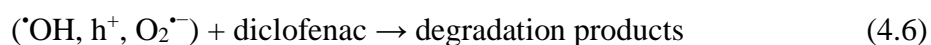
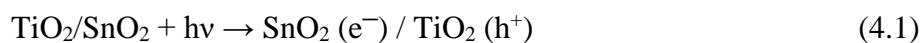


Figure 4.9 (a) Effect of different scavengers and (b) PL spectra for [•]OH radical evaluation under UV irradiation (Initial concentration = 20 mg/L, pH = 5 and catalyst loading = 0.8 g/L).

Coupling TiO₂ with another semiconductor oxide SnO₂ results in migration of electrons from CB of TiO₂ to CB of SnO₂ due to more positive CB edge of SnO₂ upon UV irradiation. Similarly, the photogenerated holes in the VB of SnO₂ are transferred to VB of TiO₂ due to the more positive VB edge of SnO₂, which leads to the separation of electron and holes. The charge carriers transfer mechanism in the heterojunction coupled photocatalytic system can effectively suppress the recombination reactions, which enhances the photocatalytic efficiency of the TiO₂-SnO₂ catalysts. The photogenerated electrons and holes could then produce O₂^{•-} and [•]OH radicals, respectively, which can further participate in the redox reaction mechanism along with some photogenerated holes.

The key reaction steps in the diclofenac reaction mechanism using the coupled TiO₂-SnO₂ mixed oxide catalyst has been summarized below:



4.1.4. Reusability and Stability

The results depicted in figure 4.10 shows that the performance of TiO₂-SnO₂ catalyst over the four-reaction cycle. The TiO₂-SnO₂ catalyst has good stability over the first three reaction cycles with a 7 % decrease in degradation efficiency.

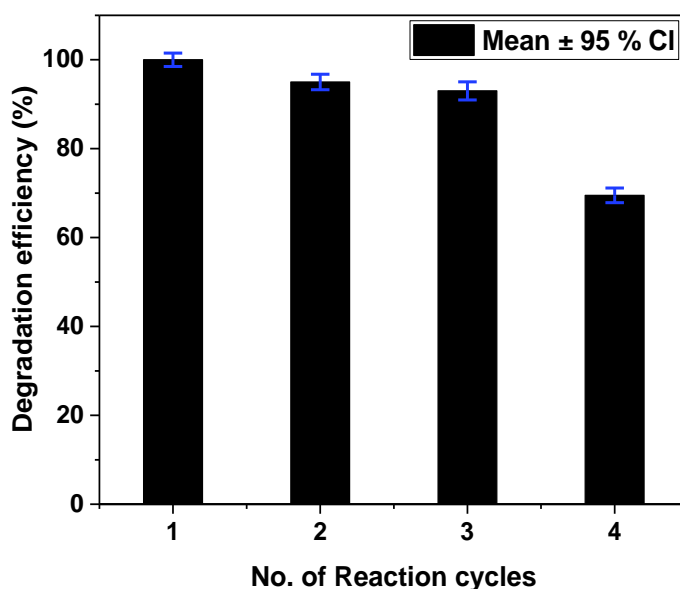


Figure 4.10. Reusability and stability of the prepared catalysts (Initial concentration = 20 mg/L, pH = 5 and catalyst loading = 0.8 g/L).

However, the degradation percentage was further reduced to 69 % for the fourth reaction cycle when compared to the initial reaction cycle. The decrease in photodegradation efficiency might be attributed to the amassment of intermediates at the

catalyst surface during each reaction cycle, which in turn reduces the number of active sites in catalysts (Chiang and Doong 2015). Hence the TiO₂-SnO₂ catalyst has the moderate capability to retain the efficiency over the repeated cycles.

4.1.5. Identification of Intermediate products

Experiments were conducted to identify the intermediates formed during the photocatalytic degradation of diclofenac under the optimum operating conditions. The LC-MS spectra of several intermediates formed during the course of irradiation were shown in figure 4.11. Decarboxylation, hydroxylation and dechlorination were the most probable reactions observed during the reduction of pollutants where three major degradation pathways were observed. The probable degradation mechanism of diclofenac is shown in figure 4.12. The peak at m/z 296 corresponds to diclofenac, which is formed by the loss of one Na from diclofenac sodium.

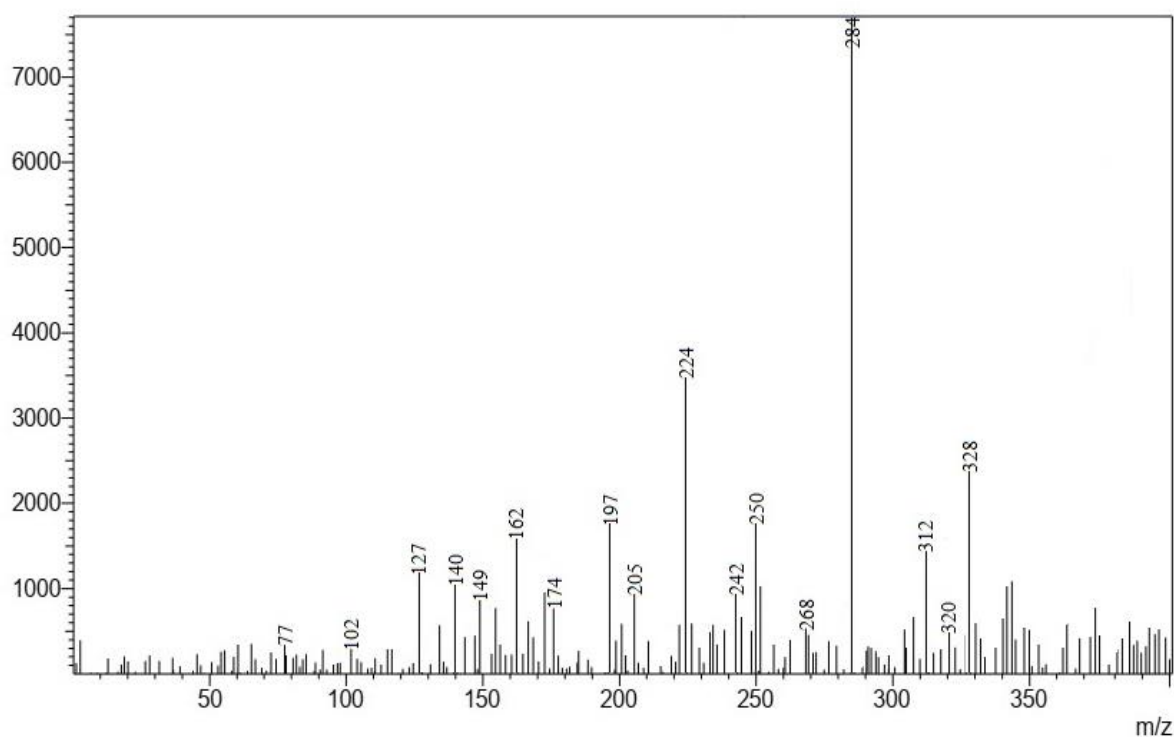


Figure 4.11. The LCMS spectra of intermediates formed (Initial concentration = 20 mg/L, pH = 5 and catalyst loading = 0.8 g/L).

The first pathway involves hydroxylation of diclofenac resulted in a peak at m/z 312, which corresponds to hydroxyl diclofenac. Loss of -COOH from molecular ion m/z 312 resulted in the formation of another fragment at m/z 267. Compound at m/z 267 again

suffers from the removal of its chlorine atoms to form another compound with m/z 197, which was reported as 2-phenylamino benzaldehyde (Martinez et al. 2011). The compound further undergoes removal of $-\text{CHO}$, resulting in the generation of diphenyl aminyl radical (m/z 169). Simultaneously, the addition of $\cdot\text{OH}$ radicals to hydroxy diclofenac (m/z 312) resulted in the formation of dihydroxy diclofenac with m/z 328, which was also reported in the literature (Calza et al. 2006; Yu et al. 2013). Dihydroxy diclofenac (m/z 328) further undergoes decarboxylation to form a major peak at m/z 284. Dechlorination of compound m/z 284 results in the formation of another fragment at m/z 250. Alternatively, the compound m/z 284 undergoes hydroxylation to produce m/z 162, which in turn suffers from the removal of Cl^- , results in another compound with m/z 127.

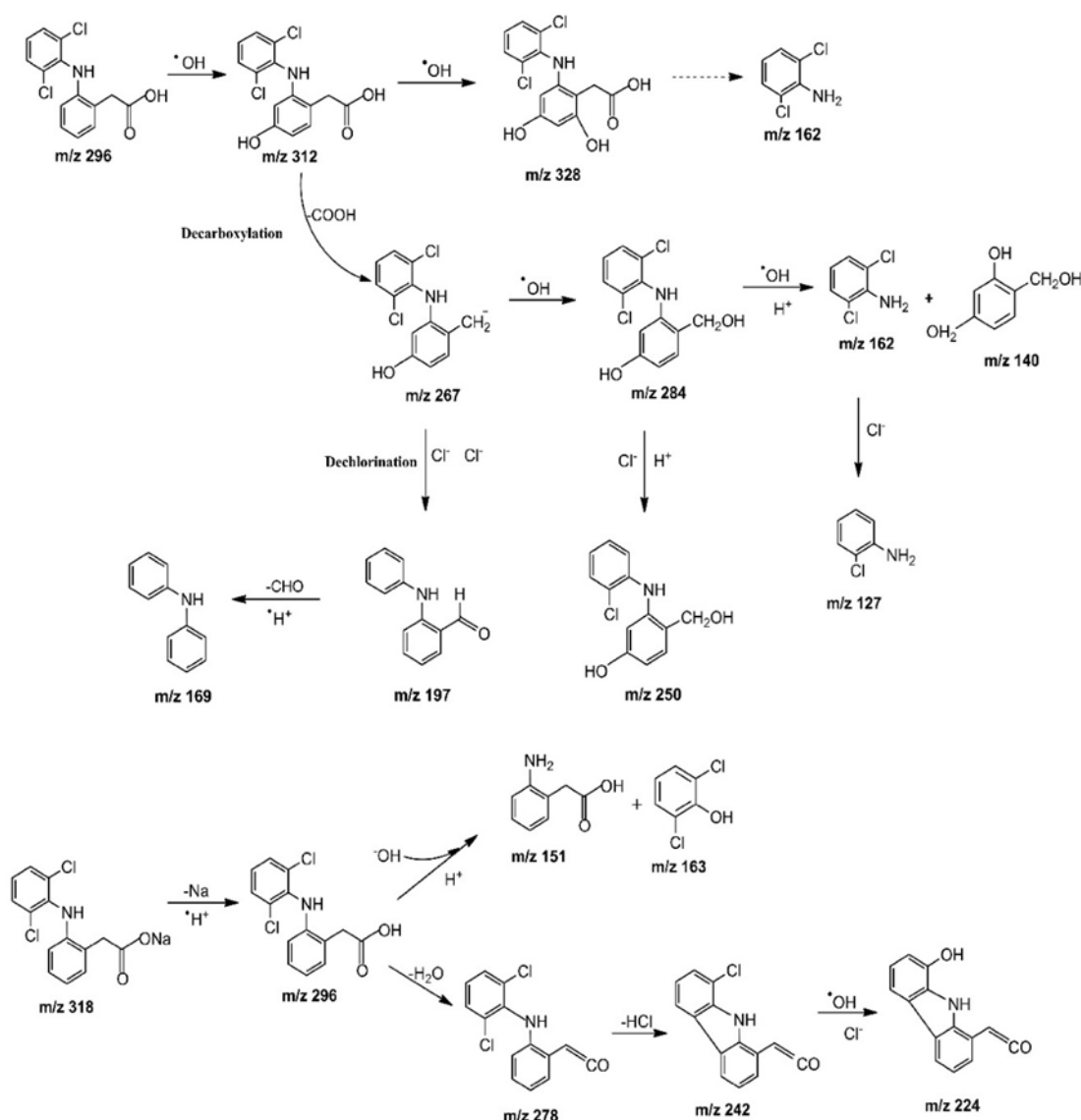


Figure 4.12. The probable degradation pathway of diclofenac using $\text{TiO}_2\text{-SnO}_2$ mixed oxide catalysts.

Another pathway involves removal of H₂O from diclofenac resulted in m/z 278, which further produces a fragment at m/z 242 due to loss HCl. The molecular ion at m/z 242 further undergoes dechlorination, and substitution of •OH resulted in another fragment at m/z 224. Similarly, hydroxylation of diclofenac (m/z 296) produces two compounds with m/z 151 and m/z 163 due to the cleavage of the C–N bond. There are various peaks that were identified during the photocatalytic degradation process at the initial stage; however, only four major peaks (m/z 284, 250, 224, 197) notably had a higher intensity and the intensity of the other peaks diminished as the reaction time increased. Several other small peaks were observed during the course of the experiments and were found to be degraded within the irradiation time of 5 h.

4.1.6. Cost analysis for TiO₂ and TiO₂-SnO₂ mixed oxides

1 unit of electricity costs Rs. 7

For the preparation of 1 g (approx.) of TiO₂,

8 ml TTIP – Rs. 37.6

Isopropanol, 30 ml – Rs. 49.7

Glacial acetic acid, 8 ml – Rs. 24.6

For Hot air oven = 2000 W * 24 h = 48 units = Rs. 336

Total cost involved for TiO₂ preparation = Rs. 37.6 + Rs. 49.7 + Rs. 24.6 + Rs. 336 = Rs. 448

For the preparation of 1 g (approx.) of TiO₂-SnO₂ mixed oxide (T20S1),

8 ml TTIP – Rs. 37.6

Isopropanol, 30 ml – Rs. 55.7

Glacial acetic acid, 8 ml – Rs. 24.6

SnCl₂.5H₂O, 0.58 g – Rs. 10.8

Ultrasonication (10 min) = 500 W * (1/6) h = 0.08 units = Rs. 0.56

For Hot air oven = 2000 W * 24 h = 48 units = Rs. 336

Total cost involved for TiO₂-SnO₂ (T20S1) preparation = Rs. 37.6 + Rs. 49.7 + Rs. 24.6 + Rs. 10.8 + Rs. 0.56 + Rs. 336 = Rs. 460

For 20 mg/L of diclofenac degradation through photocatalysis,

0.8 g of catalyst used = 0.8 * (Rs. 460) = Rs. 368

Irradiation time = 5 h

For UV irradiation = 80 W * 5 h = 0.3 units = Rs. 2.1

Total cost estimation for degradation of 20 mg of diclofenac using TiO₂-SnO₂ (T20S1) mixed oxide = Rs. 368 + Rs. 2.1 = Rs. 371

4.2. CONCLUSION

TiO₂-SnO₂ mixed oxide catalysts were found to be effective in photocatalytic degradation of diclofenac, as the complete degradation of diclofenac was achieved under UV irradiation. The catalysts were prepared by the hydrothermal method by varying the molar ratios of Ti-Sn and it was found that the T20S1 catalyst was more efficient in achieving complete degradation of diclofenac. The structural and morphological characterization of the prepared catalysts represented the presence of mixed phase crystallites in the coupled catalysts. The mineralization was also confirmed by TOC analysis, where about 88 % removal was obtained. The photocatalytic efficiency of the catalysts T30S1, T10S1 and T5S1 were also better than pure TiO₂ catalyst's performance. On the other hand, the catalyst T1S1 resulted in poor degradation efficiency due to a higher amount of Sn doping. It was observed that the addition of a small amount of Sn could enhance the photocatalytic activity of TiO₂. However, a smaller amount of Sn doping in TiO₂-SnO₂ catalyst diminishes the efficiency of charge separation and enhances electron-hole recombination.

The various optimum parameters such as pH, initial concentration and catalyst loading were evaluated. The photocatalytic degradation efficiency was maximum at pH 5 and initial diclofenac concentration of 20 mg/L and 0.8 g/L TiO₂-SnO₂ catalyst loading. The effect of different radical scavengers has been studied and the results indicated that $\cdot\text{OH}$ is the main reactive species in the diclofenac reaction mechanism, with h^+ and $\text{O}_2^{\cdot-}$ also considerably participated in the reaction mechanism. The efficient charge transfer between coupled photocatalysts was confirmed by photoluminescence analysis at 426 nm, which suppressed recombination of charge carriers and hence led to the higher catalytic activity of TiO₂-SnO₂ mixed oxides. It is observed that optimum loading of Sn in the mixed oxide heterostructure resulted in good dispersion and proper charge transfer between the TiO₂ and SnO₂. The reusability and stability of the catalyst were also evaluated and the TiO₂-SnO₂ catalyst shows good stability with only 17% reduction in degradation efficiency after three successive reaction cycles and the degradation efficiency reduced excessively in

the fourth reaction cycle. LC-MS analysis confirmed the formation of several intermediates during the process; however, the compounds with m/z 284 and m/z 224 were the main degradation products which were identified after the complete irradiation time. The probable degradation process suggests that the degradation process follows $\cdot\text{OH}$ radical attack, hydroxylation, C-N cleavage, dechlorination and decarboxylation reactions.

CHAPTER 5

PHOTOCATALYTIC DEGRADATION OF DICLOFENAC USING TiO₂-WO₃ CATALYSTS

5.1. RESULT AND DISCUSSION

5.1.1. Characterisation of TiO₂-WO₃ catalysts

X-ray diffraction patterns of all the prepared TiO₂-WO₃ catalysts were observed to be in a crystallized form which is shown in figure 5.1. Anatase and rutile phase TiO₂ and monoclinic phase WO₃ were observed in the prepared TiO₂-WO₃ catalysts. A significant increase in WO₃ content in the mixed oxides led to an increase in the intensity of the monoclinic phase of WO₃ peaks. However, the addition of WO₃ did not affect the diffraction patterns of the catalysts TW20 and TW10 as it was similar to the diffraction pattern of TiO₂ and this could be possibly due to lower WO₃ content in the mixed oxides. The diffraction peaks in the catalyst TW1 represent the anatase phase of TiO₂, rutile phase of TiO₂ and the monoclinic phase of WO₃. The peaks at $2\theta = 25.22^\circ$ and 48.21° corresponds to (101) and (200) planes of the anatase phase of TiO₂ (ICDD no. 01-071-1166) and peaks at $2\theta = 35.6^\circ$ and 54° corresponds to (101) and (111) planes of rutile phase TiO₂ (ICDD #21-1276). Peaks at $2\theta = 23.16^\circ$, 24.1° , 49.92° , and 54.3° are indicative of the (002), (200), (140) and (202) crystal planes of the monoclinic phase of WO₃ (ICDD #43-1035). The TiO₂-WO₃ mixed oxide catalysts showed a monoclinic phase of WO₃ and the WO₃ phases increase with increasing WO₃ content. The WO₃ content in the catalyst sample TW5 has been reduced such that only two weaker peaks ($2\theta = 23.16^\circ$, 24.1°) of the monoclinic phase of WO₃ were observed as seen in figure 5.1.

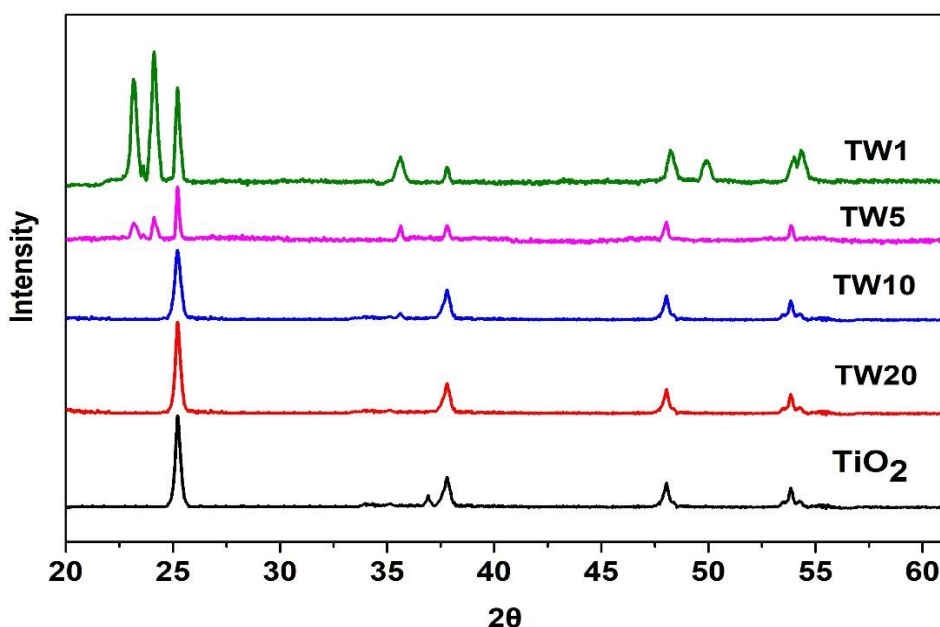


Figure 5.1. XRD patterns of the prepared TiO₂-WO₃ catalysts

TEM was used to analyze the surface morphologies of the photocatalysts synthesized by hydrothermal method, which is shown in figure 5.2. The TEM analysis unveiled that all the TiO₂-WO₃ mixed oxide catalysts were in a wide size range with different morphology. Most of the prepared catalysts were observed to be in the state of agglomeration, irregular sizes and uniform crystalline particles. The individual particle size of the catalysts TW10 and TW20 was in the range of 25–40 nm which were lesser than that of bare TiO₂ nanoparticles. As seen in figure 5.2, the TW1 catalyst has the smallest particle size compared to all the other catalysts (<10 nm). Increase in the concentration of WO₃ content led to a reduction in the size of the mixed oxides. HRTEM images displayed the presence of lattice fringes for both TiO₂ and WO₃. The lattice fringes $d = 0.37$ nm corresponds to 200 planes of WO₃ and the lattice fringes $d = 0.35$ nm indexed to 101 planes of anatase TiO₂. The HRTEM images confirm the presence of mixed-phase crystallites.

Energy-dispersive X-ray spectroscopy (EDS) analysis was done to investigate the elemental composition and weight ratios of TiO₂-WO₃ coupled semiconductor photocatalyst synthesized with various molar ratios of Ti and W precursors. The EDS of all the prepared TiO₂-WO₃ mixed oxide catalysts were illustrated in figure 5.3. It was perceived that the peaks of Ti, W, O elements were seen in the spectra which confirms the existence of coupled TiO₂-WO₃ mixed oxides. The atomic quantity ratio of all the prepared catalysts with Ti:W ratio was very much equivalent to the molar ratios of Ti and W in the prepared catalysts. The molar ratios of Ti and Sn in the prepared catalysts were also

equivalent to the weight percentage observed in the EDS analysis. The elemental weight percentage of all the mixed oxide catalysts with different molar ratios were tabulated in table 5.1.

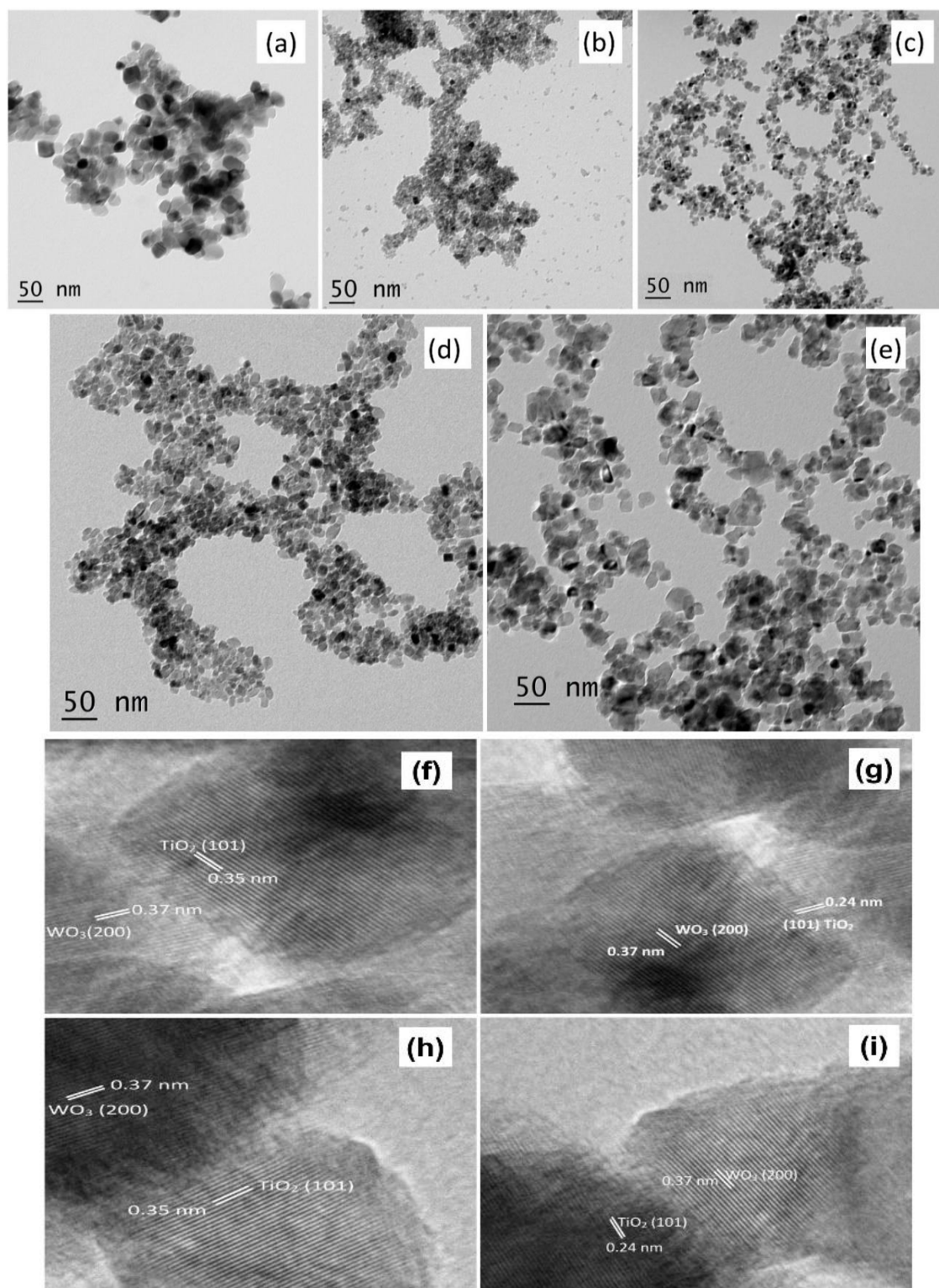


Figure 5.2. TEM images of (a) Pure TiO_2 ; (b) TW1; (c) TW5; (d) TW10 and (e) TW20 and HRTEM images (Magnification = 2 nm) of (f) TW1; (g) TW5; (h) TW10 and (i) TW20.

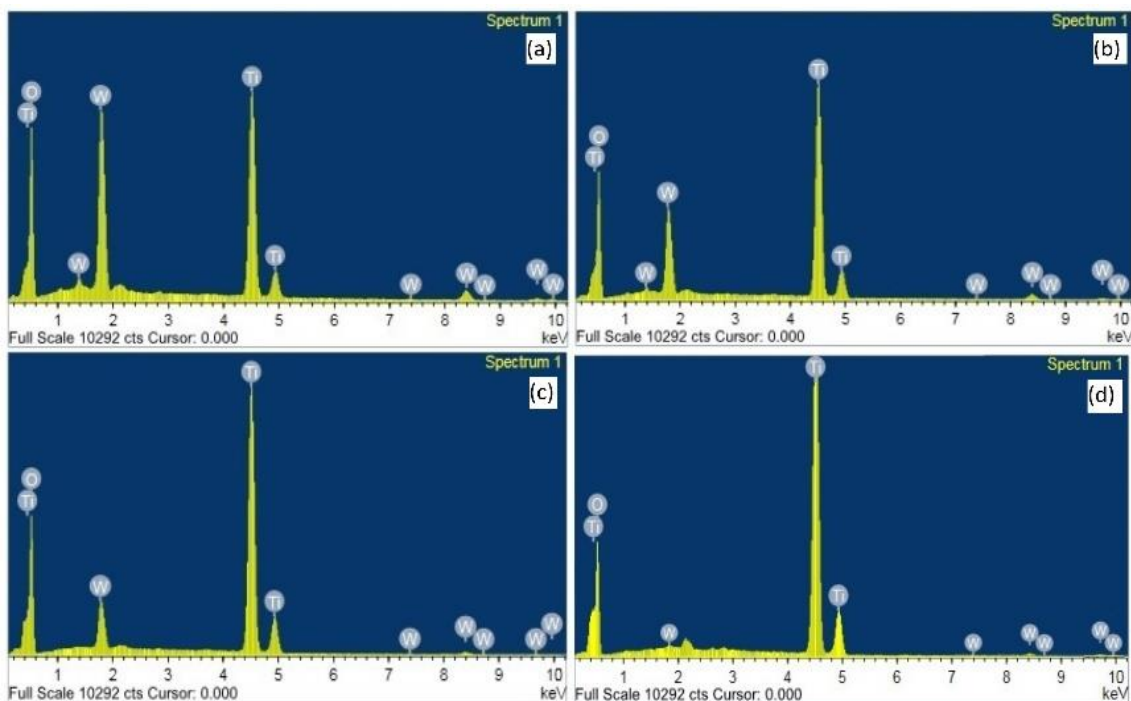


Figure 5.3. EDS of (a) TW1; (b) TW5; (c) TW10 and (d) TW20.

Table 5.1. Elemental composition and weight percentage of TiO₂-WO₃ catalysts.

Catalyst	Elements and their weight %		
	Ti	O	W
TW20	26.98	71.38	1.32
TW10	24.54	72.74	2.46
TW5	21.37	74.23	4.29
TW1	13.42	72.97	13.19

The optical band gap energy (E_g) of TiO₂-WO₃ catalysts has been determined by the Tauc plot, as shown in figure 5.4. The catalyst TW1 has the lowest bandgap energy ($E_g = 2.8$ eV). Similarly, the corresponding bandgap energy of the catalysts TW20, TW10 and TW5 was 3.1 eV, 2.95 eV and 2.9 eV respectively. It is clear that the bandgap values decrease from 3.2 eV to 2.8 eV with an increase in WO₃ loading. It is also evident that the TiO₂-WO₃ catalysts had longer wavelengths of more than 390 nm and the absorption edge of all the catalysts fall in the visible region (390-750 nm). Thus, the TiO₂-WO₃ catalysts could attract a larger section of the solar spectrum, which could be probably useful in

reducing the cost of energy consumption. Also, it could enhance the separation of photogenerated charge carriers during the visible light irradiation, and thus recombination rate of charge carriers could be reduced (Anandan et al. 2014).

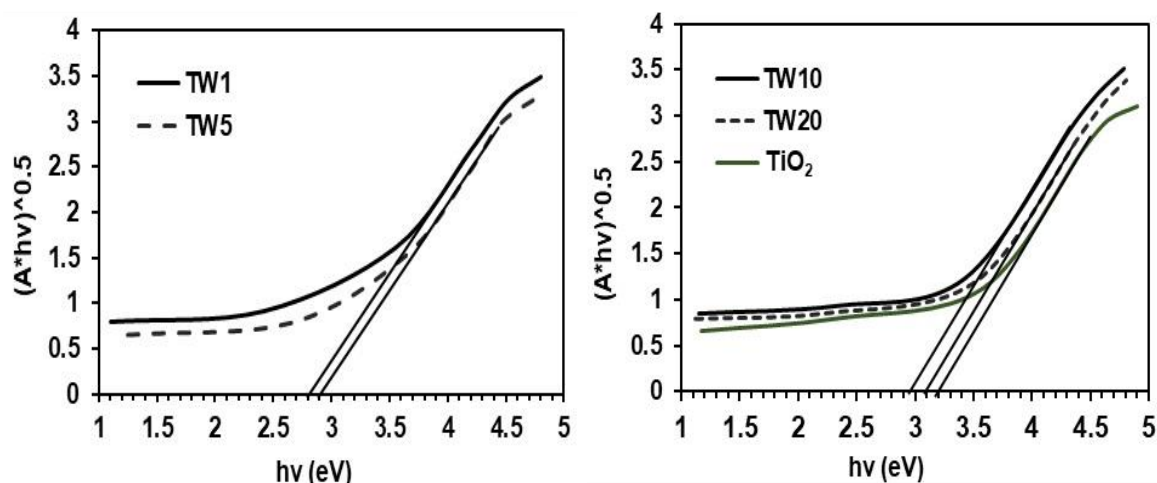


Figure 5.4. Tauc plot for calculation of band gap of all the prepared catalysts.

Table 5.2. Surface area and size of the catalysts prepared with different molar composition.

Catalyst with different molar ratios	BET surface area (m ² /g)	Total pore volume (cc/g)	Average size of the catalysts (nm)
TW20	104.28	0.2593	35 ± 8.5
TW10	103.95	0.2533	30 ± 6.1
TW5	92.99	0.1985	20 ± 3.5
TW1	80.45	0.1792	12 ± 4.5
Pure TiO₂	76.33	0.1619	40 ± 9.5

The photocatalytic activity of a catalyst is interrelated to the amount of active surface area accessible to the target molecule for promoting adsorption and desorption reactions (Bellardita et al. 2007; Subash et al. 2013). Specific surface area and pore volume of the TiO₂-WO₃ catalysts were estimated by BET and BJH method respectively. The specific surface area and pore volume of all the TiO₂-WO₃ catalyst were investigated and reported in table 5.2. The catalysts TW20, TW10 and TW5 have a higher specific surface

area and pore volume compared to pure TiO₂. But, the catalyst TW1 has a lesser pore volume and surface area among all the catalysts. It can be deduced that an increase in WO₃ molar concentration results in the reduction of surface area and total pore volume of the prepared catalysts.

5.1.1 Photocatalytic Activity Evaluation

The photocatalytic activity of all the catalysts prepared with the different molar compositions of Ti and W in the precursor solution was assessed using diclofenac solutions of different initial concentrations, catalyst loading and different pH values under visible light irradiation.

5.1.2.1 Effect of molar composition of Ti and W

The photocatalytic activity of different TiO₂-WO₃ catalysts for the degradation of diclofenac under visible light is depicted in figure 5.5. The experimental data obtained from each experiment were plotted with Eq. (3.2) and Eq (3.3) as already discussed in section 3.2. It is noted that the experimental data were well fitted to pseudo-first-order reaction ($R^2 \geq 0.98$) compared to zeroth-order reaction (where $R^2 \geq 0.668$). The apparent rate constants were tabulated in table 5.3.

Table 5.3. Apparent rate constants for all the prepared TiO₂-WO₃ catalysts.

Catalyst	Rate constant $k_{app}(\text{min}^{-1})$	R^2	Zeroth Order R^2
TW20	$0.0157 \pm 6E-4$	0.9855	0.7421
TW10	0.0226 ± 0.0027	0.9995	0.6683
TW5	$0.0115 \pm 4.7E-4$	0.9838	0.8186
TW1	$0.0095 \pm 3.5E-4$	0.9867	0.8586
TiO₂	$0.0074 \pm 2.3E-4$	0.9906	0.8904

From figure 5.5, it is observed that all the prepared catalysts have higher photodegradation efficiency compared to pure TiO₂, which indicates the presence of WO₃ has increased the degradation efficiency of TiO₂ in coupled mixed oxides. The catalyst

TW10 has the highest degradation efficiency among all the prepared catalysts. Despite that, the degradation efficiency of the catalyst TW20 was lower than that of TW10, which indicates that TW10 is the ideal catalyst for the degradation of diclofenac under visible light. Similarly, the catalyst TW1 has the lowest efficiency, which could be due to the presence of a higher amount of WO_3 content in the coupled TiO_2 - WO_3 catalyst. The presence of an excess amount of WO_3 particles could act as a center for recombination of electron and hole, thereby limiting the rate of degradation under visible light (Tian et al. 2008; Xie et al. 2014).

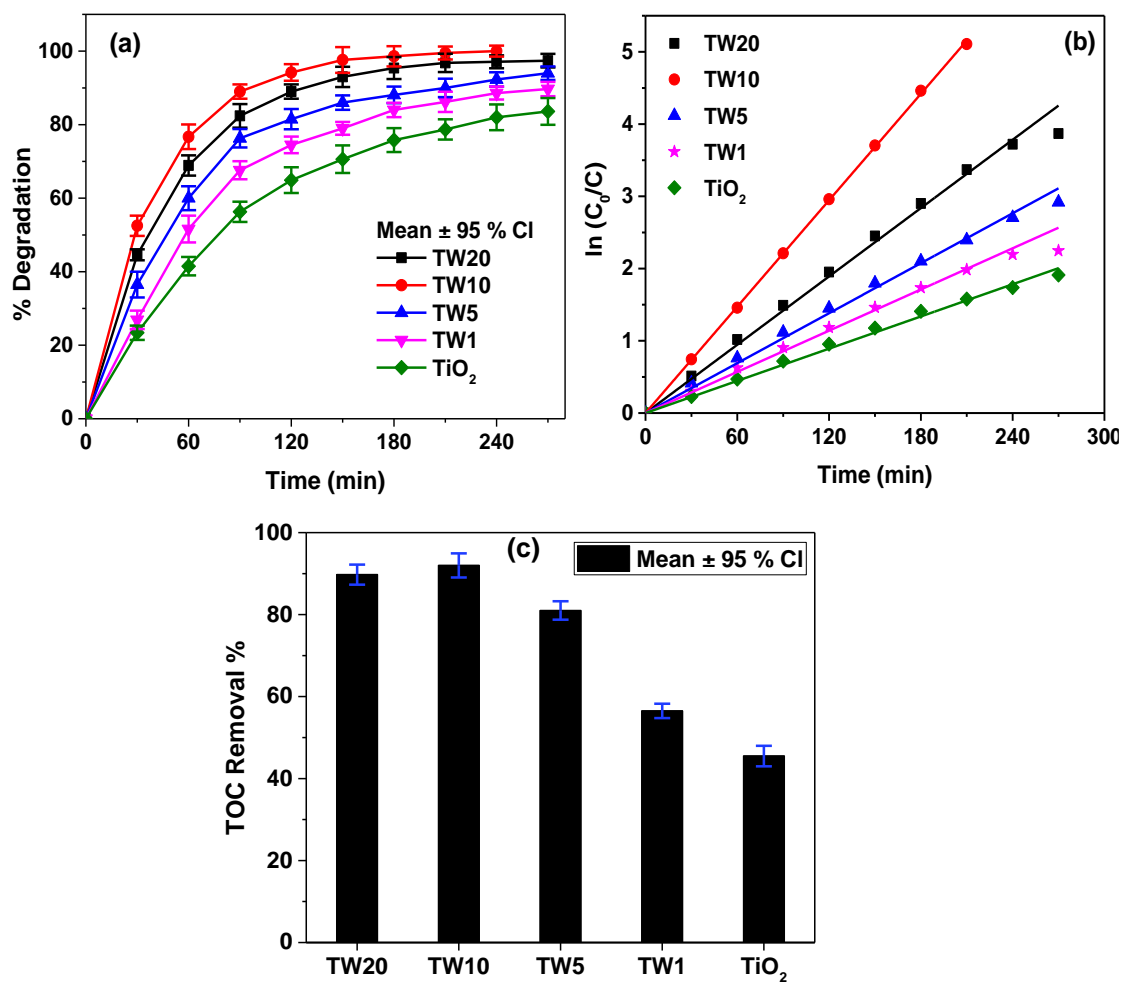


Figure 5.5. Effect of molar ratios on TiO_2 - WO_3 catalyst for photocatalytic degradation of diclofenac (a) percentage degradation of diclofenac over the time (b) kinetics of photodegradation and (c) TOC removal efficiency for different mixed oxide catalysts (Initial concentration = 25 mg/L, pH = 5 and catalyst loading = 0.6 g/L).

5.1.2.2 Effect of catalysts loading

In order to evaluate the optimal amount of catalyst concentration required for effective degradation of diclofenac, while the initial diclofenac concentration and pH were kept constant at 25 mg/L and pH 5 respectively, the experiment was performed with various quantities of catalyst dosage (0.4-0.8 g/L) in the 100 ml diclofenac solution, and the results are reported in figure 5.6. It was revealed that the photocatalytic efficiency was enhanced with an increase in catalyst dosage till catalyst concentration of 0.6 g/L and later reduced considerably. The increase in degradation efficiency might be due to the enhanced total active surface area available for adsorption of targeted diclofenac molecules. However, the addition of the excess amount of suspended photocatalysts beyond the optimum concentration could incite light scattering phenomenon and screening effects due to increased opacity and turbidity of the solution, which results in the reduction of photocatalytic efficiency of the catalysts (Achilleos et al. 2010; Herrmann 1999; Martinez et al. 2011).

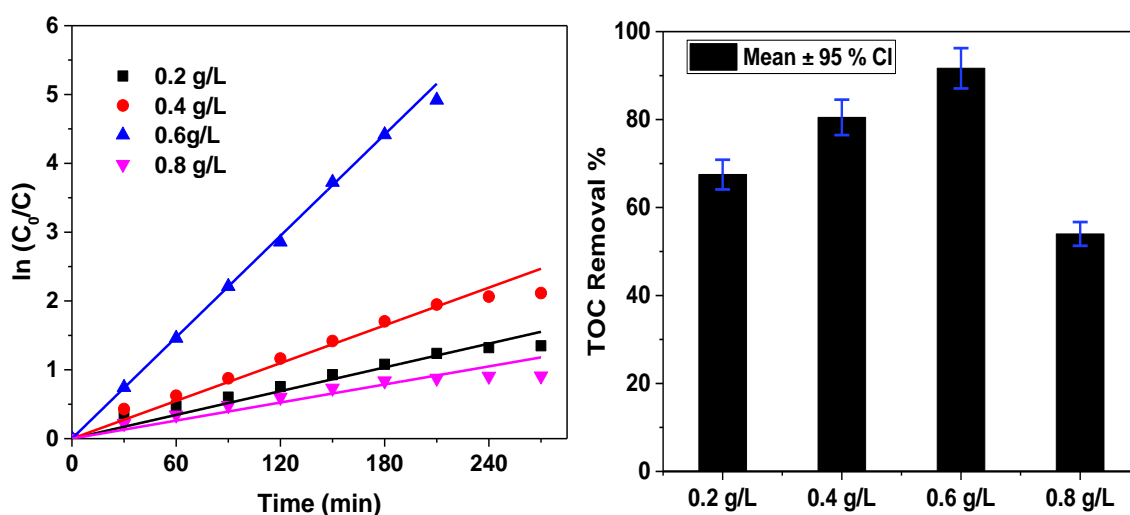


Figure 5.6. Effect of catalyst loading on photocatalytic degradation of diclofenac (pH = 5 and initial diclofenac concentration = 25 mg/L).

5.1.2.3 Effect of initial pH

TW10 catalyst was used to investigate pH effects on diclofenac removal via photocatalysis and the results are represented in figure 5.7. The study was conducted with various pH values starting from pH 4 to pH 8 with constant catalyst dosage (0.6 g/L) and initial diclofenac concentration (25 mg/L). It is found that photocatalytic degradation of

diclofenac at pH 5 was more effective compared to others. The pH_{ZPC} of the TW10 catalyst was found to be 5.7, suggesting that the catalyst surface will be positively charged at $pH < 5.7$. As already reported, pK_a value of diclofenac is 4.2 and hence diclofenac will be a negatively charged ion when the solution pH is above 4.2. The higher degradation efficiency at pH 5 was due to the electrostatic attraction between negatively charged diclofenac and positively charged TW10 catalyst, as already discussed in section 4.1.2.3. It is also reported that the acidic condition favors the hydroxyl radical generation. Thus, photocatalytic activities at pH 4 and 6 were comparatively higher at pH 8 (Bagal and Gogate 2014).

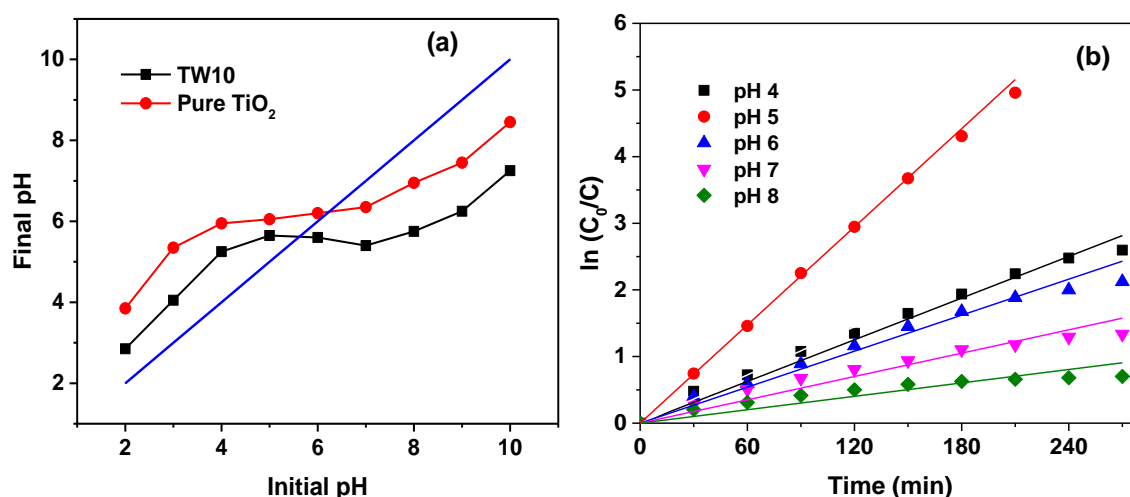


Figure 5.7. (a) The pH_{ZPC} of the TiO_2 and TW10 catalyst and (b) Effect of initial pH on photocatalytic degradation of diclofenac (Initial concentration = 25 mg/L and catalyst loading = 0.6 g/L).

5.1.2.4 Effect of initial diclofenac concentration

Further, the study was continued to estimate the optimum initial diclofenac concentration that can be mineralized under visible light irradiation with initial concentration ranging from 10mg/L to 30 mg/L. The other experimental conditions were fixed at an initial pH of 5 and a catalyst concentration of 0.6 g/L and the results are shown in figure 5.8. The catalytic efficiency was observed to be optimal with the initial diclofenac concentration ranging from 10 mg/L to 25 mg/L and then declined significantly, as shown in figure 5.8 (a). The experimental data for all the initial diclofenac concentration fit well with the pseudo-first-order reaction (figure 5.8 (b)). The rate constant values were decreasing with an increase in the initial concentration, which is shown in figure 5.8 (d).

This could be due to the fact that at higher substrate concentration, an excess amount of target molecules will be accumulated on the surface of the catalyst which could conceivably result in the reduction of the effective surface area for degradation. Consequently, increased drug molecule interaction on the active sites of the photocatalyst surface results reduction in hydroxyl radicals formation, which affects the photocatalytic activity of the catalysts (Das et al. 2015; Reza et al. 2017).

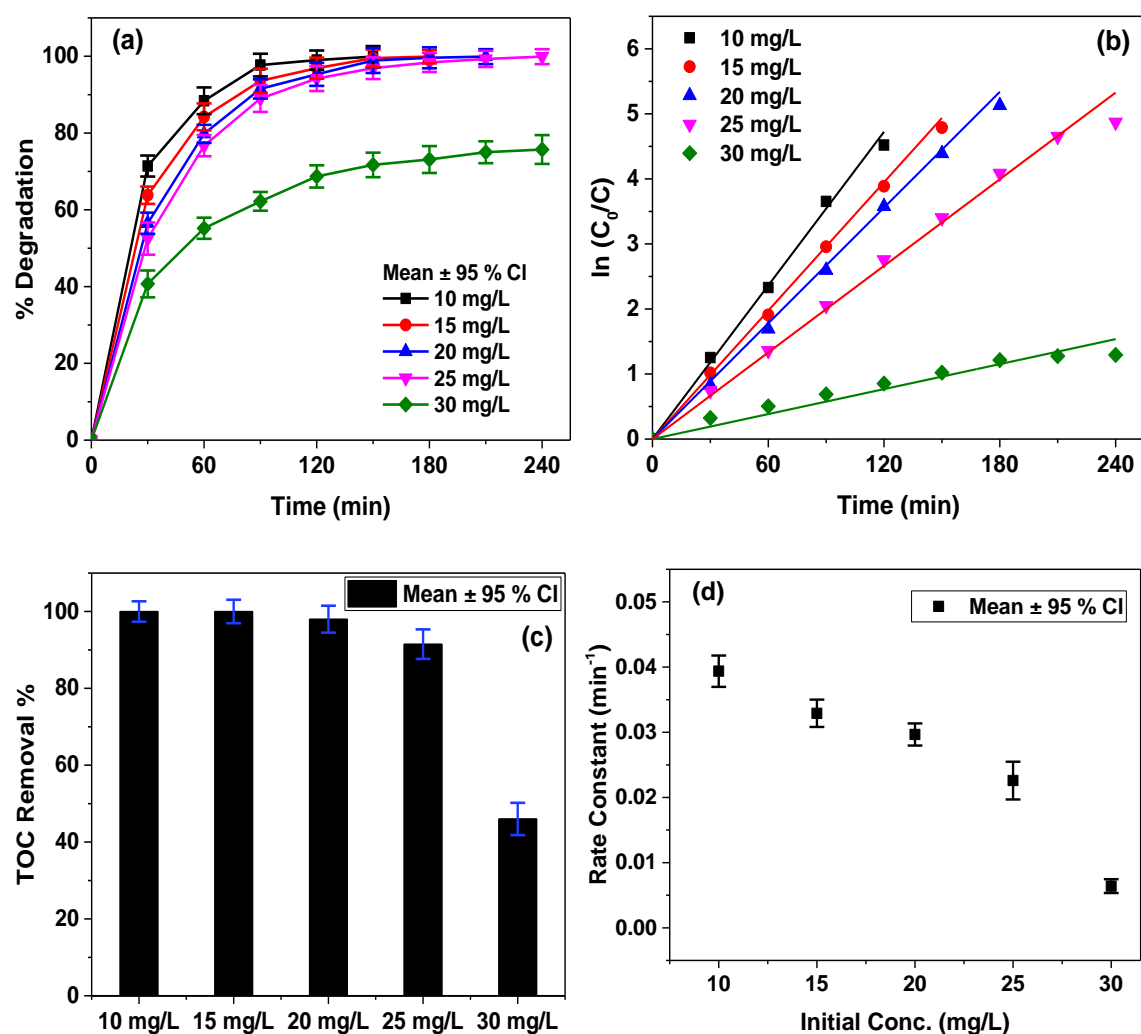


Figure 4.8. Effect of initial concentration on photocatalytic degradation of diclofenac (pH = 5 and catalyst loading = 0.6 g/L). (a) plot of percentage degradation vs time; (b) kinetics of degradation with respect to time; (c) TOC removal percentage for different initial concentrations; (d) plot of rate constant vs initial concentration.

5.1.3 Effect of radical scavengers and the role of active species

The effect of different scavengers on the degradation of diclofenac is shown in figure 5.9 (a). It can be seen that the photocatalytic degradation efficiency of diclofenac

was decreased to 27.5 %, 55 % and 97.5 % in the presence of KI, 10 % methanol and NaN₃ respectively. The degradation efficiency of diclofenac was greatly suppressed with the addition of KI suggesting that hydroxyl radicals are the prime active species in photocatalytic degradation of diclofenac. Influence of $\cdot\text{OH}$ radicals on diclofenac degradation mechanism is also confirmed by photoluminescence study as seen in figure 5.9 (b). It is observed that the catalyst TW10 showed increased photoluminescence intensity at 426 nm as compared to that of pure TiO₂ and hence degradation efficiency of TW10 was higher than that of pure TiO₂. Also, h⁺ ions are found to play a notable role in photocatalytic degradation system. However, O₂^{•-} doesn't have a significant role in the degradation mechanism. This might be due to the multi-electron reduction phenomenon that takes place in CB of WO₃, as CB of WO₃ doesn't have sufficient reduction potential to reduce adsorbed O₂ to O₂^{•-}, thereby inhibits the formation of O₂^{•-} (as explained in Eq. 5.2 and 5.3). Thus, h⁺ and $\cdot\text{OH}$ radicals were responsible for the degradation of diclofenac in an aqueous solution over the prepared TiO₂-WO₃ under visible light.

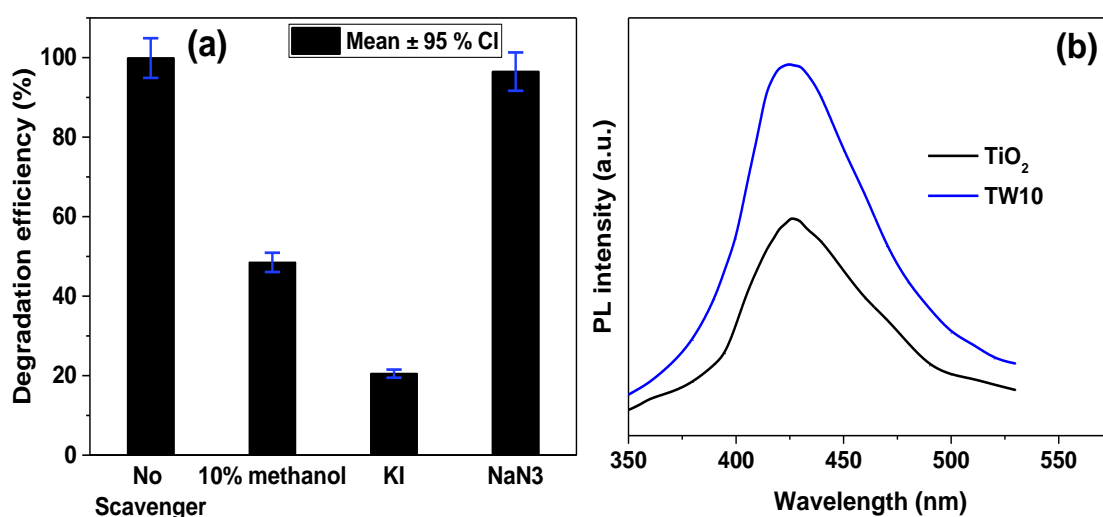
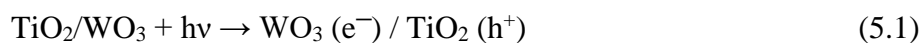
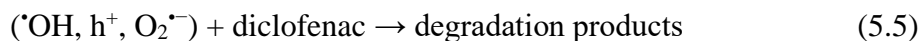


Figure 5.9 (a). Effect of different scavengers on diclofenac degradation (b) PL spectra for $\cdot\text{OH}$ radical evaluation (Initial concentration = 25 mg/L, pH = 5 and catalyst loading = 0.6 g/L).

The charge transfer reactions between the coupled TiO₂-WO₃ photocatalytic system under visible light irradiation has been explained by the following equations:





5.1.4 Catalyst stability

The experiments were further performed to evaluate the stability of TiO₂-WO₃ photocatalyst over the consecutive reaction cycles. Under the optimal experimental conditions, the same catalyst was used over the repetitive degradation reactions and the results were depicted in figure 5.10. It must be inferred that the catalyst has shown better stability throughout the repeated reaction cycles by retaining the efficiency of catalysts by 80 %. The reduction in catalyst efficiency by 19 % is possibly due to the persistence of residual organics adsorbed to the catalyst surface during repeated experiments, which successively decreased the number of active sites present in the catalysts (Chiang and Doong 2015).

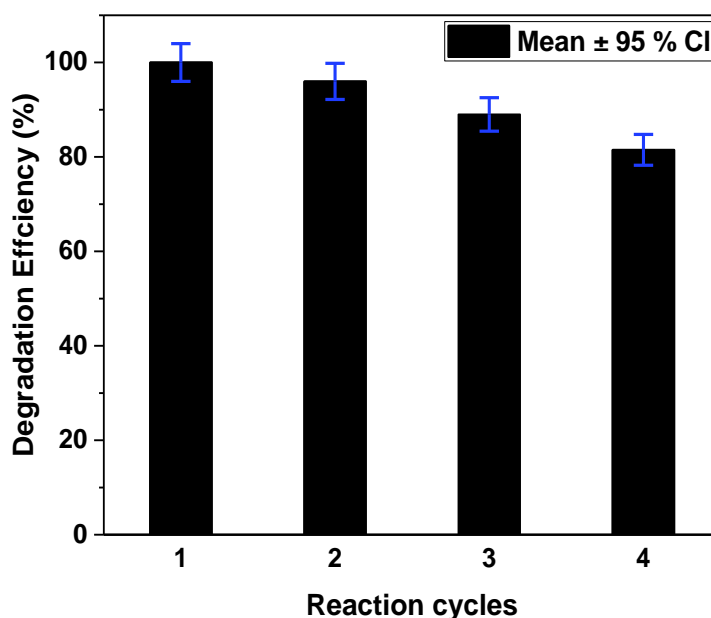


Figure 4.10. Reusability and stability of TiO₂-WO₃ photocatalysts (Initial concentration = 25 mg/L, pH = 5 and catalyst loading = 0.6 g/L).

5.1.5 Identification of degradation products

It is inferred that the degree of mineralization of diclofenac did not attain 100 %, which might be due to the presence of intermediates formed during degradation reaction. The LC-MS analysis revealed the presence of several degradation products of diclofenac.

During the initial hours of irradiation, LC-MS analysis revealed many prominent peaks and smaller peaks m/z 252, m/z 162 and m/z 152 and m/z 108 as shown in figure 5.11. Based on the LC-MS data, it is inferred that the degradation pathway of diclofenac majorly through dechlorination, decarboxylation, C-N cleavage and hydroxylation reaction.

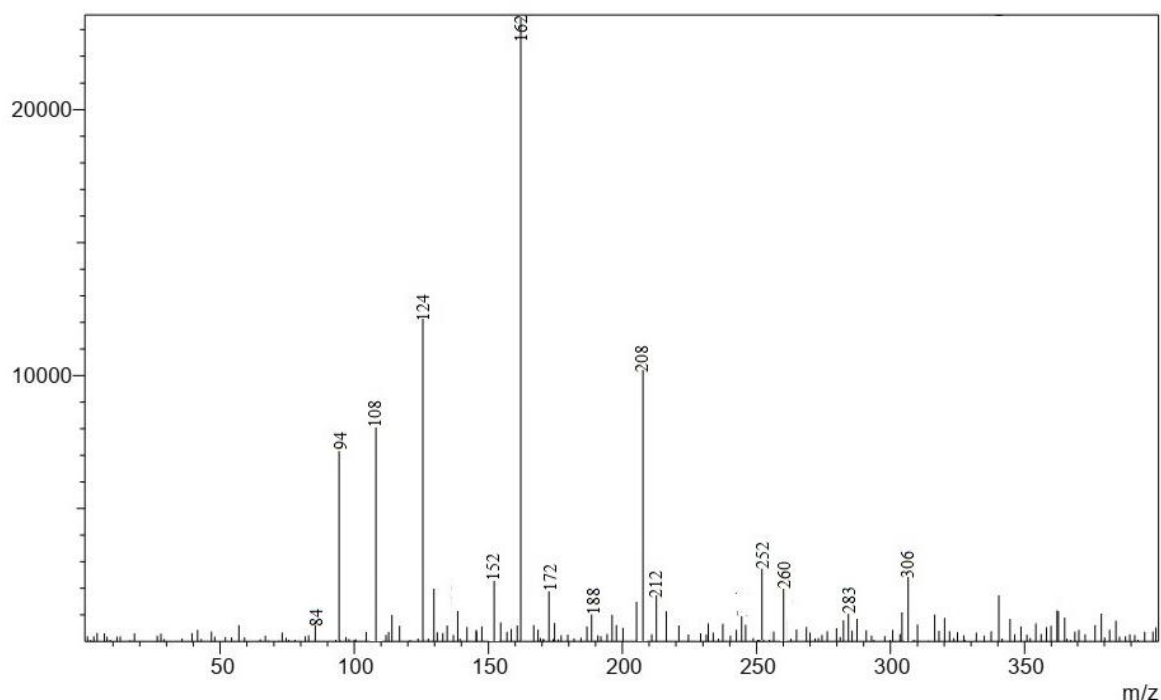


Figure 5.11. LCMS spectra corresponding to degradation products formed (Initial concentration = 25 mg/L, pH = 5 and catalyst loading = 0.6 g/L).

The probable degradation pathway for the elimination of diclofenac has been presented in figure 5.12. Removal of sodium from diclofenac sodium (m/z 318) could be affected possibly due to the reaction of sodium ions with OH^- present in the aqueous solution. Initially, the diclofenac molecule (m/z 296) undergoes decarboxylation and C-N cleavage. Decarboxylation of m/z 296 resulted in the generation of a compound with a peak at m/z 252 as in path 1, which corresponds to 2,6-dichloro-(2-methyl phenyl) aniline, which was also observed in the literature (Bagal and Gogate 2014; Madhavan et al. 2010). Further, the intermediates at m/z 252 undergo C-N cleavage due to $\cdot\text{OH}$ radical attack on the aromatic ring and produce two intermediates with m/z 161 and m/z 108. These compounds further experience a ring-opening mechanism through which mineralization might have accomplished.

Alternatively, the attack $\cdot\text{OH}$ radicals on the aromatic ring of diclofenac experiences C-N cleavage, which produces two fragments correspondingly at m/z 161 (2,6-dichloroaniline) and at m/z 152 (2-hydroxyphenyl acetic acid) as seen in path 2 which was also found in the literature (Sarasisidis et al. 2014). Further, hydroxylation and subsequent amine group removal from 2,6-dichloroaniline produces another intermediate with m/z 162. Further, dechlorination reactions from m/z 162 produce another degradation product with m/z 94, which was identified as phenol. Similarly, the intermediate product 2-hydroxyphenyl acetic acid (m/z 152) undergoes decarboxylation and hydroxylation reactions to produce another intermediate compound with m/z 124.

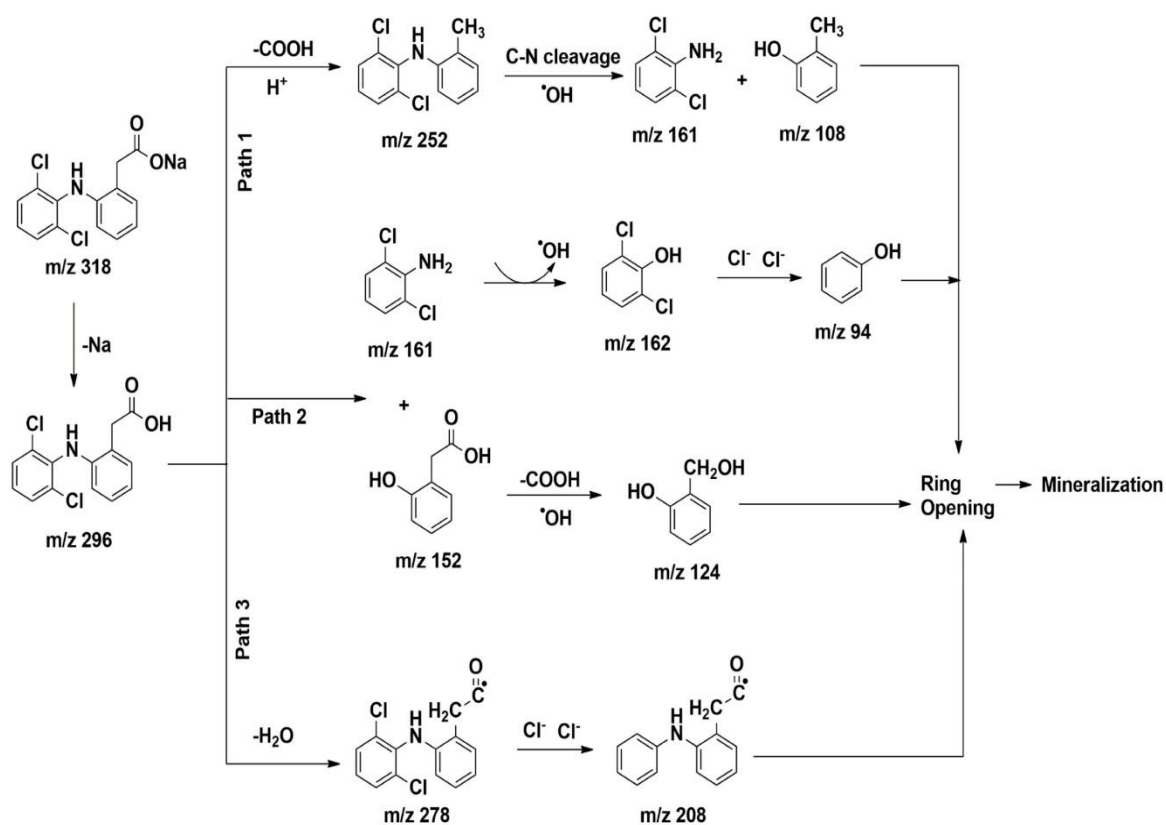


Figure 5.12. Tentative degradation pathway for diclofenac degradation.

Through dehydration process, diclofenac suffered the loss of water molecule to yield another intermediate compound at m/z 278 (path 3), which further resulted in an unknown intermediate at m/z 208 through dechlorination reaction. Consequently, the next step in the photodegradation of diclofenac involves ring-opening of aromatics which then undergoes mineralization, as seen in figure 5.12 (Chen et al. 2016a).

5.1.6 Cost analysis for TiO₂ and TiO₂-WO₃ mixed oxides

1 unit of electricity costs Rs. 7

For the preparation of 1 g (approx.) of TiO₂,

8 ml TTIP – Rs. 37.6

Isopropanol, 26 ml – Rs. 49.7

Glacial acetic acid, 10 ml – Rs. 30.7

For Hot air oven = 2000 W * 24 h = 48 units = Rs. 336

Total cost involved for TiO₂ preparation = Rs. 37.6 + Rs. 49.7 + Rs. 30.7 + Rs. 336 = Rs. 454

For the preparation of 1 g (approx.) of TiO₂-WO₃ mixed oxide (TW10),

8 ml TTIP – Rs. 37.6

Isopropanol, 26 ml – Rs. 49.7

Glacial acetic acid, 10 ml – Rs. 30.7

Sodium tungstate dihydrate, 0.88 g – Rs. 19.45

Ultrasonication (10 min) = 500 W * (1/6) h = 0.08 units = Rs. 0.56

For Hot air oven = 2000 W * 24 h = 48 units = Rs. 336

Total cost involved for TiO₂-WO₃ mixed oxide (TW10) preparation = Rs. 37.6 + Rs. 49.7 + Rs. 30.7 + Rs. 19.45 + Rs.0.56 + Rs. 336 = Rs. 474

For 20 mg/L of degradation of diclofenac,

0.6 g of catalyst used = (Rs. 474) * 0.6 = Rs. 284.4

Irradiation time = 3 h

For visible light irradiation = 400 W * 3 h = 1.2 units = Rs. 8.4

Total cost estimation for degradation of 20 mg of diclofenac using TiO₂-WO₃ (TW10) mixed oxide = Rs. 284.4 + Rs. 8.4 = Rs. 293

Hence, total cost required for degradation of 20 mg/L of initial concentration of diclofenac through photocatalysis is equivalent to Rs. 293.

5.2 CONCLUSION

TiO₂-WO₃ mixed oxide catalysts were found to be effective in photocatalytic degradation of diclofenac, as the complete degradation of diclofenac was achieved under visible light irradiation. The structural and morphological analysis of the prepared catalyst

showed that all the prepared mixed oxide catalysts were well crystalline and spherical shaped particles with uniform distribution. The catalysts were prepared by hydrothermal method by varying the molar ratios of $\text{TiO}_2\text{-WO}_3$ and it was found that the TW10 catalyst was more efficient in achieving complete degradation of diclofenac within the irradiation time of 4 h. The mineralization was also confirmed by TOC analysis, where about 92 % removal was obtained. The photocatalytic efficiency of the catalysts TW20, TW5 and TW1 were also better than that of pure TiO_2 . The various parameters such as pH, initial concentration and catalyst loading were optimized and the optimum conditions for efficient photodegradation were found to be at pH 5 and initial diclofenac concentration of 25 mg/L and 0.6 g/L of catalyst loading. It is revealed that $\cdot\text{OH}$ radicals are the main active species in the diclofenac degradation mechanism. The coupled heterojunctions of $\text{TiO}_2\text{-WO}_3$ resulted in superior charge carrier separation and reduced recombination rate, which corresponds to the higher photocatalytic efficiency in the mixed oxides. The stability and reusability of the catalyst were also evaluated and the $\text{TiO}_2\text{-WO}_3$ mixed oxide catalyst shows good stability with 80 % of degradation efficiency after four successive reaction cycles. LC-MS analysis confirmed the formation of several intermediates during the process and the probable degradation process suggests that the degradation process majorly followed hydroxylation, dechlorination, C-N cleavage and decarboxylation reactions.

CHAPTER 6

PHOTOCATALYTIC DEGRADATION OF DICLOFENAC USING ZnO-WO₃ CATALYSTS

6.1 RESULT AND DISCUSSION

6.1.1 Characterisation of the prepared catalysts

The diffraction pattern of the synthesized ZnO-WO₃ mixed oxides and the pure ZnO were presented in figure 6.1. All the observed diffraction peaks of bare ZnO at $2\theta = 31.7^\circ$, 34.38° , 36.25° , 47.53° , 56.56° , 62.86° , 67.95° and 69.1° were indexed to (100), (002), (101), (102), (110), (103), (112) and (201) planes of the hexagonal phase of ZnO, which was well matched to ICDD standard card (65-4311). The results revealed that the ZnW20 and ZnW10 catalysts exhibited weaker peaks at 23.14° , 23.62° , and 24.38° corresponds to the monoclinic phase of WO₃ (ICDD No: 01-072-0677). The standard WO₃ ICDD card was added as the reference for monoclinic phase peaks. The remaining stronger peaks observed in figure 6.1 corresponded to the hexagonal phase of ZnO, which is similar to that of pure ZnO.

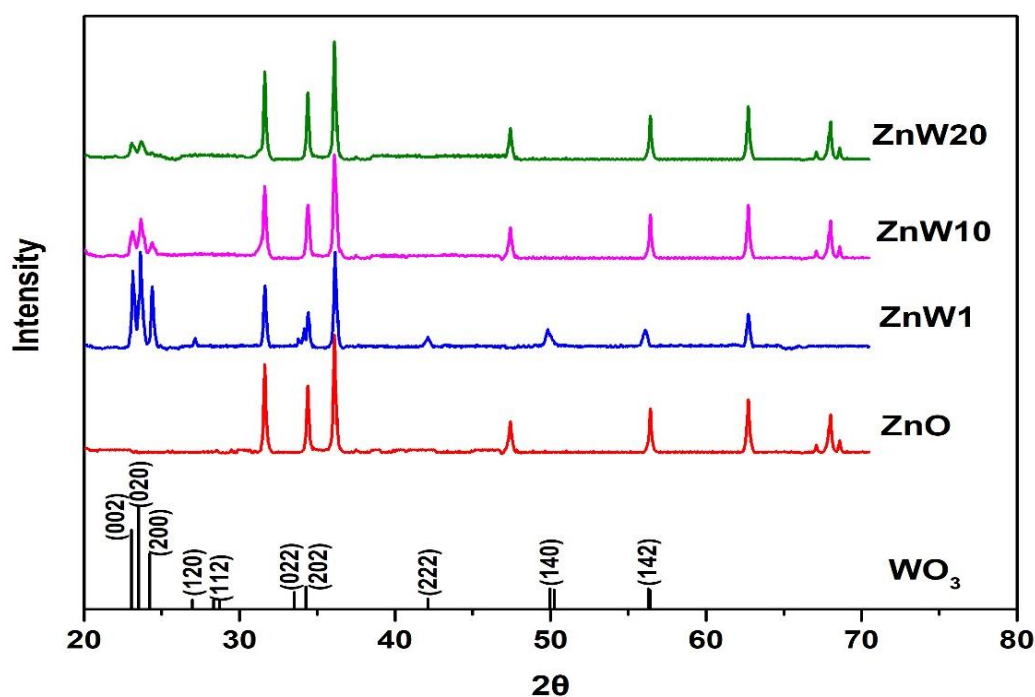


Figure 6.1. X-ray diffraction patterns of ZnO-WO₃ mixed oxide catalysts.

The intensity of ZnO peaks reduced slightly with the increase in tungsten concentration. Alternatively, ZnW1 exhibited stronger peaks of both WO₃ and ZnO, which was mainly due to the presence of a higher amount of tungsten concentration compared to other mixed oxides. No other impurity peaks were observed in the ZnO-WO₃ mixed oxide catalysts, indicating the non-existence of organic compounds in the mixed oxides. The prepared catalysts were also well crystalline in nature.

TEM observations of the prepared catalysts revealed that the synthesized nanoparticles were in rod-like morphology, and the size of the particles was uneven. The bare ZnO nanoparticles exhibited rod-shaped nanostructures of different sizes, and the average diameter was around 15 nm, and the average length was around 70 nm. All the prepared ZnO-WO₃ mixed catalysts were also observed to have rod-like nanostructures, as shown in figure 6.2. ZnW20 exhibited similar morphology as pure ZnO, and the changes in the nanostructure of ZnW20 were evident as the amount of tungsten molar ratios decreased. The amount of the tungsten used in the reaction mixture has caused the variation in their size and shape, which can be observed in ZnW10 and ZnW1 catalysts. The ZnW10 catalyst was observed to be in nearly rod-shaped nanostructures, and the size of the rod-like structure varied considerably. The ZnW1 catalysts were observed to have a greatly irregular morphology composed of blocky particles mainly due to the increased formation of WO₃ in the mixed oxides. The increased amount of W⁶⁺ in the starting solution hinders the formation of rod-like ZnO in ZnW1 (Lam et al. 2015).

Figure 6.2 (e, f, and g) shows the HRTEM analysis of ZnW1, ZnW10, and ZnW20, respectively. The lattice fringes of 0.28 and 0.26 correspond to (100) and (002) planes of hexagonal phase ZnO and the lattice fringes of 0.37 can be indexed to (200) plane of monoclinic WO₃ structure, thus indicating the formation of mixed crystallites of ZnO and WO₃ in the nanoparticles. However, the HRTEM image of ZnW20 shown in figure 6.2 (g) indicates the lattice fringes of 0.28 attributed to (100) plane of the hexagonal phase of ZnO and no clear indication of WO₃ lattice fringes which might be due to the concentration of tungsten in the preparation of ZnW20 was much lower compared to other catalysts. The results were in good accordance with XRD results.

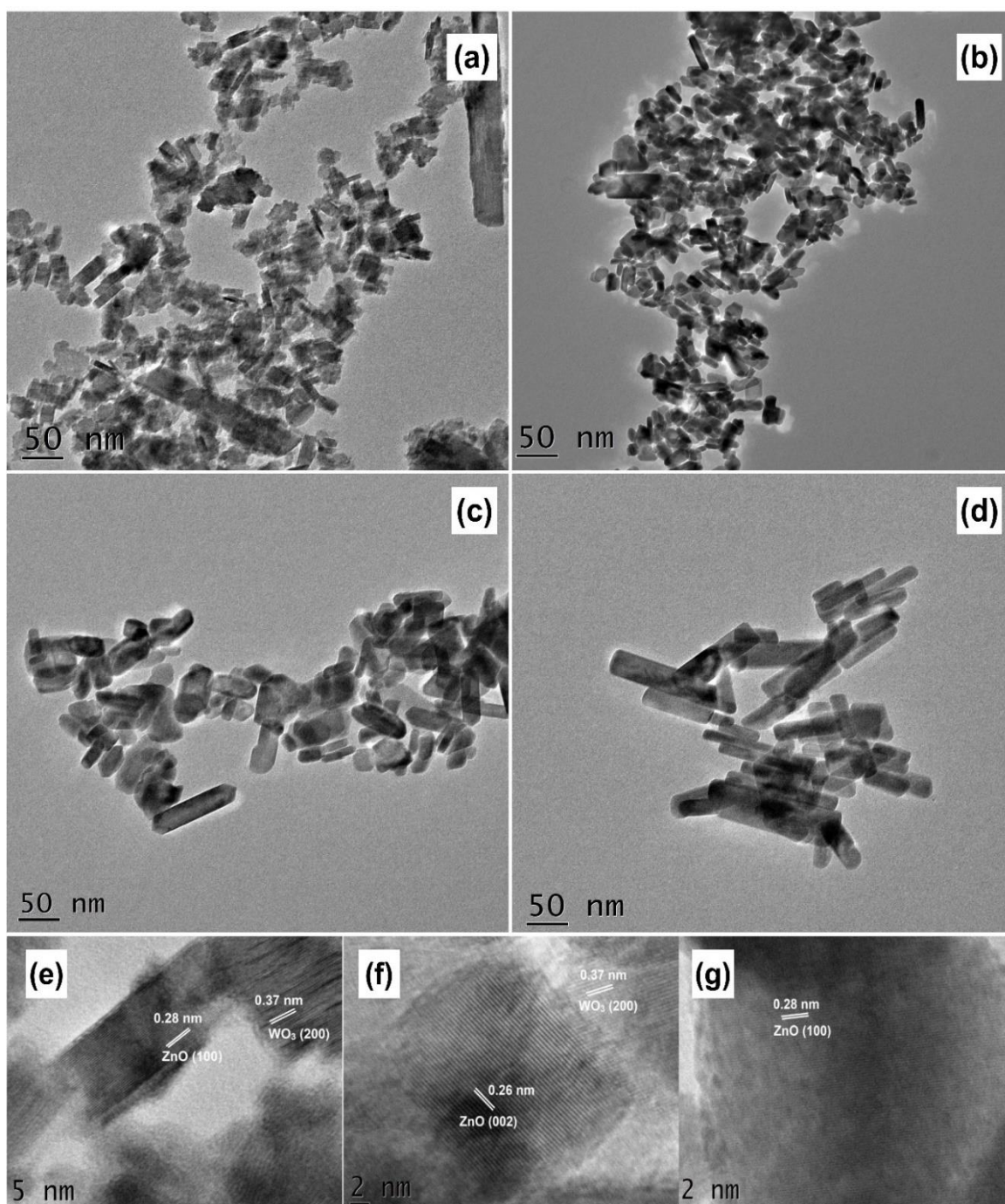


Figure 6.2. TEM and HR-TEM images of ZnW1 (a and e); ZnW10 (b and f); ZnW20 (c and g) and Bare ZnO (d).

EDS spectrum confirmed the presence of Zn, W, and O in the mixed oxide catalysts, as shown in figure 6.3. In the EDS spectrum of pure ZnO, only Zn and O peaks were present. On the other hand, W peaks were observed in ZnW1, ZnW10 and ZnW20 catalysts and the variation in the intensity of W peaks designates the corresponding molar concentrations of W in the mixed oxide catalysts. The atomic concentration of each element

was also noted to be equivalent to their molar ratios of zinc and tungsten, which were presented in table 6.1.

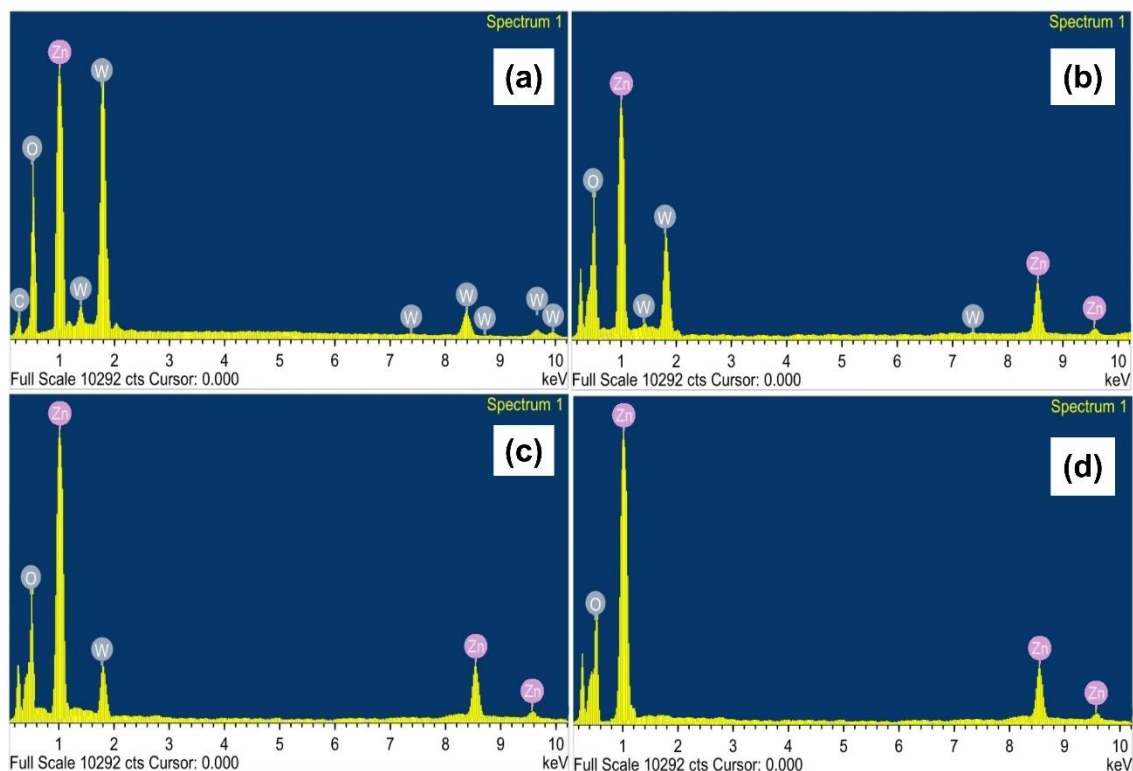


Figure 6.3. EDS spectrum of (a) ZnW1; (b) ZnW10; (c) ZnW20 and (d) Bare ZnO.

Table 6.1. Elemental composition and weight percentage of ZnO-WO₃ catalyst.

Catalyst	Elements and their weight %		
	Zn	O	W
ZnW20	28.61	69.58	1.45
ZnW10	26.76	70.49	2.62
ZnW1	15.45	69.17	14.89
ZnO	39.97	59.76	-

Optical bandgap energy is the significant variable in determining the absorption spectrum of the catalysts and identification of the type of illumination source needed to activate the catalyst (Kaur et al. 2016). The bandgap energy values have been inferred from the Tauc plots and the bandgap energy of the ZnO-WO₃ catalysts was shown in figure 6.4.

From the figure, it has been observed that the bandgap values of pure ZnO were estimated to be 3.2 eV. The calculated energy bandgap values of all the mixed oxide catalysts like ZnW1, ZnW10, and ZnW20 were 2.7 eV, 2.8 eV, and 2.9 eV, respectively. It is revealed that all the mixed oxide catalysts have excellent absorption towards the visible light (400-700 nm) compared to that of the pure ZnO, whereas the absorption range was only limited to the ultraviolet range (<400 nm). The decrease in the energy bandgap values of ZnO-WO₃ catalyst was proportional to the increase in the tungsten loading. It was reported that the defect energy levels formation within the forbidden band of ZnO and WO₃ resulted in the decrease of their bandgap energy values of the prepared ZnO-WO₃ mixed oxide catalysts (Xie et al. 2014).

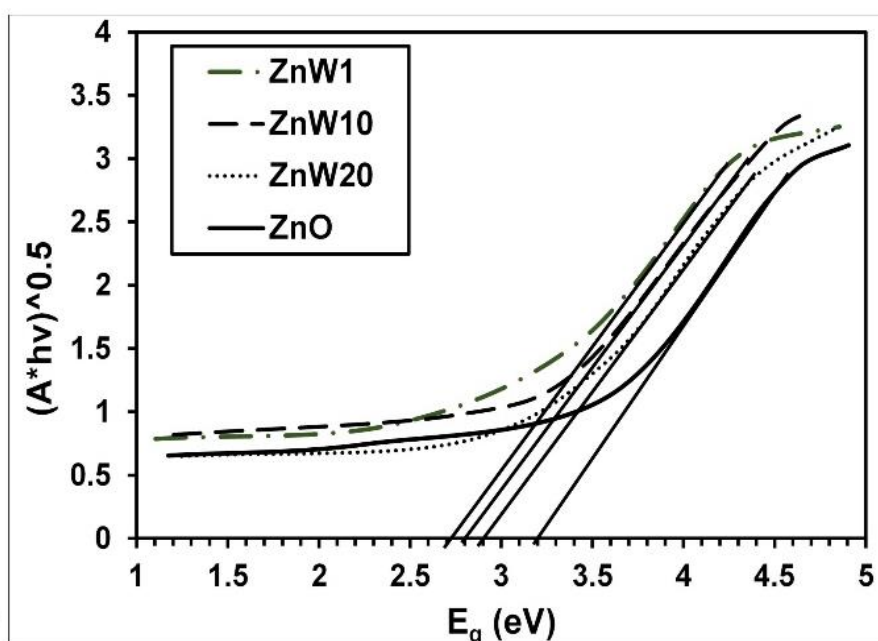


Figure 6.4. Tauc plot for all the prepared ZnO-WO₃ mixed oxide catalysts.

The surface area of the catalysts is a significant factor in determining the photocatalytic activity of the catalysts (Subash et al. 2013). The surface area of the prepared ZnO-WO₃ mixed oxide catalyst was determined using the nitrogen adsorption method. The BET surface area and pore volume of the catalyst were given in table 6.2. The ZnW10 catalyst had the highest surface area of 41.2 m²/g compared to other mixed oxide catalysts, and it was higher than the pure ZnO (21.4 m²/g).

Table 6.2. Surface area and pore volume of all the prepared photocatalysts

Catalyst with different molar ratios	BET surface area (m²/g)	Total pore volume (cc/g)
ZnW20	33.96 ± 1.26	0.0733
ZnW10	41.21 ± 2.08	0.0993
ZnW1	34.37 ± 1.89	0.0812
ZnO	21.4 ± 2.47	0.0678

6.2 Photocatalytic activity of mixed oxide catalysts

The catalytic performance of different ZnO-WO₃ mixed oxide catalysts was tested through the degradation of diclofenac under visible light irradiation. The photocatalytic activity of all the mixed oxide catalyst was analyzed by the operating variable like initial pH, catalyst loading, and initial diclofenac concentration.

6.1.2.1 Effect of molar ratios of Zn and W

The kinetic mechanism of diclofenac degradation using ZnO-WO₃ mixed oxide catalyst was also studied under different reaction conditions. The experimental data obtained from each experiment were plotted with Eq. (3.2) and Eq. (3.3) as already discussed in section 3.5. Series of mixed oxide catalysts, namely ZnW20, ZnW10, ZnW1, and the pure ZnO were sequentially analyzed to evaluate their photocatalytic efficiency, and the results were depicted in figure 6.5. The results show that the catalyst ZnW10 showed a better degradation rate compared to other catalysts. The apparent reaction rate constants for photocatalytic degradation of diclofenac were evaluated from experimental data using linear regression. The experimental data resulted that R² values of pseudo-first-order reaction were ≥ 0.96 as compared to zeroth-order reaction (R² ≥ 0.738). Thus, degradation kinetics was best fitted to the pseudo-first-order kinetic model and the apparent rate constants for all the prepared catalysts were tabulated in table 6.3. The apparent rate constant for first-order kinetics for ZnW10 was 0.01292 min⁻¹.

Table 6.3. Apparent rate constant for all the prepared ZnO-WO₃ catalysts.

Catalyst	Rate constant $k_{app}(\text{min}^{-1})$	R^2	Zereth Order R^2
ZnW20	$0.00914 \pm 2.8E-4$	0.9905	0.8698
ZnW10	$0.01292 \pm 2.4E-4$	0.9964	0.7385
ZnW1	$0.00693 \pm 1.3E-4$	0.9962	0.8915
ZnO	$0.00251 \pm 1.5E-4$	0.9661	0.8921

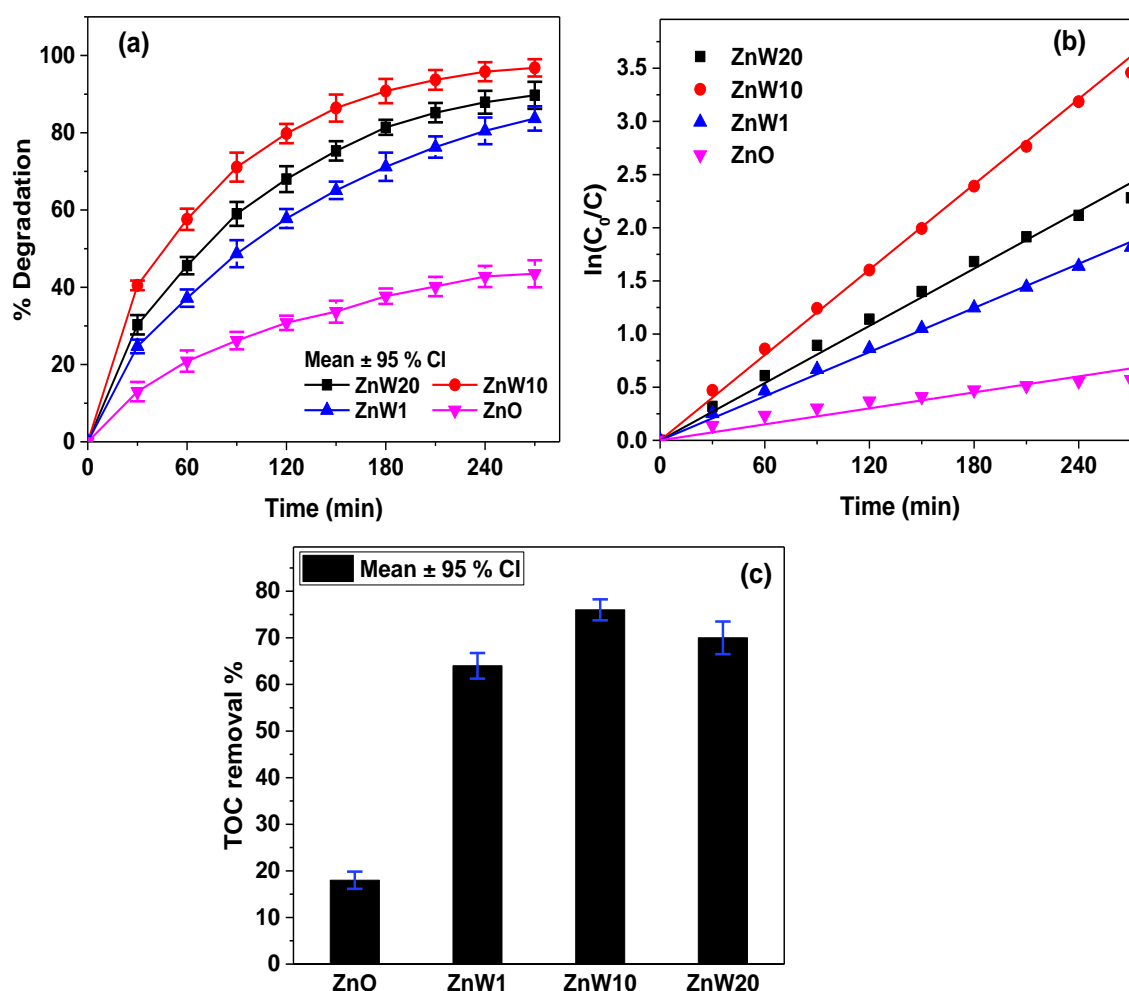


Figure 6.5. Photocatalytic degradation of diclofenac using the ZnO-WO₃ catalysts prepared with different molar ratios (a) Degradation efficiency of all the prepared catalysts; (b) Kinetics of photodegradation and (c) TOC removal % for all the prepared catalysts (Catalyst loading = 0.8 g/L, Initial diclofenac concentration = 20 mg/L, solution pH = 6)

The mineralization of diclofenac was analyzed, and the results revealed that the catalyst ZnW10 showed 76 % TOC reduction during the irradiation time of 270 min. The pure ZnO exhibited poor TOC removal efficiency (< 20 %) which apparently due to the bandgap energy of the catalyst (3.2 eV), which limits its absorption band edge in the visible light. The results revealed that the catalyst ZnW1 has the least photocatalytic efficiency than the other prepared mixed oxide catalysts. It might be due to the higher concentration of WO₃ that would have resulted in poor dispersion of WO₃ in ZnO, and an excessive amount of WO₃ could act as a recombination center for charge carriers (Fallah Shojaei et al. 2015; Xie et al. 2014).

6.1.2.2 Effect of catalyst loading

The influence of catalyst dosage on photocatalytic degradation of diclofenac was studied with various catalyst concentrations ranging from 0.4-1.0 g/L, as shown in figure 6.6. The results revealed that the increase in the catalyst concentration to 0.8 g/L resulted in the increased rate constant of 0.01355 min⁻¹ and a maximum TOC removal of 76 % was achieved in 4 hrs of irradiation. It can be accredited to the presence of an increased number of active sites and enhanced adsorption rate between the catalyst and the target molecule in the reaction mixture (Kaur et al. 2016). Further, an increase in the catalyst concentration (1 g/L) resulted in a drastic reduction in photocatalytic efficiency due to the presence of an excess amount of catalyst particles.

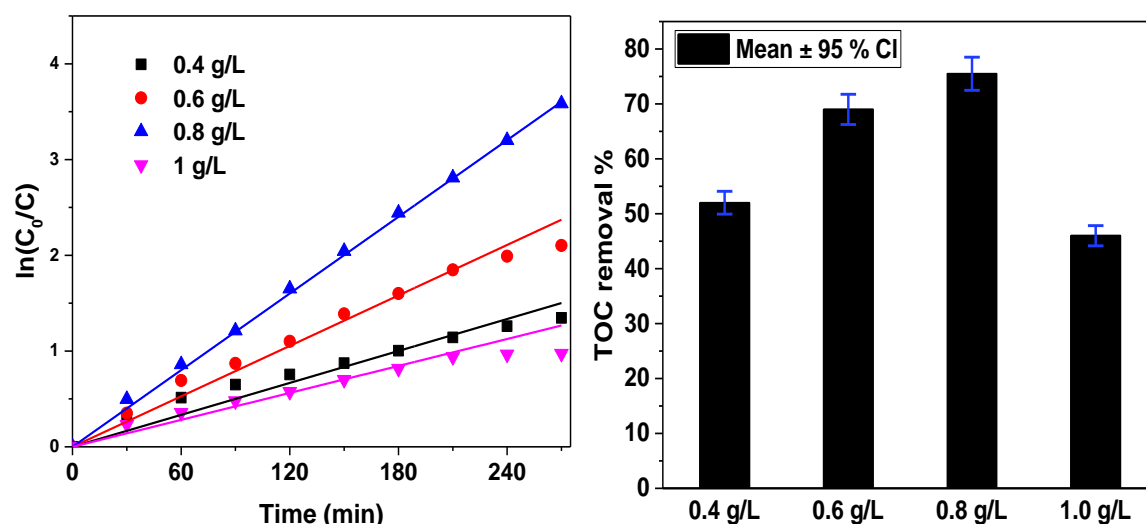


Figure 6.6. Effect of catalyst loading on photocatalytic degradation of diclofenac using the ZnO-WO₃ catalysts under constant initial diclofenac concentration = 20 mg/L and at pH 6.

6.1.2.3 Effect of initial pH

The study on the effects of solution pH on diclofenac photocatalytic degradation is one of the important factors as there are higher possibilities of pH influence on the rate of photo-degradation. The effect of pH was analyzed over different pH values starting from pH 5 to pH 8. The results were depicted in figure 6.7, and it was observed that the rate constant was found to be maximum (0.01372 min^{-1}) at pH 6. The higher rate constant at pH 6 can be explained by the fact that the photocatalytic degradation mostly depended on the surface charge property of the photocatalyst material (Kaur et al. 2016; Khodja et al. 2001). The pH_{ZPC} of the pure ZnO was found to be 8.9 ± 0.2 , and pH_{ZPC} of the prepared catalyst was found to be 7.35 ± 0.2 , which was shown in figure 6.7 (a). Thus at pH value, less than 7.2, the surface of ZnW10 catalyst should be positively charged, and the surface charge of diclofenac should be negatively charged as pK_a value of diclofenac was reported to be 4.35 ± 0.2 (Hiew et al. 2018). Hence the rate constant of ZnW10 catalyst at pH 6 was found to be maximum in the investigated pH range of 5-8.

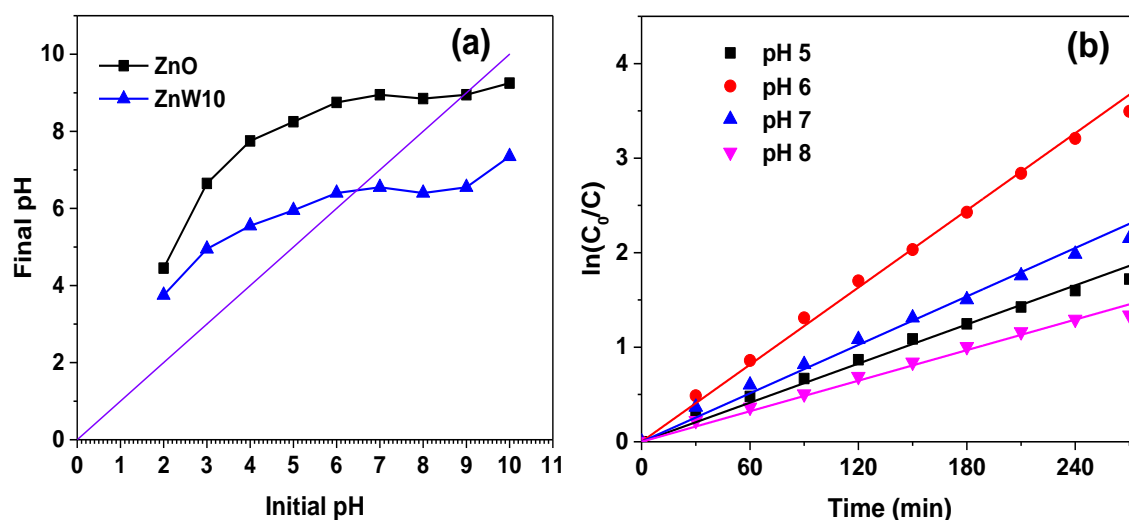


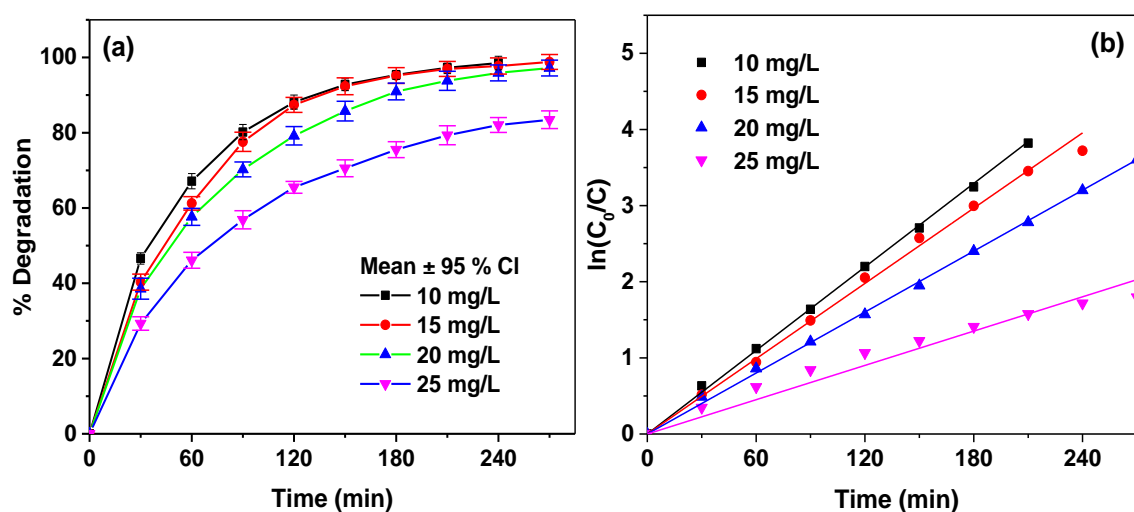
Figure 6.7 (a) pH of zero-point charge of bare ZnO and ZnW10 catalyst and (b) Effect of pH on photocatalytic degradation of diclofenac using the ZnO-WO₃ catalysts under constant catalyst dosage = 0.8 g/L and Initial diclofenac concentration = 20 mg/L.

When the reaction was carried at pH 7, the reduction in the number of positive charge groups was experienced as the solution pH was closer to pH_{ZPC} of the catalyst and also the pH of the solution alleged to decrease as the reaction proceeds. Hence photocatalytic degradation was high at pH 6 as the adsorption percentage was also higher at the same pH. ZnO photocatalyst is usually unstable in acidic solution, but we observed

that the stability of the ZnO was improved considerably with the addition of WO₃ loading in the mixed oxide catalyst. However, the mediocre photocatalytic efficiency in the pH 5 might be due to the dissolution of ZnO in an acidic medium, and we observed that the pH of the solution decreases as the reaction proceeds, thus affecting the surface charge property of the catalyst.

6.1.2.4 Effect of initial diclofenac concentration

The photocatalytic degradation efficiency could also be largely influenced by the amount of initial drug concentration. Thus, in order to analyze the effect of initial diclofenac concentration, the solution with various concentrations (10-25 mg/L) of diclofenac was used in the photocatalytic degradation experiments under the constant catalyst dosage (0.8 g/L) at a pH 5. The results revealed that the degradation efficiency was approximately equivalent for the initial diclofenac concentration up to 20 mg/L. All the experimental data corresponding to different initial concentrations were fitted to pseudo-first-order reaction (figure 6.8b). Mineralization of diclofenac was also decreased marginally when the initial diclofenac concentration increased from 10 mg/L to 20 mg/L, as shown in figure 6.8 (c). The rate constant for degradation of diclofenac with an initial concentration of 20 mg/L was found to be 0.01359 min⁻¹ and the rate constant decreased drastically when initial concentration increased to 25 mg/L as seen in figure 6.8 (d).



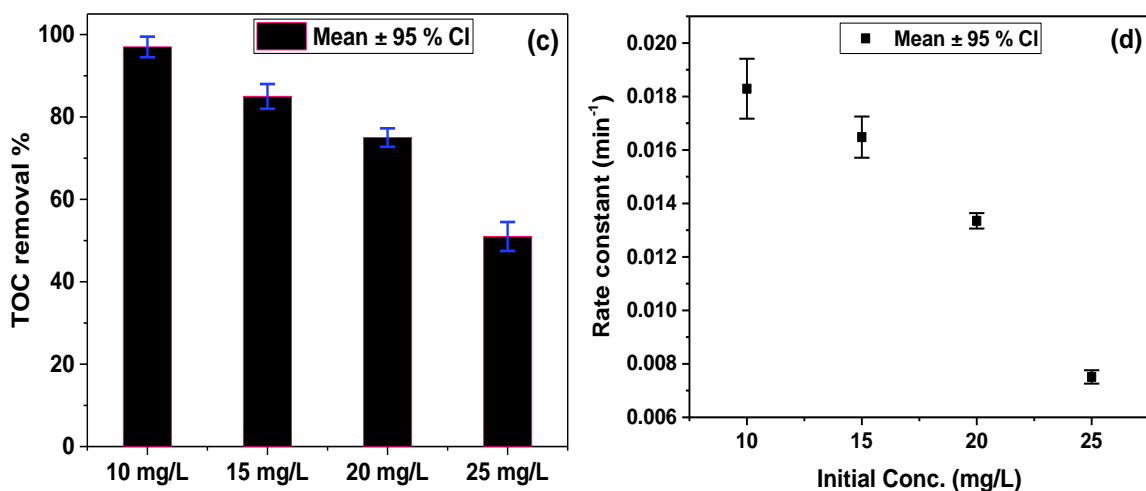


Figure 6.8. Effect of initial diclofenac concentration on photocatalytic degradation of diclofenac using the ZnO-WO₃ catalysts (a) Degradation percentage with respect to time; (b) Kinetics of degradation; (c) TOC removal efficiency under different initial concentration and (d) Rate constant with respect to different initial concentration (constant catalyst dosage = 0.8 g/L and at solution pH 6).

On the other hand, the degradation efficiency for the initial diclofenac concentration of 25 mg/L was much lower compared to other values due to the reduction in the available surface area of the catalyst surface leading to photocatalyst deactivation (Reza et al. 2017; Sarasidis et al. 2014).

6.1.3 Role of active species and reaction mechanism

Photocatalytic degradation mechanism could be well elucidated by evaluating the active species responsible for diclofenac degradation. The degradation experiment was performed using ZnW10 catalyst with different quenchers such as 10 % methanol solution, KI and NaN₃ under optimum conditions obtained from the previous experiments. The results were shown in figure 6.9 (a) revealed that the reduction in degradation efficiency compared to the experiment without the scavengers. The efficiency reduced to 29 %, 42 % and 94 % in the presence of KI, 10 % methanol and NaN₃, respectively. Thus, holes and [•]OH radicals were the main active species involved in the degradation mechanism of diclofenac using ZnW10 catalyst. The photogenerated holes can either directly oxidize or react with H₂O to generate the powerful [•]OH radical which possesses strong oxidation capability. Coupling ZnO and WO₃ results in the transfer of charge carriers due to the narrow bandgap in the coupled oxides and thus reducing the rate of recombination of charge carriers (Sajjad et al. 2018). The transfer of charge carriers can be confirmed by [•]OH radical

measurement, as reported in the literature (Huang et al. 2009; Yuan et al. 2014). The photoluminescence spectra shown in figure 6.9 (b) reveals the increased fluorescence intensity as compared to the bare ZnO. At a fixed irradiation time of 20 min, PL intensity generated on the prepared ZnW10 catalyst was higher than that of pure ZnO, which reveals the enhanced generation of $\cdot\text{OH}$ radicals than the bare ZnO and hence increased photocatalytic activity for the coupled oxides. This result suggests that $\cdot\text{OH}$ radicals certainly plays an important role in the degradation process.

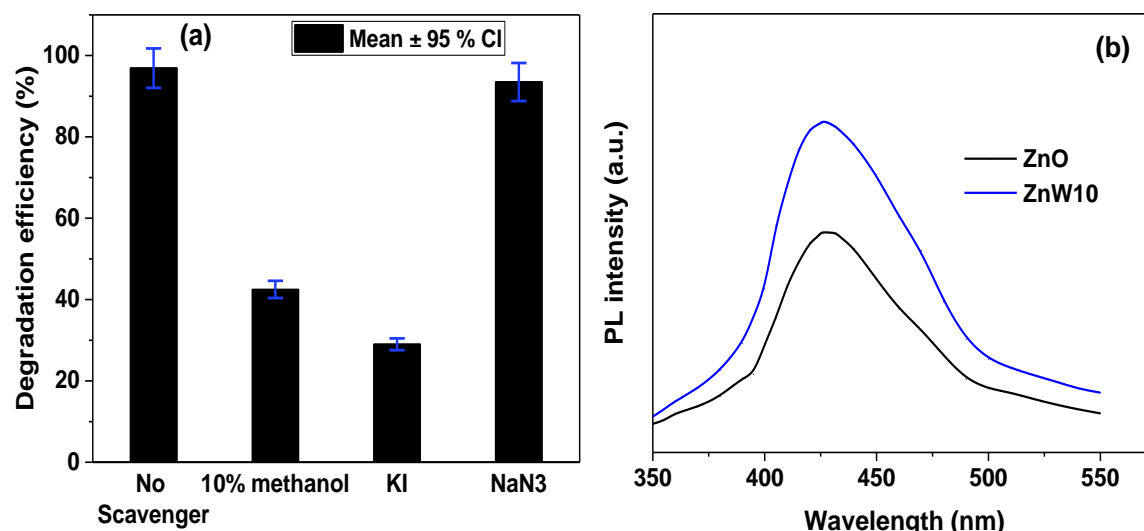
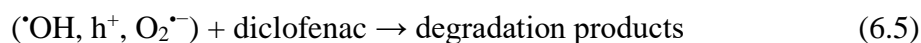
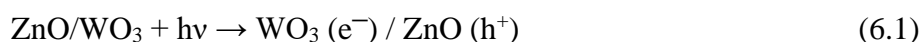


Figure 6.9. (a) Role of active species evaluation and (b) PL spectra for $\cdot\text{OH}$ radical evaluation of pure ZnO and ZnW10 irradiated samples.

When WO_3 is coupled with ZnO, results in the transfer of an electron from CB of ZnO to CB of WO_3 due to the more positive band edge of WO_3 , so that WO_3 can function as a sink for electrons in the coupled oxide (SHU et al. 2011; Subash et al. 2013). Therefore, recombination of photogenerated electron-hole pairs is suppressed, leading to increased photocatalytic activity of the coupled oxide. In addition, the standard redox potentials of ($\cdot\text{OH}/\text{OH}^\cdot$) (1.99 eV vs. NHE) and ($\cdot\text{OH}/\text{H}_2\text{O}$) (2.7 eV vs. NHE) were lies within the VB edge position of ZnO (2.9 eV vs. NHE) and hence holes generated in the VB of ZnO could oxidize OH^- groups or adsorbed H_2O to yield powerful $\cdot\text{OH}$ radicals (Lam et al. 2015; Lei et al. 2019). However, it is thermodynamically impossible for the electrons accumulated in the CB of WO_3 to reduce adsorbed O_2 to superoxide anion ($\text{O}_2^{\cdot-}$) due to the more positive CB edge potential (0.5 eV vs. NHE) than the standard redox potential of ($\text{O}_2/\text{O}_2^{\cdot-}$) (-0.33 V vs. NHE) (Lam et al. 2015). Therefore, the electrons in the CB of WO_3 can be preceded via multi-electron reduction of O_2 to yield H_2O_2 since the CB edge of WO_3 was more

negative than the potential of (O₂/H₂O₂) (0.682 eV vs. NHE) (Hori et al. 2017; Lam et al. 2015; Tomita et al. 2014). According to the above phenomenon, it is clear that superoxide radical (O₂^{•-}) formation is inhibited in the TiO₂-WO₃ coupled catalysts under visible light irradiation and hence negligible reduction efficiency in the presence of NaN₃ was obtained (as seen in figure 6.9 (a)). Further, the [•]OH radicals were produced through the reaction of H₂O₂ with the photogenerated electron. Thus, the generated [•]OH was successively involved in diclofenac degradation reactions. It is also reported that the presence of coupling effect between ZnO and WO₃ was mainly due to optimal loading of WO₃ since good dispersion of WO₃ in coupled oxides benefits the formation of heterojunction structures between the two coupled oxides (Lam et al. 2015; SHU et al. 2011). The higher amount of WO₃ concentration in coupled oxide could also result in poor contact between two semiconductors, which would hinder the charge separation and reduces photocatalytic activity (Lam et al. 2015). Hence, ZnW10 catalyst shows better photocatalytic activity than the other mixed oxide catalyst since it was found to be the optimum molar ratio for diclofenac degradation. The main reaction steps in the diclofenac degradation reaction mechanism have been explained in the following equations:



6.1.4 Stability and reusability of the catalyst

In order to evaluate the stability of the photocatalyst, the same catalyst was recycled and used for the successive experiments. The results revealed that the ZnO-WO₃ photocatalyst remained stable and the maximum efficiency was retained up to 80 % compared to the first run. The 20 % drop in their efficiency, as shown in figure 6.10 was primarily due to the accumulation of some of the intermediates formed during each reaction cycle.

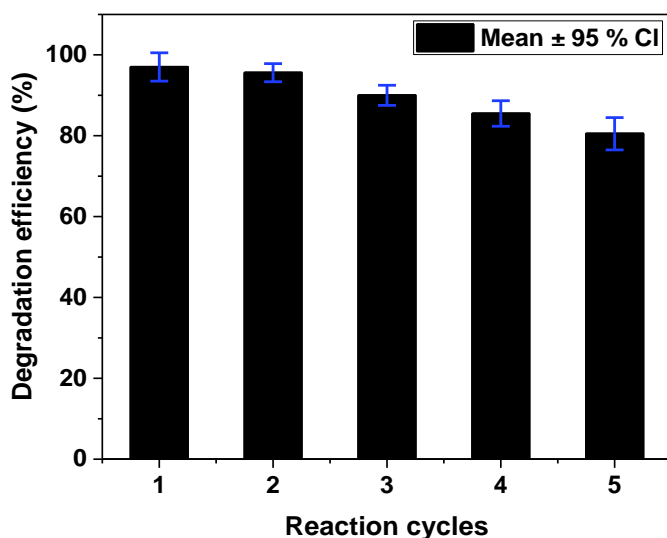


Figure 6.10. Stability and reusability of ZnO-WO₃ photocatalysts under optimum reaction conditions (pH = 6, initial diclofenac concentration = 20 mg/L and catalyst dosage = 0.8 g/L).

6.1.5 Identification of degradation products

LC-MS analysis was carried out to investigate the number of photocatalytic intermediates formed during the irradiation. The LC-MS results confirmed the formation of several degradation products, as shown in figure 6.11. Based on the LC-MS data, the probable degradation mechanism has been deduced, as shown in figure 6.12.

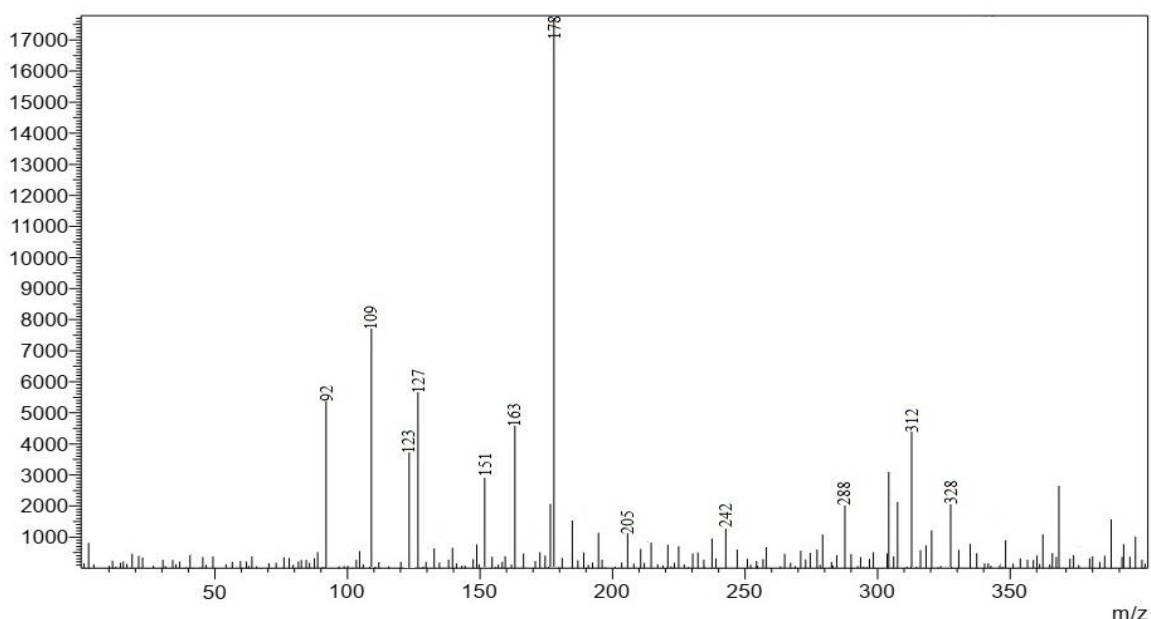


Figure 6.11. LCMS peaks of intermediates formed during diclofenac degradation (pH = 6, initial diclofenac concentration = 20 mg/L and catalyst dosage = 0.8 g/L).

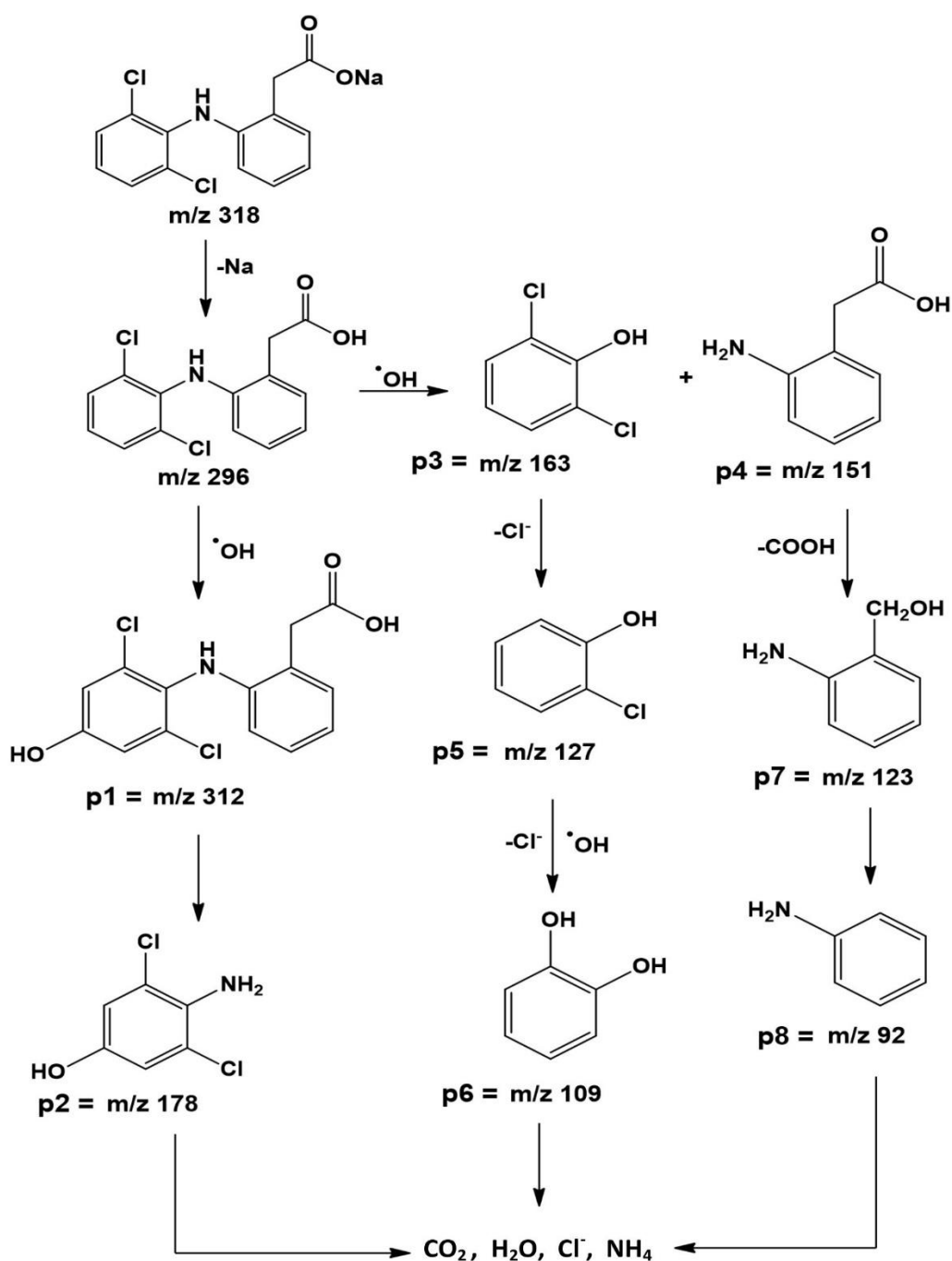


Figure 6.12. The probable degradation pathway for diclofenac degradation.

As discussed in section 6.1.4, photocatalytic degradation is mainly preceded by an attack of $\cdot OH$ radicals. Initially, sodium from diclofenac sodium salt has been removed and resulted in diclofenac molecule (m/z 296). The primary intermediates for diclofenac degradation were at m/z 312, 178, 163, 151, 127, and 109. Hydroxylated intermediate p1

(m/z 312) was formed due to the addition of $\cdot\text{OH}$ radicals to the diclofenac molecule. It is reported that aryl-hydroxy diclofenac intermediates were commonly formed due to the attack of $\cdot\text{OH}$ radicals (Calza et al. 2006; Zhang et al. 2016). The intermediate p1 (m/z 312) suffered C-N bond cleavage and resulted in an unknown intermediate p2 (m/z 178), which was also reported in the literature (Zhang et al. 2017). The attack of $\cdot\text{OH}$ radicals on diclofenac subsequently resulted in C-N cleavage through another pathway, which has led to the formation of two compounds with p3 (m/z 163) and p4 (m/z 151). The intermediate p3 was reportedly identified as 2, 6-dichlorophenol (Espino-Estévez et al. 2016) which further undergoes the loss of chlorine and hydrogen atoms to form another intermediate p5 (m/z 127). The substitution of Cl^- by OH^- resulted in the formation of another intermediate, p6 (m/z 109).

On the other hand, the intermediate p4 (m/z 151) undergoes decarboxylation to produce another intermediate p7 (m/z 123) and the subsequent removal of CH_2OH to produce another organic compound aniline, p8 (m/z 92) which was also reported in the literature (Gou et al. 2017). These intermediates formed were finally mineralized to CO_2 and H_2O . The chloride ions resulted from dechlorination reactions eventually reacted with a water molecule to form hydrochloric acid, which was confirmed by the pH analysis during the degradation, where the solution pH changed from 6 to 4.5.

6.1.6 Cost analysis for ZnO and ZnO-WO₃ mixed oxides

1 unit of electricity costs Rs. 7

For the preparation of 1 g (approx.) of ZnO,

$\text{Zn}(\text{NO}_3)_2 \cdot 6\text{H}_2\text{O}$, 2 g – Rs. 45.2

NH_4OH , 11 ml (approx.) – Rs. 17.38

NaCl , 0.04 g – Rs. 0.2

For Hot air oven = 2000 W * 24 h = 48 units = Rs. 336

Total cost involved for ZnO preparation = Rs. 45.2 + Rs. 17.38 + Rs. 0.2 + Rs. 336 = Rs. 399

For the preparation of 1 g (approx.) of ZnO-WO₃ mixed oxide (ZnW10),

$\text{Zn}(\text{NO}_3)_2 \cdot 6\text{H}_2\text{O}$, 2 g – Rs. 45.2

NH_4OH , 11 ml (approx.) – Rs. 11.06

NaCl, 0.04 g – Rs. 0.1

Sodium tungstate dihydrate, 0.24 g – Rs. 5.3

Ultrasonication (30 min) = $500 \text{ W} * (1/2) \text{ h} = 0.25 \text{ units} = \text{Rs. } 1.75$

For Hot air oven = $2000 \text{ W} * 24 \text{ h} = 48 \text{ units} = \text{Rs. } 336$

Total cost involved for ZnO-WO₃ mixed oxide (ZnW10) preparation = $\text{Rs. } 45.2 + \text{Rs. } 17.38 + \text{Rs. } 0.2 + \text{Rs. } 5.3 + \text{Rs. } 1.75 + \text{Rs. } 336 = \text{Rs. } 406$

For 20 mg/L of degradation of diclofenac,

0.8 g of catalyst used = $0.8 \text{ g} * (\text{Rs. } 406) = \text{Rs. } 324.8$

Irradiation time = 4.5 h

For visible light irradiation = $400 \text{ W} * 4.5 \text{ h} = 1.8 \text{ units} = \text{Rs. } 12.6$

Total cost estimation for degradation of 20 mg of diclofenac using ZnO-WO₃ (ZnW10) mixed oxide = $\text{Rs. } 324.8 + \text{Rs. } 12.6 = \text{Rs. } 338$.

6.2 CONCLUSION

Photocatalytic degradation of diclofenac has been effectively achieved using ZnO-WO₃ nanocatalyst prepared using the hydrothermal method. To investigate the required optimum tungsten concentration for the effective utilization of ZnO-WO₃ catalyst, various molar ratios of ZnO-WO₃ catalyst has been prepared and successively tested its performance in the photocatalytic degradation of diclofenac under visible light irradiation. Degradation kinetic study revealed that the experimental data were well fitted to the pseudo-first-order reaction. The photocatalytic degradation studies revealed that the degradation efficiency of all the ZnO-WO₃ mixed oxide catalysts was reportedly higher than the bare ZnO. The molar ratio of Zn:W \approx 10:1 was found to be the optimum molar concentration of Zn and W, and the ZnW10 catalyst has displayed excellent degradation efficiency under visible light irradiation. The ZnO-WO₃ catalyst has extended the optical absorption to the visible region, which was the prime reason for enhanced performance under visible light irradiation.

Moreover, the optimum parameters such as initial solution pH, initial diclofenac concentration and catalyst loading concentration were also evaluated, and the results revealed that the photocatalytic efficiency was maximum at pH 6, with an initial diclofenac concentration of 20 mg/L and catalyst concentration of 0.8 g/L. Photogenerated holes and $\cdot\text{OH}$ radicals were the primary active species involved in photocatalytic degradation of

diclofenac. The stability of the ZnO-WO₃ mixed oxide catalyst under aqueous solution was improved considerably, and the catalysts showed better stability in retaining the catalyst efficiency by 80 % even after five consecutive reaction cycles. LC-MS analysis revealed the formation of several degradation products during photocatalytic degradation and the number of photoproducts were identified and reported. Degradation of diclofenac primarily undergoes attack of [•]OH radicals, hydroxylation, dechlorination, decarboxylation, and C-N cleavage reactions.

CHAPTER 7

PHOTOCATALYTIC DEGRADATION OF DICLOFENAC USING TiO₂-CdS CATALYSTS

7.1 RESULT AND DISCUSSION

7.1.1 Characterization of TiO₂-CdS catalysts

The crystal phase analysis and crystalline nature of prepared samples were determined using the X-ray diffraction (XRD) technique. The XRD pattern of TiO₂-CdS mixed oxide catalysts seen in figure 7.1 showed anatase phase TiO₂ and hexagonal phase CdS, respectively. The characteristic TiO₂ peaks are found to be at $2\theta = 25.4^\circ, 37.8^\circ, 48.2^\circ, 53.8^\circ, 54.1^\circ$ and 62.8° conforming to the crystal planes of (101), (004), (200), (105), (211) and (204) respectively, which were well indexed to anatase TiO₂ standard card (ICDD no. 01-071-1166). Similarly, the peaks at $26.6^\circ, 28.2^\circ, 26.6^\circ, 43.8^\circ$ and 52.1° could be assigned to the hexagonal phase of CdS (002), (101), (110) and (112) respectively (Kaur et al. 2018; Shen et al. 2015). The hexagonal phase of CdS increases with increase in CdS loading as seen in TC1, where more of the CdS peaks were present. In contrast, the less content of CdS in mixed oxide resulted in the gradual weakening of CdS peaks as seen in TC5 and TC10. Due to a very less amount of CdS, the TC10 catalyst shows only a weaker peak of CdS at 26° , and other stronger peaks were assigned to anatase TiO₂. The sharp and strong diffraction peaks validate the high crystallinity nature of the prepared nanoparticles. The diffraction pattern of TiO₂-CdS catalysts reckoned the co-occurrence of hexagonal CdS and anatase TiO₂ components in the synthesized mixed oxides catalysts. Furthermore, the well crystalline nature of the prepared mixed oxide catalysts was confirmed by the non-existence of impurity peaks.

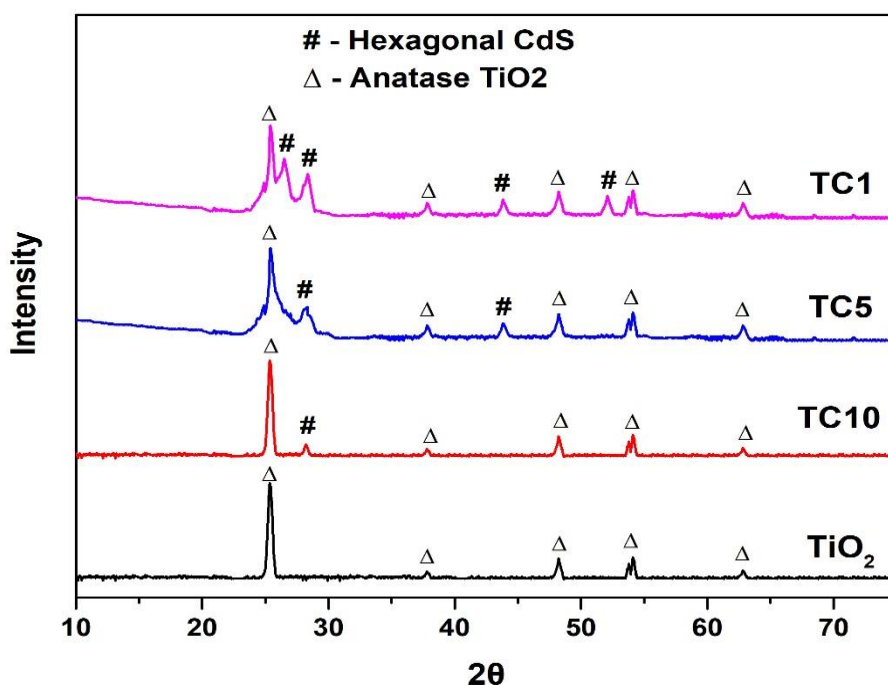


Figure 7.1. XRD patterns of all the prepared TiO₂-CdS catalysts.

The surface morphology of hydrothermally prepared mixed oxide catalysts was analyzed using TEM. The TEM analysis showed in figure 7.2 revealed that all the TiO₂-CdS mixed oxide catalysts were observed to be in broad sized nanoparticles with different morphology. Also, some of the nanoparticles were observed to be blocky and irregular sized particles (Fig. 7.2 b). The individual particle size of the catalysts TC5 and TC10 were in the range of 15-30 nm and 10-20 nm, respectively and they exhibited nearly octahedral or hexagonal-shaped particles. The particle size of TC1 photocatalyst has been the largest compared to other prepared mixed oxide catalysts as displayed in figure 7.2 and the approximate particle size ranges from 30-60 nm. The higher concentration of CdS in mixed oxide catalysts had affected the morphology and size of the mixed oxides. Henceforth, TC1 catalyst was irregular in morphology and resulted in higher sized particles due to higher loading of CdS. The particle size of all the TiO₂-CdS mixed oxide catalysts is listed in table 7.2. Figure 7.2 (e, f, and g) shows the HRTEM analysis of TC1, TC5 and TC10, respectively. The lattice fringes of 0.33 nm and 0.316 nm correspond to (002) and (101) planes of hexagonal phase CdS and the lattice fringes of 0.35 can be indexed to (101) plane of anatase TiO₂, thus indicating the formation of mixed crystallites of TiO₂ and CdS in the nanoparticles. The results were in accordance well with XRD results.

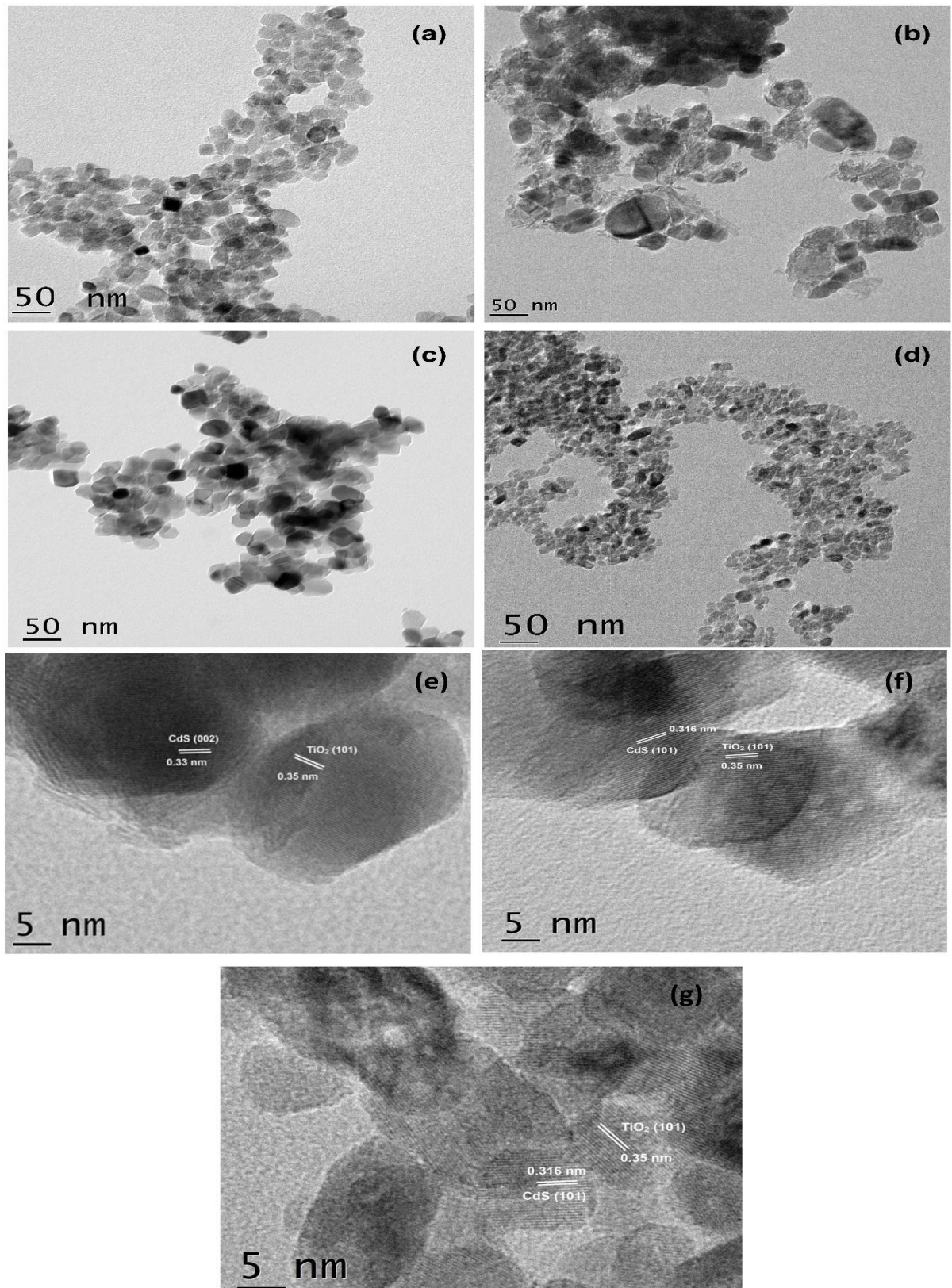


Figure 7.2. TEM images of (a) Pure TiO₂; (b) TC1; (c) TC5; (d) TC10 and HRTEM images of (e) TC1; (f) TC5 and (g) TC10.

Energy-dispersive X-ray spectroscopy (EDS) analysis was performed for all the prepared TiO₂-CdS photocatalysts to examine the elements present in the surface of the catalysts and its molar composition of Ti and Cd precursors. The EDS spectra of the as-prepared TC1, TC5, TC10 and TiO₂ catalysts were shown in figure 7.3. It is noted that only Ti, Cd, O and S elements were displayed in the EDS images of the prepared catalysts, which confirms the occurrence of coupled TiO₂-CdS mixed oxides. From EDS analysis, it is apparent that the prepared catalysts didn't show any impurity peaks.

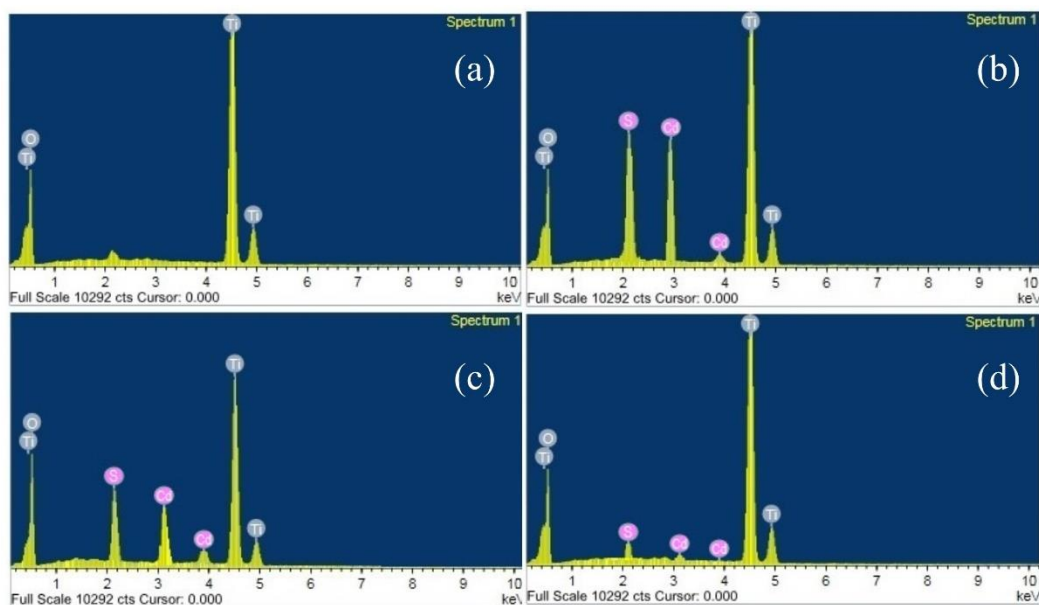


Figure 7.3. EDS of (a) TiO₂; (b) TC1; (c) TC5 and (d) TC10.

Table 7.1. Elemental composition and weight percentage of TiO₂-CdS catalyst.

Catalyst	Elements and their weight %			
	Ti	O	Cd	S
TC10	30.92	62.08	3.14	3.11
TC5	28.84	58.26	5.84	5.89
TC1	19.71	39.97	19.79	19.72
TiO ₂	33.17	66.79	-	

Tauc plot has been used to evaluate the optical bandgap energy (E_g) of all the prepared TiO₂-CdS mixed oxide catalysts and was shown in figure 7.4. The bandgap energy

of all the prepared catalyst samples was found to be in the range of 2.7-2.9 eV. The catalyst TC1 has the lowest energy bandgap value of 2.7 eV and the corresponding bandgap energy of the prepared catalysts increases linearly with the reduction in the molar concentration of CdS. From the bandgap energy analysis, it is obvious that the corresponding excitation wavelength of all the prepared TiO₂-CdS mixed oxide catalysts was more than 390 nm and all the catalysts could be irradiated using the visible light source.

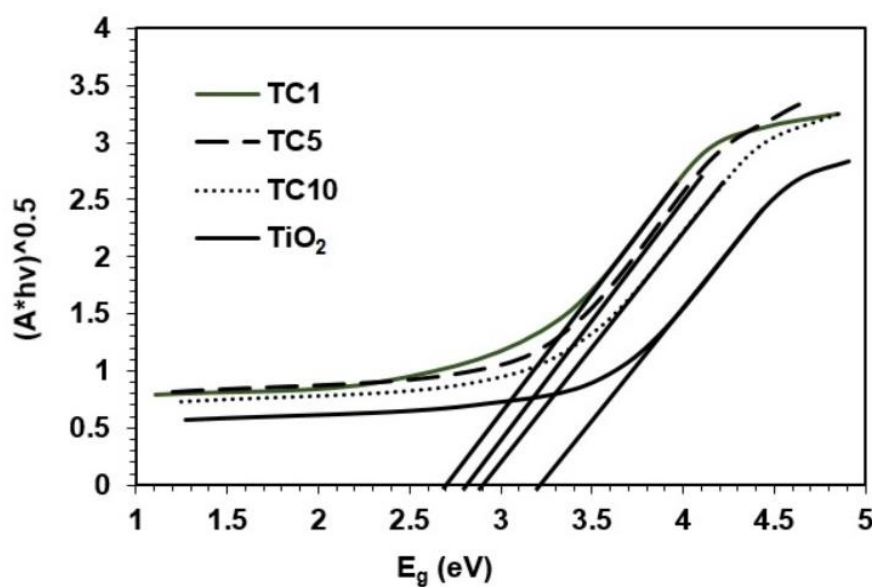


Figure 7.4. Tauc plot for calculation of bandgap of all the prepared catalysts.

Higher amount of available active surface area of the catalysts is a necessity for promoting adsorption and desorption reactions (Mazinani et al. 2014; Subash et al. 2013). The available surface area and the total pore volume of the prepared TiO₂-CdS catalyst samples were estimated by BET and BJH method, respectively. The results divulged that the TC10 photocatalyst has a higher surface area among others (91.28 m²/g). The surface area of the TC5 catalyst was slightly lesser than that of TC10 catalyst. Nevertheless, the TC1 catalyst has the lowest surface area compared to others. This can be attributed due to their bigger particle size. The results suggest that the decrease in the molar ratio of TiO₂-CdS reduces the surface area and pore volume of the prepared catalysts. The active surface area and the total pore volume of the prepared TiO₂-CdS catalyst determined by BET and BJH method were reported in table 7.2.

Table 7.2. Surface area and Size of all the prepared TiO₂-CdS photocatalysts.

Catalyst with different molar ratios	BET surface area (m ² /g)	Total pore volume (cc/g)	Average size of the catalysts (nm)
TC10	91.28	0.2343	15 ± 3.5
TC5	83.95	0.2267	20 ± 4.5
TC1	56.99	0.0785	55 ± 14.5
Pure TiO₂	72.33	0.1019	22 ± 7.5

7.1.2 Photocatalytic Activity Evaluation

7.1.2.1 Effect of different molar ratios

The photocatalytic activity of all the prepared TC10, TC5 TC1 and pure TiO₂ photocatalysts were evaluated and compared under visible light irradiation. Further, various operating conditions like initial diclofenac concentration, desired catalyst concentration and pH values were optimized. The photocatalytic activity of different molar ratios of TiO₂-CdS catalysts used for the degradation of diclofenac under visible light is represented in figure 7.5. It is noted that the experimental data were well fitted to pseudo-first-order reaction ($R^2 \geq 0.95$) as compared to zeroth-order reaction (where $R^2 \geq 0.547$). The apparent rate constants were tabulated in table 7.3.

Table 7.3. Apparent rate constant for all the prepared catalyst

Catalyst	Rate constant $k_{app}(\text{min}^{-1})$	R^2	Zeroth Order R^2
TC10	0.01326 ± 8.7E-4	0.9581	0.8224
TC5	0.02326 ± 5.7E-4	0.9976	0.5475
TC1	0.00743 ± 2.3E-4	0.9906	0.8984
TiO₂	0.00688 ± 1.4E-4	0.9956	0.9062

From figure 7.5, it is observed that all the prepared mixed oxide catalysts exhibited higher catalytic efficiency as compared to pure TiO_2 , which might be due to the coexistence effect of optimum CdS loading in the coupled TiO_2 -CdS heterojunction system. The prepared coupled catalyst TC5 has the highest rate constant (0.02326 min^{-1}) among all the other catalysts.

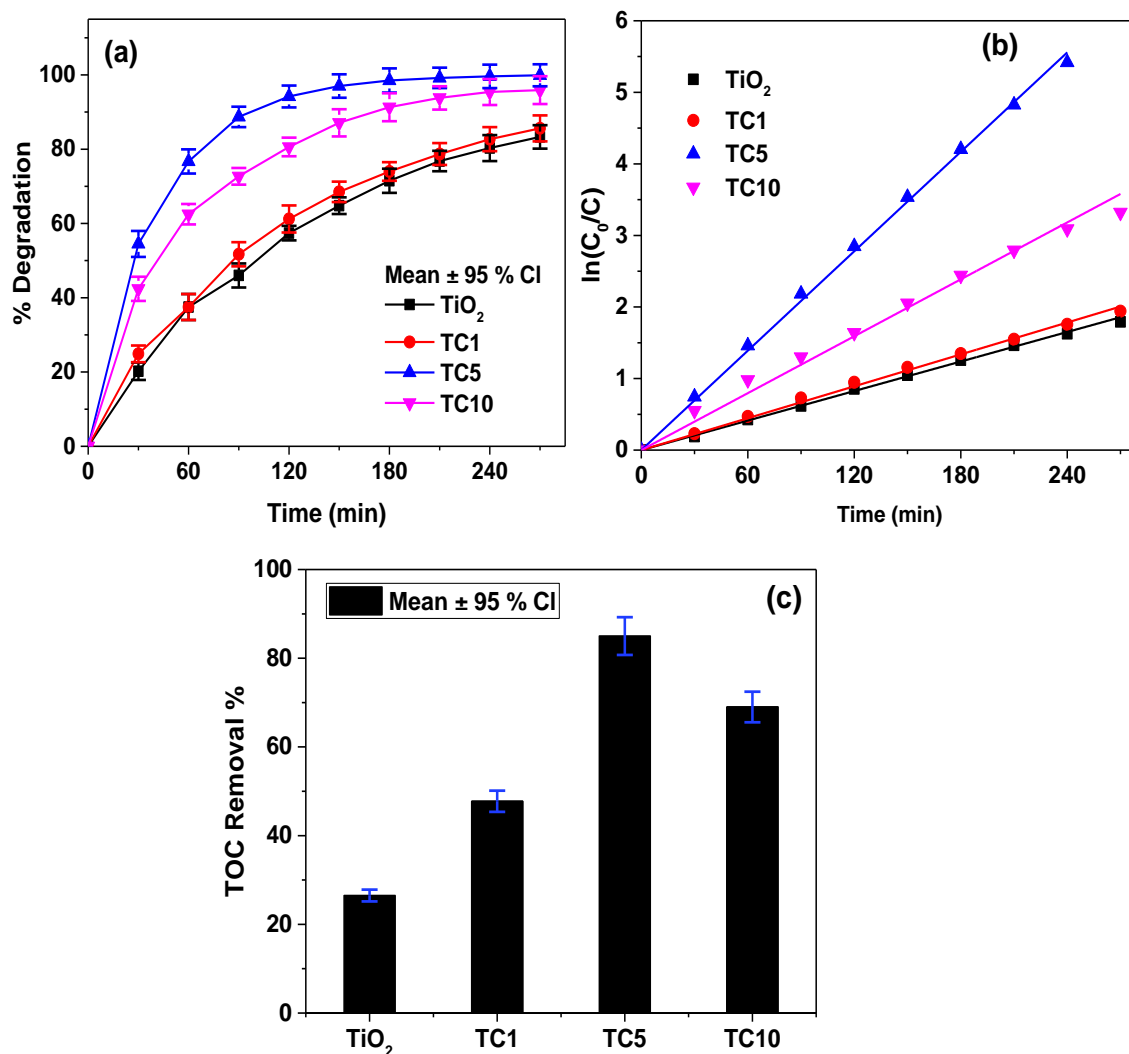


Figure 7.5. Effect of molar ratios on TiO_2 -CdS catalyst for photocatalytic degradation of diclofenac (a) Degradation efficiency for all the mixed oxide catalysts; (b) Kinetics of photodegradation and (c) TOC removal efficiency for all the mixed oxide catalysts (Initial concentration = 20 mg/L, pH = 5 and catalyst loading = 0.6 g/L).

In contrast, the degradation efficiency of the coupled catalyst TC10 was lower as compared to the TC5 catalyst. It can be correlated that the presence of CdS content in TC10 catalyst was insufficient to enhance the charge transfer between the coupled heterojunction

system. TC5 is preferably the best performing coupled photocatalysts among the prepared catalysts. The optimum molar ratio for the preparation mixed-phase TiO₂-CdS catalyst was also evaluated as 5:1. On the other hand, the catalyst TC1 has a poorer degradation rate among the other coupled catalysts, which can be related to the presence of an excess amount of CdS in the TiO₂-CdS heterojunction system. These increased loading of CdS particles coupled system might result in the accumulation of CdS onto TiO₂ surface, thereby resulting in reduced surface area available and inefficient charge transfer under visible light (Cui et al. 2017; Tian et al. 2017).

7.1.2.2 Effect of catalyst dosage

TC5 catalyst was used further to study the effect of catalyst dosage on diclofenac degradation efficiency was investigated in the range of 0.4 to 0.8 g/L, as seen in figure 7.6. The initial diclofenac concentration and pH of the solution were fixed at 20 mg/L and pH 5, respectively. It is revealed that the complete degradation efficiency was reached when the catalyst dosage increased to 0.6 g/L. At the same time, the higher catalyst dosage of 0.8 g/L resulted in poorer photocatalytic efficiency as higher catalyst dosage in solution increases the turbidity and affects the light absorption. Since the photocatalysts were added in suspended form, the excessive suspended catalysts could intensify light scattering phenomenon and screening effects (Achilleos et al. 2010; Herrmann 1999; Martinez et al. 2011).

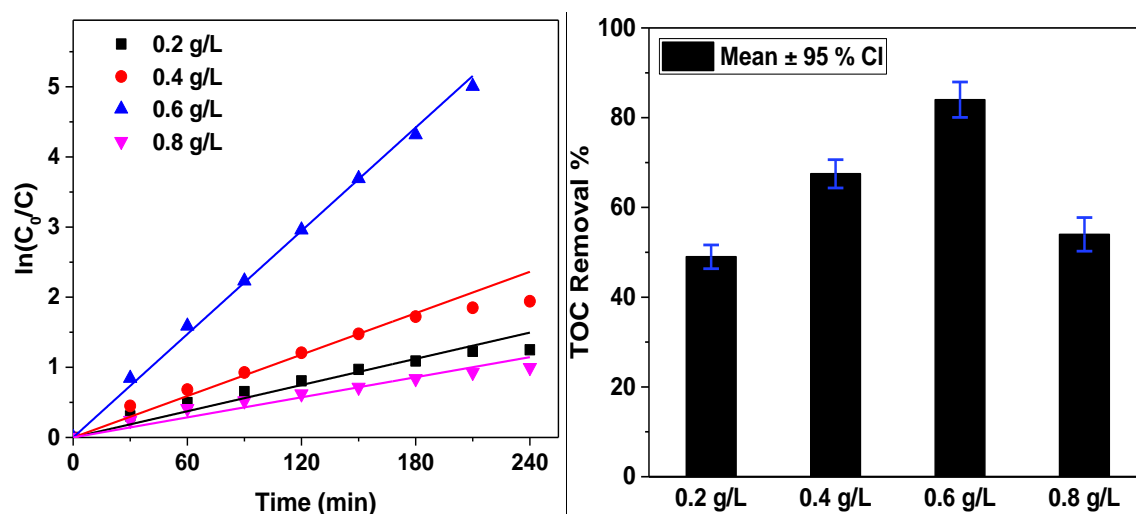


Figure 7.6. Effect of catalyst loading on photocatalytic degradation of diclofenac (pH = 5 and initial diclofenac concentration = 20 mg/L).

7.1.2.3 Effect of pH

Further to study the effect of solution pH for photocatalytic degradation of diclofenac, the experiment was sequentially performed with 20 mg/L of diclofenac solution at different solution pH values (pH 4-7) with a constant catalyst dosage of 0.6 g/L. The photocatalytic degradation of various pharmaceutical compounds generally relied on the surface charge of photocatalyst material and electrostatic interaction between target pollutant and photocatalyst (Kaur et al. 2016; Khodja et al. 2001). The results from figure 7.7 (b) indicate that the catalytic efficiency at solution pH 5 was more effective than at other pH values. The pH_{ZPC} of the TC5 catalyst was found to be 5.8 (Figure 7.7 a), suggesting that the catalyst surface is positively charged at $pH < 5.8$. The pK_a value of diclofenac was reported to be 4.35 (Hiew et al. 2018) and diclofenac will be in negatively charged ion when the pH of the solution was above 4.35. Thus, the higher degradation efficiency at pH 5 was due to the electrostatic attraction between negatively charged diclofenac and positively charged TC5 catalyst. The surface charge of the TC5 catalyst at solution $pH > 5.8$ (pH_{ZPC} of TC5) will be negatively charged. Thus, degradation rate at pH 6 was lower than at pH 5, and still, the rate was higher than at solution pH 7, which might be due to the increased hydroxyl radical generation in the acidic medium (Bagal and Gogate 2014). However, degradation efficiency at pH 4 was poorer than the efficiency at other pH values, which might be due to the molecular form of diclofenac at $pH < pK_a$, where the electrostatic attraction between the TC5 catalyst and diclofenac will not be possible.

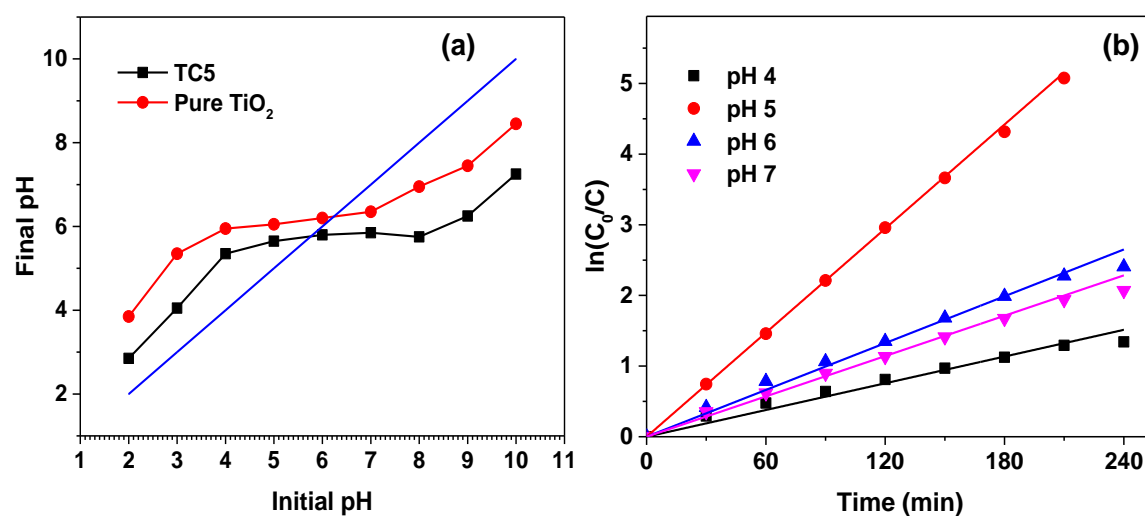


Figure 7.7. (a) The pH_{ZPC} of the TiO_2 and TC5 catalyst and (b) Effect of initial pH on photocatalytic degradation of diclofenac (Initial concentration = 20 mg/L and catalyst loading = 0.6 g/L).

7.1.2.4 Effect of Initial concentration

Effect of initial diclofenac concentration was analyzed at a solution pH 5 and catalyst dosage of 0.6 g/L. Series of initial diclofenac concentrations ranging from 10 mg/L to 25 mg/L were studied and the results are depicted in figure 7.8.

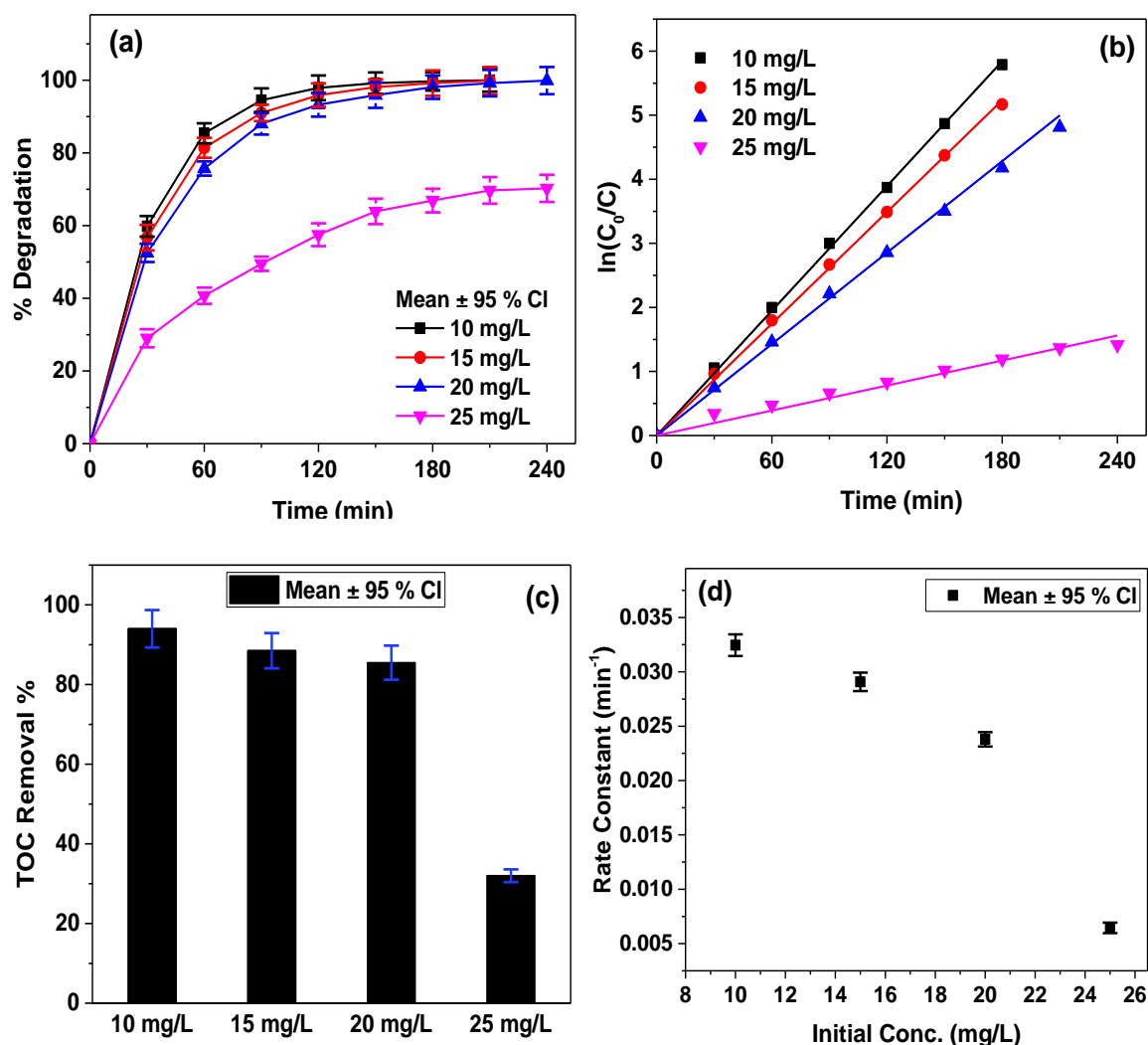


Figure 7.8. Effect of initial concentration on photocatalytic degradation of diclofenac (a) Plot of degradation percentage vs time; (b) Kinetics of photodegradation; (c) TOC removal % for different initial concentration and (d) Rate constant values with respect to initial diclofenac concentration (pH = 5 and catalyst loading = 0.6 g/L).

Primarily it is observed that complete degradation efficiency achieved till the initial diclofenac concentration increased up to 20 mg/L. The degradation kinetics can be expressed by pseudo-first-order reaction with a higher rate constant of 0.03245 min⁻¹ and 0.02379 min⁻¹ for 10 mg/L and 20 mg/L of initial diclofenac concentration, respectively.

However, at 25 mg/L initial concentration, the rate constant reduced immensely as shown in figure 7.8 (d). Generally, at higher substrate concentration, the presence of excessive target molecules could easily be amassed on to the catalyst surface, which could possibly reduce the possibility of photons reaching the surface of photocatalysts. Also, at higher pollutant concentrations, the active radical formation will be sufficient due to the lesser available surface area of the catalysts (Das et al. 2015; Reza et al. 2017).

7.1.3 Effect of scavengers and the role of active species

The study of different scavengers on diclofenac degradation is illustrated in figure 7.9(a). The results revealed that the photocatalytic degradation efficiency of diclofenac was decreased to 26.5 %, 72 % and 42.5 % prominently due to the inhibitory effects of KI, 10 % methanol and NaN_3 , respectively. The photocatalytic efficiency of diclofenac was significantly reduced with the addition of KI. (scavenger for both h^+ and $\cdot\text{OH}$ radicals), signifying that hydroxyl radicals are the prime active species in photocatalytic degradation of diclofenac. Similarly, $\text{O}_2^{\cdot-}$ were also other important species involved in photocatalytic degradation mechanism. However, holes produced in the heterojunction system could be significantly involved in the formation of more $\cdot\text{OH}$ radicals. Holes were also directly involved in degradation mechanism in the reduced amount as the efficiency in the presence of 10 % methanol results in around 30 % reduction in its efficiency.

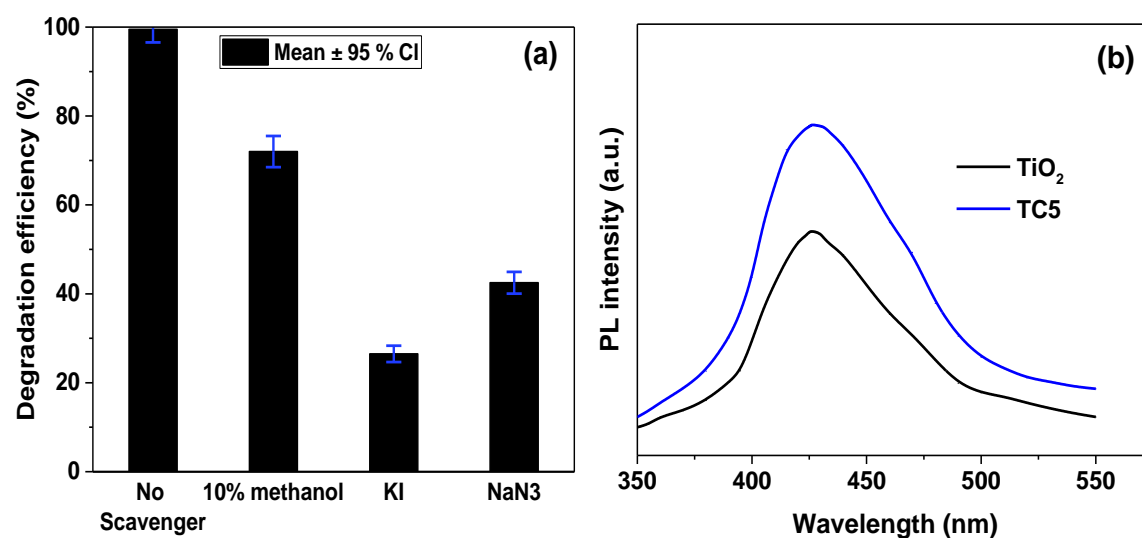
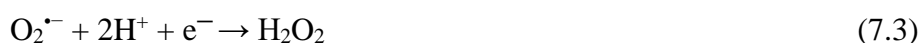
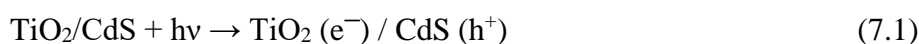


Figure 7.9 (a) Effect of different scavengers on diclofenac degradation and (b) PL spectra for $\cdot\text{OH}$ radical evaluation of pure TiO_2 and TC5 irradiated samples.

The PL spectra depicted in figure 7.9(b) indicate that the mixed-phase catalyst TC5 showed higher fluorescence intensity at 425 nm as compared to pure TiO₂, confirms the generation of hydroxyl radicals and increased charge transfer between heterojunction structure. The effective charge transfer and high hydroxyl radical generation could be well correlated to excellent degradation efficiency shown in photocatalytic experiments.

The presence of coupling effects between TiO₂ and CdS was achieved due to the loading of the optimum concentration of CdS, which promotes the good dispersion of CdS in the coupled photocatalytic system. The coupling of one mixed oxide to other results in reduced electron-hole recombination and increased degradation efficiency in coupled oxides. It is known that CdS nanoparticles have a narrow bandgap, due to which it can be excited by the visible light source to produce electrons and holes. The main redox reaction steps in diclofenac degradation mechanism have been summarized below:



7.1.4 Catalyst stability

The stability and durability of the prepared coupled photocatalyst were evaluated using the same catalysts recycled for five successive reaction cycles, as shown in figure 7.10. The experiments were performed with the optimized operating parameters such as catalyst dosage 0.6 g/L, solution pH 5 and initial concentration of 20 mg/L. In the first cycle efficiency of the catalyst was slightly reduced and in the successive reaction cycles, the photocatalytic efficiency was decreased slowly owing to the presence of intermediates at each reaction cycle and agglomeration of TiO₂-CdS heterojunction catalyst. Nevertheless, the catalyst still has retained its efficiency up to 80 % over the five reaction cycles, signifying the photochemical stability and durability of prepared photocatalysts.

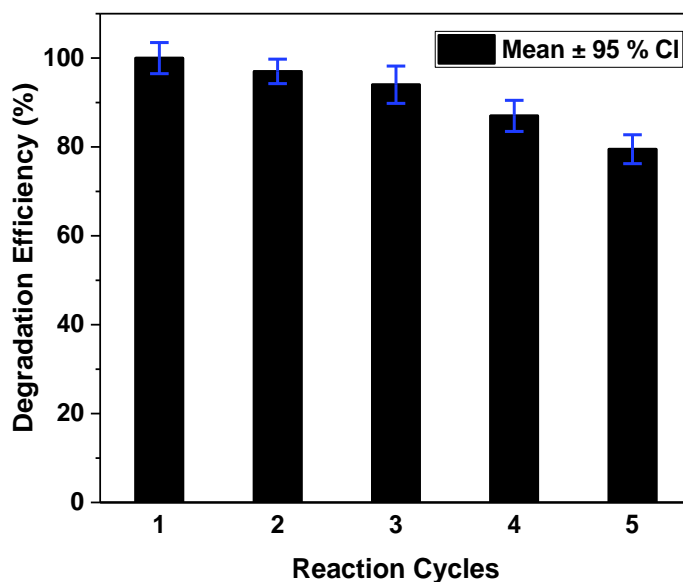


Figure 7.10. Reusability and stability of TiO₂-CdS photocatalysts under optimum reaction conditions (Initial diclofenac concentration = 20 mg/L; pH = 5 and catalyst loading = 0.6 g/L).

7.1.5 Identification of degradation products

Even though complete degradation of diclofenac is achieved, mineralization of organic intermediates has not reached 100 % as observed in TOC removal efficiency i.e. 86 %. To evaluate the number of intermediates formed, LC-MS analysis was performed. The results revealed the formation of several intermediates during the reaction which are visible in LC-MS analysis with peaks at m/z 312, m/z 260, m/z 252, m/z 224, m/z 178, m/z 161, m/z 152, m/z 124 and m/z 108 as shown in figure 7.11.

LC-MS data suggests that the photocatalytic degradation of diclofenac using TiO₂-CdS catalyst can be primarily progressed via hydroxylation reaction and hydroxyl radical attack. Based on the available literature, a tentative diclofenac degradation pathway has been proposed (as shown in figure 7.12) including decarboxylation, C-N cleavage and dechlorination reaction through which diclofenac may well undergo mineralization. Firstly, diclofenac sodium (m/z 318) on reaction with H₂O and the possible formation of NaOH in the aqueous solution, results in diclofenac molecule (m/z 296). Primarily hydroxylation of diclofenac (m/z 296) could result in a new product with an unchanged structure reported as hydroxydiclofenac (m/z 312). The product m/z 312 further endures bond cleavage due to hydroxyl radical attack, resulting in another degradation product m/z 178 as already reported (Liu et al. 2019; Yu et al. 2013). On the other side, decarboxylation of diclofenac

resulted in another intermediate compound at m/z 252, which correlates to 2,6-dichloro-(2-methyl phenyl) aniline, as already reported in the literature (Bagal and Gogate 2014; Madhavan et al. 2010). At the successive reaction path, intermediate at m/z 252 undergoes $\cdot\text{OH}$ radical attack and subsequent C-N cleavage yielding two more degradation products at m/z 161 and m/z 108.

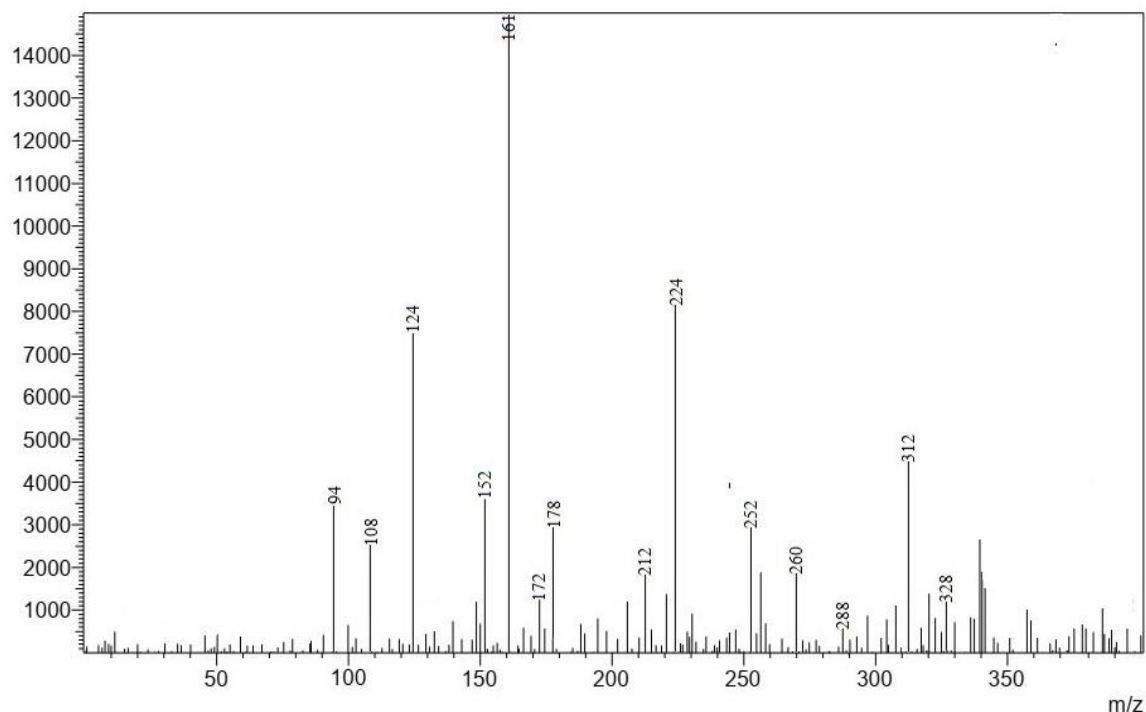


Figure 7.11. LCMS spectra of intermediates formed during the visible light irradiation (Initial diclofenac concentration = 20 mg/L; pH = 5 and catalyst loading = 0.6 g/L).

Diclofenac on different reaction pathways endures C-N cleavage due to $\cdot\text{OH}$ radical attack and results in two new degradation products correspondingly at m/z 161 and at m/z 152 which were reportedly accredited as dichloroaniline and hydroxy phenylacetic acid (Sarasidis et al. 2014). On the secondary step, m/z 161 suffers $\cdot\text{OH}$ radical attack and subsequent dechlorination reactions and further undergoes NH_2 substitution by OH which results in the formation of another degradation product, leading to the formation phenolic derivative with m/z 94. Correspondingly, the secondary reaction at m/z 152 preceded by decarboxylation and hydroxylation reactions leads to the formation of another degradation product with m/z 124.

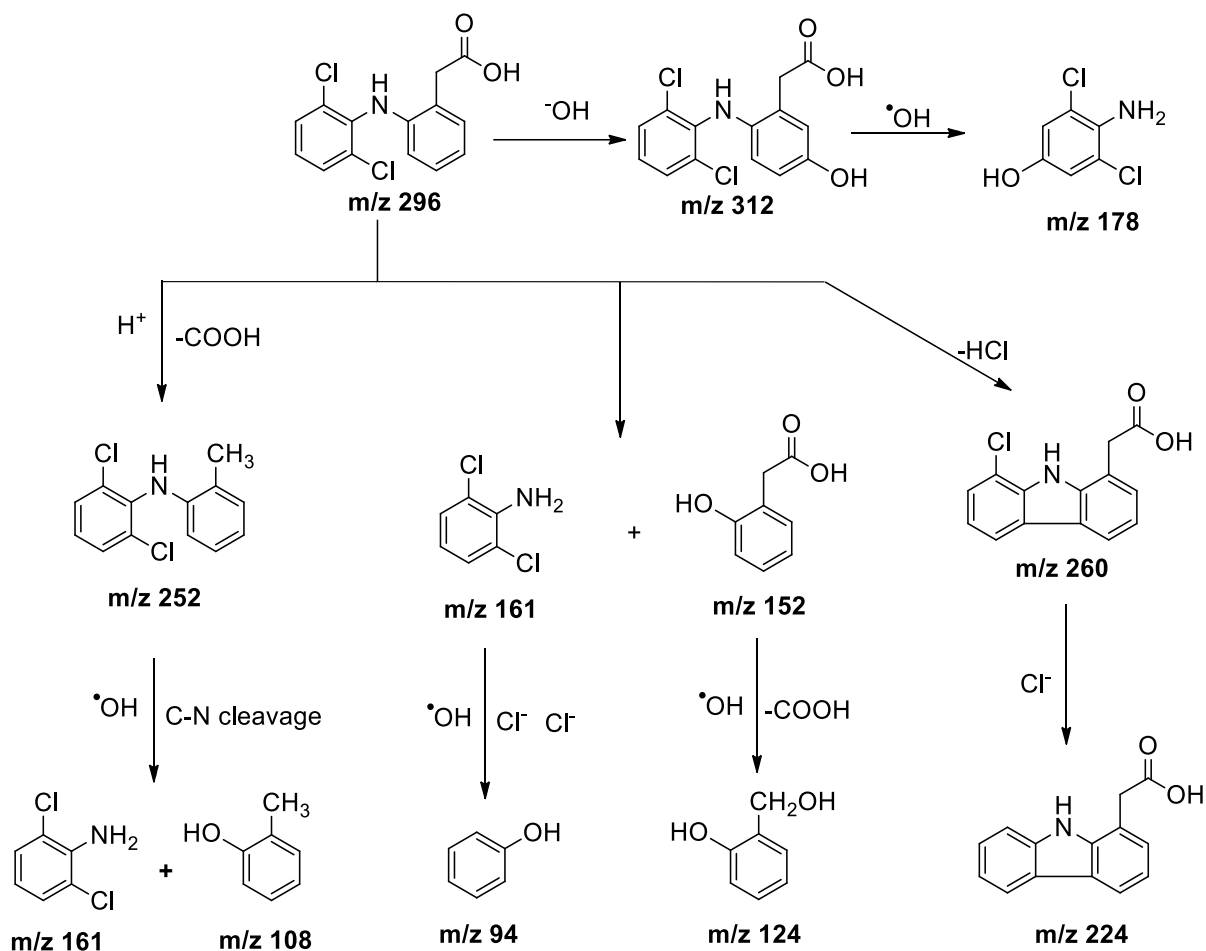


Figure 7.12. Probable diclofenac degradation pathway.

Similarly, diclofenac suffered HCl removal and ring closure mech to another intermediate compound at m/z 260, followed by dechlorination reaction leading to the formation of another unknown intermediate at m/z 224, similar degradation product was also listed in the literature (Yu et al. 2013). The degradation products with m/z 224, m/z 161 and m/z 124 were found out to be stable and the products persisted even at the end of the experiment. The other smaller m/z degradation products are apparently mineralized via cleavage of aromatic rings and transformation of aliphatic compounds (Calza et al. 2006).

7.1.6 Cost estimation of TiO_2 and $\text{TiO}_2\text{-CdS}$ mixed oxides

1 unit of electricity costs Rs. 7

For the preparation of 1 g (approx.) of TiO_2 ,

8 ml TTIP – Rs. 37.6

Isopropanol, 26 ml – Rs. 49.7

Glacial acetic acid, 10 ml – Rs. 30.7

For Hot air oven = 2000 W * 24 h = 48 units = Rs. 336

Total cost involved for TiO₂ preparation = Rs. 37.6 + Rs. 49.7 + Rs. 30.7 + Rs. 336 = Rs. 454

For the preparation of 1 g (approx.) of TiO₂-CdS mixed oxides (TC5),

1 g of TiO₂ as prepared (as reported earlier) = Rs. 454

Cadmium acetate, 2.87 g – Rs. 85.8

Thiourea, 0.95 g – Rs. 8.9

Ethylene glycol, 10 ml – Rs. 21.5

Pluronic, 1 g – Rs. 15.26

Ultrasonication (30 min) = 500 W * (1/2) h = 0.25 units = Rs. 1.75

For Hot air oven = 2000 W * 20 h = 40 units = Rs. 280

Total cost involved for TiO₂-CdS mixed oxide (TC5) preparation = Rs. 454 + Rs. 85.8 + Rs. 8.9 + Rs. 21.5 + Rs. 15.26 + Rs. 1.75 + Rs. 280 = Rs. 867

For 20 mg/L of degradation of diclofenac,

0.8 g of catalyst used = 0.8 g * (Rs. 867) = Rs. 693.6

Irradiation time = 4 h

For visible light irradiation = 400 W * 4 h = 1.6 units = Rs. 11.2

Total cost estimation for degradation of 20 mg of diclofenac using TiO₂-CdS (TC5) mixed oxide = Rs. 693.6 + Rs. 11.2 = Rs. 705.

7.2 CONCLUSION

The preparation of different molar composition of heterojunction TiO₂-CdS photocatalysts was achieved through the two-step hydrothermal treatment. All the prepared photocatalysts were proven to be efficient in photocatalytic degradation of diclofenac with complete removal efficiency was accomplished under irradiation of visible light source. The TC10, TC5 and TC1 coupled photocatalysts were prepared with variation in the molar ratios of Ti and Cd precursors. Among these catalysts, TC5 was found to ideal catalysts for photodegradation of diclofenac within the irradiation time of 4 h. The experimental data was best suited to the pseudo-first-order reaction with the TC5 catalyst exhibiting a rate constant of 0.02316 min⁻¹. The mineralization of diclofenac was also efficient, with 86%

removal was observed over the course of irradiation. The photodegradation efficiency of the TC10 catalyst was considerably lesser than that of TC5 catalyst, which might be due to an insufficient amount of CdS in their coupled photocatalytic system. At the same time, TC1 catalyst exhibited poorer efficiency among the other coupled catalysts. The optimization of variable operating parameters such as solution pH, initial concentration and catalyst dosage was performed successively and the optimum conditions for efficient photodegradation were found to be at pH 5, initial diclofenac concentration of 20 mg/L and 0.6 g/L of catalyst concentration. Effect of different scavengers on diclofenac degradation using TiO₂-CdS was also studied and the results revealed that the powerful hydroxyl radicals ($\cdot\text{OH}$) and superoxide anions ($\text{O}_2^{\cdot-}$) was the dominant active species involved in efficient degradation mechanism for mineralization of diclofenac. The catalyst stability and reusability were also assessed and the prepared coupled TiO₂-CdS photocatalysts displayed good stability and recycling capability with retaining around 80 % of photocatalytic efficiency for over five successive reaction cycles. The formation of several degradation products was assessed and confirmed by LC-MS analysis and it was found that only m/z 224, m/z 124 and m/z 178 were persisted even at the end of irradiation. The remaining other peaks were possibly mineralized through the aromatic ring cleavage mechanism. The tentative degradation pathway was elucidated and the degradation mechanism primarily succeeded via hydroxyl radical attack and hydroxylation reaction. Dechlorination, C-N cleavage and decarboxylation reactions were also involved in the degradation pathway as the further steps.

CHAPTER 8

SUMMARY AND CONCLUSION

The mixed oxide photocatalysts prepared in the present study was found to be effective in photocatalytic degradation system. All the prepared $\text{TiO}_2\text{-SnO}_2$, $\text{TiO}_2\text{-WO}_3$, ZnO-WO_3 and $\text{TiO}_2\text{-CdS}$ mixed oxide catalysts showed excellent photocatalytic activity in the degradation of diclofenac under UV and visible light irradiation. The catalysts were prepared through the hydrothermal method with different molar ratios and characterized with XRD, TEM and EDS. The significant results from this study have been summarised below:

- ❖ The catalyst characterizations revealed that the prepared coupled oxide catalysts were well crystallized and the existence of mixed-phase crystallite formation.
- ❖ The bandgap energy of the coupled oxides was estimated and most of the mixed oxide catalysts have good absorption in the visible light region.
- ❖ The optimum molar ratios of the precursor were analyzed and it was found that the photocatalytic degradation of diclofenac using T20S1 exhibited around 89 % TOC removal over the period of 5 h under UV irradiation whereas ZnW10 exhibited around 76 % TOC removal under visible irradiation.
- ❖ TW10 catalysts attained around 92 % of TOC removal and 86 % of TOC removal was achieved using the TC5 catalyst over a period of 5 h under visible light irradiation.
- ❖ The various optimum parameters such as pH, initial concentration and catalyst loadings were evaluated. The photocatalytic degradation efficiency using $\text{TiO}_2\text{-SnO}_2$ catalyst was maximum at pH 5 and initial diclofenac concentration of 20 mg/L and 0.8 g/L catalyst loading. Similarly, optimum conditions for efficient photodegradation using $\text{TiO}_2\text{-WO}_3$ catalyst were found to be at pH 5 and initial diclofenac concentration of 25 mg/L and 0.6 g/L of catalyst loading.
- ❖ The ZnO-WO_3 catalyst exhibited maximum efficiency at pH 6 and the initial diclofenac concentration of 20 mg/L and 0.8 g/L catalyst loading. Meanwhile, diclofenac

degradation using TiO₂-CdS catalysts showed maximum efficiency at pH 5 and initial diclofenac concentration of 20 mg/L and 0.6 g/L of catalyst loading.

- ❖ The prepared photocatalysts had exhibited better photocatalytic activities as compared to the other catalysts for diclofenac degradation, which is tabulated in table 8.1.

Table 8.1. Performance of as-prepared catalysts in comparison with other researchers.

Catalyst	Catalyst loading	Initial diclofenac concentration	Light source	TOC removal Efficiency	References
Degussa P25	1.6 g/L	20 mg/L	UV Irradiation	65 % (COD)	(Rizzo et al. 2009b)
Degussa P25	0.8 g/L	10 mg/L	UV-A Irradiation	85 %	(Achilleos et al. 2010)
CuBi ₂ O ₄	0.025 g/L	10 mg/L	Visible light	38 %	(Chen et al. 2015)
C doped WO ₃ /TiO ₂	1 g/L	10 mg/L	Visible light	82 %	(Cordero-García et al. 2016)
AgI/g-C ₃ N ₄	0.01 g/L	1 mg/L	Visible light	79 %	(Zhang et al. 2017)
B doped TiO ₂	0.1 g/L	15 mg/L	UV Irradiation	38 %	(Gil et al. 2017)
Ag ₃ PO ₄	0.02 g/L	4 mg/L	Visible light	97 %	(Gou et al. 2017)
Ce@TiO ₂	0.075 g/L	20 µM	UV Irradiation	85 %	(Thiruppathi et al. 2018)
TiO ₂ -SnO ₂	0.8 g/L	20 mg/L	UV Irradiation	89 %	Present Study
TiO ₂ -WO ₃	0.6 g/L	25 mg/L	Visible light (Metal halide,	92 %	
ZnO-WO ₃	0.8 g/L	20 mg/L		400 W)	
TiO ₂ -CdS	0.6 g/L	20 mg/L		86 %	

- ❖ Degradation kinetics was analyzed and it is evident that pseudo-first-order kinetics is well suited for all the mixed oxide catalysts.
- ❖ The presence of the Sn, Cd and W in an optimum amount in the coupled catalytic system is sufficient to enhance the degradation property of bare TiO₂ and ZnO respectively, which resulted in extended absorption range towards the solar spectrum and reducing the recombination of charge carriers.
- ❖ Effect of different scavengers under optimum reaction conditions was studied and it is revealed that the holes and [•]OH radicals were the prominent active species in degradation reaction mechanism for TiO₂-WO₃ and ZnO-WO₃ catalysts. Superoxide radicals (O₂^{•-}) formation is inhibited in these mixed oxide catalysts since degradation mechanism precedes via multi-electron reduction pathway.
- ❖ However, for TiO₂-SnO₂ and TiO₂-CdS catalyst, holes, O₂^{•-} and [•]OH radicals noticeably played a role, but [•]OH radicals were the most prominent species in degradation reaction mechanism for all the mixed oxide catalysts. Effective charge transfer between coupled oxides was confirmed by the increased photoluminescence intensity at 426 nm of mixed oxide as compared to that of bare semiconductor oxides and hence higher photocatalytic activity achieved in mixed oxide catalysts.
- ❖ Several degradation products were formed during the photocatalytic degradation process and it is observed that the hydroxylation, dechlorination, C-N cleavage and decarboxylation were predominant reactions that resulted in diclofenac degradation for all the mixed oxide catalysts.
- ❖ The photocatalytic degradation of diclofenac using the different mixed oxide catalysts in this study was also compared with the degradation/removal of diclofenac through other treatment techniques were presented in table 8.2.
- ❖ It is observed from Table 8.2 that the prepared mixed oxide catalysts were effective for photocatalytic degradation of diclofenac and was better than most of the removal treatment techniques and was comparable with the other treatment techniques.
- ❖ The cost analysis for the preparation of each catalyst was calculated and it is found that the ZnO-WO₃ catalysts were slightly cheaper than other mixed oxide catalysts in terms of preparation of 1 g of catalyst. For the synthesis of 1 g of ZnO-WO₃ catalysts, the estimated cost of about Rs. 406 is required.

Table 8.2. Degradation efficiency for diclofenac removal using different methods and cost analysis comparison for the prepared mixed oxide catalysts

Initial diclofenac concentration	Treatment technique	Degradation efficiency	References	Cost estimation
100 mg/L	Membrane bioreactor	50 % rejection	Kimura et al. (2005)	-
100 mg/L	Photo-Fenton process	94 %	Alalm et al. (2015)	-
20 mg/L	Catalyst Ozonation	76 %	Chen et al. (2016b)	-
6 mg/L	Photocatalysis (Ag ₃ PO ₄)	92 %	Gou et al. (2017)	-
10 mg/L	Photocatalysis C doped WO ₃ /TiO ₂	100 %	(Cordero-García et al. 2016)	-
200 mg/L	Electrochemical Oxidation	91 %	Fernández-Aguirre et al. (2020)	-
20 mg/L	Nanofiltration	99 %	Cuhorka et al. (2020)	-
20 mg/L	Photocatalysis TiO ₂ -SnO ₂	100 %	Present study	Rs. 371
20 mg/L	TiO ₂ -WO ₃	100 %		Rs. 293
20 mg/L	ZnO-WO ₃	97.5 %		Rs. 338
20 mg/L	TiO ₂ -CdS	100 %		Rs. 705

- ❖ However, cost estimation for the overall degradation process for complete degradation of diclofenac, $\text{TiO}_2\text{-WO}_3$ mixed oxides was cost-effective in terms of preparation and complete removal of diclofenac and higher TOC removal efficiency with about Rs. 293 only was required for degradation of 20 mg/L of the initial concentration of diclofenac through photocatalysis under visible light.
- ❖ The total cost estimation for photocatalytic treatment of each catalyst for 20 mg/L of initial diclofenac concentration is compared in table 8.2 and it is found that $\text{TiO}_2\text{-WO}_3$ mixed oxide catalyst was best in terms of degradation efficiency as well as cost-effective compared to other mixed oxides.

8.1 SCOPE FOR FUTURE WORK

- ❖ Even though the prepared coupled photocatalysts showed great efficiency in the degradation of diclofenac, it could be further enhanced by co-doping with metals or by fabricating ternary composite material.
- ❖ The above-prepared catalysts can be coated with a glass substrate and further analyzed for its efficiency in a continuous mode photocatalytic reactor.
- ❖ The prepared mixed oxide photocatalysts showed enhanced activity and it could be applied to photocatalytic hierarchical nanomembrane based water treatment.

REFERENCES

- Abellán, M. N., Giménez, J., and Esplugsas, S. (2009). "Photocatalytic degradation of antibiotics: The case of sulfamethoxazole and trimethoprim." *Catal. Today*, 144(1–2), 131–136.
- Achilleos, A., Hapeshi, E., Xekoukoulotakis, N. P., Mantzavinos, D., and Fatta-Kassinos, D. (2010). "Factors affecting diclofenac decomposition in water by UV-A/TiO₂ photocatalysis." *Chem. Eng. J.*, 161(1–2), 53–59.
- Acuña, V., Ginebreda, A., Mor, J. R., Petrovic, M., Sabater, S., Sumpter, J., and Barceló, D. (2015). "Balancing the health benefits and environmental risks of pharmaceuticals: Diclofenac as an example." *Environ. Int.*, 85, 327–333.
- Ahmed, M. A., Fahmy, A., and Hashem, E. M. (2020). "Fabrication of novel AgIO₄/SnO₂ heterojunction for photocatalytic hydrogen production through direct Z-scheme mechanism." *Journal Photochem. Photobiol. A Chem.*, 112660.
- Ahmed, M. B., Zhou, J. L., Ngo, H. H., Guo, W., Thomaidis, N. S., and Xu, J. (2017). "Progress in the biological and chemical treatment technologies for emerging contaminant removal from wastewater: A critical review." *J. Hazard. Mater.*, 323, 274–298.
- Akpan, U. G., and Hameed, B. H. (2009). "Parameters affecting the photocatalytic degradation of dyes using TiO₂-based photocatalysts: A review." *J. Hazard. Mater.*, 170(2–3), 520–529.
- Al-Rifai, J. H., Gabelish, C. L., and Schäfer, A. I. (2007). "Occurrence of pharmaceutically active and non-steroidal estrogenic compounds in three different wastewater recycling schemes in Australia." *Chemosphere*, 69(5), 803–815.
- Alalm, M. G., Tawfik, A., and Ookawara, S. (2015). "Degradation of four pharmaceuticals by solar photo-Fenton process: Kinetics and costs estimation." *J. Environ. Chem. Eng.*, 3(1), 46–51.

Anandan, S., Sivasankar, T., and Lana-Villarreal, T. (2014). "Synthesis of TiO₂/WO₃ nanoparticles via sonochemical approach for the photocatalytic degradation of methylene blue under visible light illumination." *Ultrason. Sonochem.*, 21(6), 1964–1968.

Artero, V., and Fontecave, M. (2011). "Light-driven bioinspired water splitting: Recent developments in photoelectrode materials." *Comptes Rendus Chim.*, 14(9), 799–810.

Badawy, M. I., Wahaab, R. A., and El-Kalliny, A. S. (2009). "Fenton-biological treatment processes for the removal of some pharmaceuticals from industrial wastewater." *J. Hazard. Mater.*, 169(1–3), 567–574.

Bagal, M. V., and Gogate, P. R. (2014). "Degradation of diclofenac sodium using combined processes based on hydrodynamic cavitation and heterogeneous photocatalysis." *Ultrason. Sonochem.*, 21(3), 1035–1043.

Bartels, P., and Jr, W. V. T. (2007). "Solar radiation influence on the decomposition process of diclofenac in surface waters." *Sci. Total Environ.*, 374(1), 143–155.

Bellardita, M., Addamo, M., Paola, A. Di, and Palmisano, L. (2007). "Photocatalytic behaviour of metal-loaded TiO₂ aqueous dispersions and films." *Chem. Phys.*, 339(1–3), 94–103.

Benotti, M. J., Trenholm, R. A., Vanderford, B. J., Holady, J. C., Stanford, B. D., and Snyder, S. A. (2009). "Pharmaceuticals and Endocrine Disrupting Compounds in US Drinking Water." *Environ. Sci. Technol.*, 43(3), 597–603.

Bonnefille, B., Arpin-Pont, L., Gomez, E., Fenet, H., and Courant, F. (2017). "Metabolic profiling identification of metabolites formed in Mediterranean mussels (*Mytilus galloprovincialis*) after diclofenac exposure." *Sci. Total Environ.*, 583, 257–268.

Brillas, E., Garcia-Segura, S., Skoumal, M., and Arias, C. (2010). "Electrochemical incineration of diclofenac in neutral aqueous medium by anodic oxidation using Pt and boron-doped diamond anodes." *Chemosphere*, 79(6), 605–612.

Brillas, E., Sirés, I., Arias, C., Cabot, P. L., Centellas, F., Rodríguez, R. M., and Garrido,

- J. A. (2005). "Mineralization of paracetamol in aqueous medium by anodic oxidation with a boron-doped diamond electrode." *Chemosphere*, 58(4), 399–406.
- Calza, P., Sakkas, V. A., Medana, C., Baiocchi, C., Dimou, A., Pelizzetti, E., and Albanis, T. (2006). "Photocatalytic degradation study of diclofenac over aqueous TiO₂ suspensions." *Appl. Catal. B Environ.*, 67(3–4), 197–205.
- Chen, W., Li, X., Pan, Z., Ma, S., and Li, L. (2016a). "Effective mineralization of Diclofenac by catalytic ozonation using Fe-MCM-41 catalyst." *Chem. Eng. J.*, 304, 594–601.
- Chen, W., Li, X., Pan, Z., Ma, S., and Li, L. (2016b). "Effective mineralization of Diclofenac by catalytic ozonation using Fe-MCM-41 catalyst." *Chem. Eng. J.*, 304, 594–601.
- Chen, X., Dai, Y., and Guo, J. (2015). "Hydrothermal synthesis of well-distributed spherical CuBi₂O₄ with enhanced photocatalytic activity under visible light irradiation." *Mater. Lett.*, 161, 251–254.
- Chiang, L. F., and Doong, R. A. (2015). "Enhanced photocatalytic degradation of sulfamethoxazole by visible-light-sensitive TiO₂ with low Cu addition." *Sep. Purif. Technol.*, 156, 1003–1010.
- Cleuvers, M. (2004). "Mixture toxicity of the anti-inflammatory drugs diclofenac, ibuprofen, naproxen, and acetylsalicylic acid." *Ecotoxicol. Environ. Saf.*, 59(3), 309–315.
- Cordero-García, A., Guzman-Mar, J. L., Hinojosa-Reyes, L., Ruiz-Ruiz, E., and Hernandez-Rami-rez, A. (2016). "Effect of carbon doping on WO₃/TiO₂ coupled oxide and its photocatalytic activity on diclofenac degradation." *Ceram. Int.*, 42(8), 9796–9803.
- Cuhorka, J., Wallace, E., and Mikulášek, P. (2020). "Removal of micropollutants from water by commercially available nanofiltration membranes." *Sci. Total Environ.*, 720, 137474.
- Cui, S., Li, X., Li, Y., Zhao, H., Wang, Y., Li, N., Li, X., and Li, G. (2017). "Synthesis of

CdS/m-TiO₂ mesoporous spheres and their application in photocatalytic degradation of rhodamine B under visible light.” *Chem. Res. Chinese Univ.*, 33(3), 436–441.

Dalrymple, O. K., Yeh, D. H., and Trotz, M. A. (2007). “Removing pharmaceuticals and endocrine-disrupting compounds from wastewater by photocatalysis.” *J. Chem. Technol. Biotechnol.*, 82(2), 121–134.

Dantas, R. F., Contreras, S., Sans, C., and Esplugas, S. (2008). “Sulfamethoxazole abatement by means of ozonation.” *J. Hazard. Mater.*, 150(3), 790–794.

Das, L., Barodia, S. K., Sengupta, S., and Basu, J. K. (2015). “Aqueous degradation kinetics of pharmaceutical drug diclofenac by photocatalysis using nanostructured titania–zirconia composite catalyst.” *Int. J. Environ. Sci. Technol.*, 12(1), 317–326.

Daya Mani, A., Nandy, S., and Subrahmanyam, C. (2015). “Synthesis of CdS/CeO₂ nanomaterials for photocatalytic H₂ production and simultaneous removal of phenol and Cr(VI).” *J. Environ. Chem. Eng.*, 3(4), 2350–2357.

Domínguez, J. R., González, T., Palo, P., Sánchez-Martín, J., Rodrigo, M. A., and Sáez, C. (2012). “Electrochemical degradation of a real pharmaceutical effluent.” *Water. Air. Soil Pollut.*, 223, 2685–2694.

El-Kemary, M., El-Shamy, H., and El-Mehasseb, I. (2010). “Photocatalytic degradation of ciprofloxacin drug in water using ZnO nanoparticles.” *J. Lumin.*, 130(12), 2327–2331.

Elakhya, N., Gayatri, G., Aparna, S., Rajesh, P., and Ramasamy, P. (2017). “Effect of tin oxide crystallite size on the efficacy of polyaniline-tin oxide nanocomposite based counter electrode for DSSC applications.” *Optik (Stuttg.)*, 142, 436–445.

Espino-Estévez, M. R., Fernández-Rodríguez, C., González-Díaz, O. M., Araña, J., Espinós, J. P., Ortega-Méndez, J. A., and Doña-Rodríguez, J. M. (2016). “Effect of TiO₂-Pd and TiO₂-Ag on the photocatalytic oxidation of diclofenac, isoproturon and phenol.” *Chem. Eng. J.*, 298, 82–95.

Fallah Shojaei, A., Shams-Nateri, A., and Ghomashpasand, M. (2015). “Comparative study

of photocatalytic activities of magnetically separable $\text{WO}_3/\text{TiO}_2/\text{Fe}_3\text{O}_4$ nanocomposites and TiO_2 , WO_3/TiO_2 and $\text{TiO}_2/\text{Fe}_3\text{O}_4$ under visible light irradiation.” *Superlattices Microstruct.*, 88, 211–224.

Fernández-Aguirre, M. G., Berenguer, R., Beaumont, S., Nuez, M., Rosa-Toro, A. La, Peralta-Hernández, J. M., and Morallón, E. (2020). “The generation of hydroxyl radicals and electro-oxidation of diclofenac on Pt-doped SnO_2 –Sb electrodes.” *Electrochim. Acta*, 354, 136686.

Ferrari, B., Paxéus, N., Giudice, R. Lo, Pollio, A., and Garric, J. (2003). “Ecotoxicological impact of pharmaceuticals found in treated wastewaters: Study of carbamazepine, clofibrac acid, and diclofenac.” *Ecotoxicol. Environ. Saf.*, 55(3), 359–370.

Fujishima, A., and Honda, K. (1972). “Electrochemical photolysis of water at a semiconductor electrode.” *Nature*, 238(5358), 37–38.

Gadipelly, C., Pérez-González, A., Yadav, G. D., Ortiz, I., Ibáñez, R., Rathod, V. K., and Marathe, K. V. (2014). “Pharmaceutical Industry Wastewater: Review of the Technologies for Water Treatment and Reuse.” *Ind. Eng. Chem. Res.*, 53(29), 11571–11592.

Gar Alalm, M., Ookawara, S., Fukushi, D., Sato, A., and Tawfik, A. (2016). “Improved WO_3 photocatalytic efficiency using ZrO_2 and Ru for the degradation of carbofuran and ampicillin.” *J. Hazard. Mater.*, 302, 225–231.

Giger, W., Alder, A. C., Golet, E. M., Kohler, H.-P. E., McArdell, C. S., Molnar, E., Siegrist, H., and Suter, M. J.-F. (2003). “Occurrence and Fate of Antibiotics as Trace Contaminants in Wastewaters, Sewage Sludges, and Surface Waters.” *Chim. Int. J. Chem.*, 57(9), 485–491.

Gil, A., García, A. M., Fernández, M., Vicente, M. A., González-Rodríguez, B., Rives, V., and Korili, S. A. (2017). “Effect of dopants on the structure of titanium oxide used as a photocatalyst for the removal of emergent contaminants.” *J. Ind. Eng. Chem.*, 53, 183–191.

Gou, J., Ma, Q., Cui, Y., Deng, X., Zhang, H., Cheng, X., Li, X., Xie, M., Cheng, Q., and Liu, H. (2017). “Visible light photocatalytic removal performance and mechanism of

diclofenac degradation by Ag_3PO_4 sub-microcrystals through response surface methodology.” *J. Ind. Eng. Chem.*, 49, 112–121.

Haap, T., Triebkorn, R., and Köhler, H. R. (2008). “Acute effects of diclofenac and DMSO to *Daphnia magna*: Immobilisation and hsp70-induction.” *Chemosphere*, 73(3), 353–359.

Halling-Sorensen, B., Halling-Sorensen, B., Nielsen, S. N., Nielsen, S. N., Lanzky, P. F., Lanzky, P. F., Ingerslev, F., Ingerslev, F., Holten Lutzhoft, H. C., Holten Lutzhoft, H. C., S.E., J., and S.E., J. (1998). “Occurrence, fate and effects of pharmaceuticals substance in the environment - A review.” *Chemosphere*, 36(2), 357–393.

Hashim, N., Natarajan, P., and Ray, A. K. (2014). “Intrinsic Kinetic Study for Photocatalytic Degradation of Diclofenac under UV and Visible Light.” *Ind. Eng. Chem. Res.*, 53(49), 18637–18646.

Hassani, A., Khataee, A., and Karaca, S. (2015). “Photocatalytic degradation of ciprofloxacin by synthesized TiO_2 nanoparticles on montmorillonite: Effect of operation parameters and artificial neural network modeling.” *J. Mol. Catal. A Chem.*, 409, 149–161.

Heberer, T. (2002). “Occurrence, fate, and removal of pharmaceutical residues in the aquatic environment: a review of recent research data.” *Toxicol. Lett.*, 131, 5–17.

Herrmann, J. (1999). “Heterogeneous photocatalysis: fundamentals and applications to the removal of various types of aqueous pollutants.” *Catal. Today*, 53(1), 115–129.

Hiew, B. Y. Z., Thangalazhy-Gopakumar, S., Lai, K. C., Lee, L. Y., Pan, G.-T., Yang, T. C.-K., and Gan, S. (2018). “Adsorptive decontamination of diclofenac by three-dimensional graphene-based adsorbent: Response surface methodology, adsorption equilibrium, kinetic and thermodynamic studies.” *Environ. Res.*, 168(August 2018), 241–253.

Hoffmann, M. R., Martin, S. T., Choi, W. Y., and Bahnemann, D. W. (1995). “Environmental Applications of Semiconductor Photocatalysis.” *Chem. Rev.*, 95(1), 69–96.

Hori, H., Takashima, M., Takase, M., and Ohtani, B. (2017). “Pristine Bismuth-tungstate Photocatalyst Particles Driving Organics Decomposition through Multielectron Reduction of Oxygen.” *Chem. Lett.*, 46(9), 1376–1378.

Hu, L., Chen, F., Hu, P., Zou, L., and Hu, X. (2016). “Hydrothermal synthesis of SnO₂/ZnS nanocomposite as a photocatalyst for degradation of Rhodamine B under simulated and natural sunlight.” *J. Mol. Catal. A Chem.*, 411, 203–213.

Hu, L., Flanders, P. M., Miller, P. L., and Strathmann, T. J. (2007). “Oxidation of sulfamethoxazole and related antimicrobial agents by TiO₂ photocatalysis.” *Water Res.*, 41(12), 2612–2626.

Huang, J., Ding, K., Wang, X., and Fu, X. (2009). “Nanostructuring Cadmium Germanate Catalysts for Photocatalytic Oxidation of Benzene at Ambient Conditions.” *Langmuir*, 25(14), 8313–8319.

Huang, M., Yu, J., Li, B., Deng, C., Wang, L., Wu, W., Dong, L., Zhang, F., and Fan, M. (2015). “Intergrowth and coexistence effects of TiO₂-SnO₂ nanocomposite with excellent photocatalytic activity.” *J. Alloys Compd.*, 629, 55–61.

Jonker, M. A. J., Svendsen, C., Bedaux, J. J. M., Bongers, M., and Kammenga, J. E. (2005). “Significance Testing of Synergistic/Antagonistic, Dose Level–Dependent, or Dose Ratio–Dependent Effects in Mixture Dose–Response Analysis.” *Environ. Toxicol. Chem.*, 24(10), 2701–2713.

Kanakaraju, D., Glass, B. D., and Oelgemöller, M. (2014). “Titanium dioxide photocatalysis for pharmaceutical wastewater treatment.” *Environ. Chem. Lett.*, 12(1), 27–47.

Kaur, A., Umar, A., Anderson, W. A., and Kansal, S. K. (2018). “Facile synthesis of CdS/TiO₂ nanocomposite and their catalytic activity for ofloxacin degradation under visible illumination.” *J. Photochem. Photobiol. A Chem.*, 360, 34–43.

Kaur, J., Bhukal, S., Gupta, K., Tripathy, M., Bansal, S., and Singhal, S. (2016). “Nanocomposite of CeO₂ and ZnO: An active material for the treatment of contaminated

water.” *Mater. Chem. Phys.*, 177, 512–520.

Khodja, A. A., Sehili, T., Pilichowski, J.-F., and Boule, P. (2001). “Photocatalytic degradation of 2-phenylphenol on TiO₂ and ZnO in aqueous suspensions.” *J. Photochem. Photobiol. A Chem.*, 141(2–3), 231–239.

Kim, J., Lee, C. W. E. E., and Choi, W. (2010). “Platinized WO₃ as an Environmental Photocatalyst that Generates OH Radicals under Visible Light.” *Environ. Sci. Technol.*, 44(17), 6849–6854.

Kimura, K., Hara, H., and Watanabe, Y. (2005). “Removal of pharmaceutical compounds by submerged membrane bioreactors (MBRs).” *Desalination*, 178(1-3 SPEC. ISS.), 135–140.

Kleywegt, S., Pileggi, V., Yang, P., Hao, C., Zhao, X., Rocks, C., Thach, S., Cheung, P., and Whitehead, B. (2011). “Pharmaceuticals, hormones and bisphenol A in untreated source and finished drinking water in Ontario, Canada - Occurrence and treatment efficiency.” *Sci. Total Environ.*, 409(8), 1481–1488.

Kosma, C. I., Lambropoulou, D. A., and Albanis, T. A. (2014). “Investigation of PPCPs in wastewater treatment plants in Greece: Occurrence, removal and environmental risk assessment.” *Sci. Total Environ.*, 466–467, 421–438.

Kümmerer, K. (2004). *Pharmaceuticals in the environment: Sources, Fate, Effects and Risks. 2nd Ed., Springer Sci. Bus. Media.*

Kyzas, G. Z., Fu, J., Lazaridis, N. K., Bikiaris, D. N., and Matis, K. A. (2015). “New approaches on the removal of pharmaceuticals from wastewaters with adsorbent materials.” *J. Mol. Liq.*, 209, 87–93.

Lam, S. M., Sin, J. C., Abdullah, A. Z., and Mohamed, A. R. (2015). “Sunlight responsive WO₃/ZnO nanorods for photocatalytic degradation and mineralization of chlorinated phenoxyacetic acid herbicides in water.” *J. Colloid Interface Sci.*, 450, 34–44.

Lamba, R., Umar, A., Mehta, S. K., and Kansal, S. K. (2015). “ZnO doped SnO₂

nanoparticles heterojunction photo-catalyst for environmental remediation.” *J. Alloys Compd.*, 653, 327–333.

Lei, R., Zhang, H., Ni, H., Chen, R., Gu, H., and Zhang, B. (2019). “Novel ZnO nanoparticles modified WO₃ nanosheet arrays for enhanced photocatalytic properties under solar light illumination.” *Appl. Surf. Sci.*, 463(August 2018), 363–373.

Li, H., Wang, X., Zhang, L., and Hou, B. (2015). “Preparation and photocathodic protection performance of CdSe/reduced graphene oxide/TiO₂ composite.” *Corros. Sci.*, 94, 342–349.

Lin, H. H. H., and Lin, A. Y. C. (2014). “Photocatalytic oxidation of 5-fluorouracil and cyclophosphamide via UV/TiO₂ in an aqueous environment.” *Water Res.*, 48(1), 559–568.

Liu, S., Huang, J., Cao, L., Li, J., Ouyang, H., Tao, X., and Liu, C. (2014). “One-pot synthesis of TiO₂-WO₃ composite nanocrystallites with improved photocatalytic properties under natural sunlight irradiation.” *Mater. Sci. Semicond. Process.*, 25, 106–111.

Liu, W., Li, Y., Liu, F., Jiang, W., Zhang, D., and Liang, J. (2019). “Visible-light-driven photocatalytic degradation of diclofenac by carbon quantum dots modified porous g-C₃N₄: Mechanisms, degradation pathway and DFT calculation.” *Water Res.*, 150, 431–441.

Liu, Z. hua, Kanjo, Y., and Mizutani, S. (2009). “Removal mechanisms for endocrine disrupting compounds (EDCs) in wastewater treatment - physical means, biodegradation, and chemical advanced oxidation: A review.” *Sci. Total Environ.*, 407(2), 731–748.

Lonappan, L., Brar, S. K., Das, R. K., Verma, M., and Surampalli, R. Y. (2016). “Diclofenac and its transformation products: Environmental occurrence and toxicity - A review.” *Environ. Int.*, 96, 127–138.

Loos, R., Tavazzi, S., Mariani, G., Suurkuusk, G., Paracchini, B., and Umlauf, G. (2017). “Analysis of emerging organic contaminants in water, fish and suspended particulate matter (SPM) in the Joint Danube Survey using solid-phase extraction followed by UHPLC-MS-MS and GC-MS analysis.” *Sci. Total Environ.*, 607–608, 1201–1212.

Lv, Z., Zhong, Q., and Ou, M. (2016). “Utilizing peroxide as precursor for the synthesis of

CeO₂/ZnO composite oxide with enhanced photocatalytic activity.” *Appl. Surf. Sci.*, 376, 91–96.

Madhavan, J., Kumar, P. S. S., Anandan, S., Zhou, M., Grieser, F., and Ashokkumar, M. (2010). “Ultrasound assisted photocatalytic degradation of diclofenac in an aqueous environment.” *Chemosphere*, 80(7), 747–752.

Madikizela, L. M., Tavengwa, N. T., and Chimuka, L. (2017). “Status of pharmaceuticals in African water bodies: Occurrence, removal and analytical methods.” *J. Environ. Manage.*, 193, 211–220.

Martinez, C., Canle L., M., Fernandez, M. I., Santaballa, J. A., and Faria, J. (2011). “Aqueous degradation of diclofenac by heterogeneous photocatalysis using nanostructured materials.” *Appl. Catal. B Environ.*, 107(1–2), 110–118.

Mazinani, B., Masrom, A. K., Beitollahi, A., and Luque, R. (2014). “Photocatalytic activity, surface area and phase modification of mesoporous SiO₂-TiO₂ prepared by a one-step hydrothermal procedure.” *Ceram. Int.*, 40(8 PART A), 11525–11532.

Méndez-Arriaga, F., Esplugas, S., and Giménez, J. (2008). “Photocatalytic degradation of non-steroidal anti-inflammatory drugs with TiO₂ and simulated solar irradiation.” *Water Res.*, 42(3), 585–594.

Meng, A., Zhu, B., Zhong, B., Zhang, L., and Cheng, B. (2017). “Direct Z-scheme TiO₂/CdS hierarchical photocatalyst for enhanced photocatalytic H₂ -production activity.” *Appl. Surf. Sci.*, 422, 518–527.

Mestre, A. S., Pires, J., Nogueira, J. M. F., and Carvalho, A. P. (2007). “Activated carbons for the adsorption of ibuprofen.” *Carbon N. Y.*, 45(10), 1979–1988.

Mingyan, W., Wei, Z., Dongen, Z., Shuan, L., Weixing, M., Zhiwei, T., and Jun, C. (2014). “CeO₂ hollow nanospheres decorated reduced graphene oxide composite for efficient photocatalytic dye-degradation.” *Mater. Lett.*, 137, 229–232.

Mishra, M., and Chun, D. M. (2015). “ α -Fe₂O₃ as a photocatalytic material: A review.”

Appl. Catal. A Gen., 498, 126–141.

Nikolaou, A., Meric, S., and Fatta, D. (2007). “Occurrence patterns of pharmaceuticals in water and wastewater environments.” *Anal. Bioanal. Chem.*, 387(4), 1225–1234.

Oaks, J. L., Gilbert, M., Virani, M. Z., Watson, R. T., Meteyer, C. U., Rideout, B. A., Shivaprasad, H. L., Ahmed, S., Jamshed, M., Chaudhry, I., Arshad, M., Mahmood, S., Ali, A., and Khan, A. A. (2004). “Diclofenac residues as the cause of vulture population decline in Pakistan.” *Nature*, 427(February), 630–633.

Paola, A. Di, Garcia-Lopez, E., Marci, G., and Palmisano, L. (2012). “A survey of photocatalytic materials for environmental remediation.” *J. Hazard. Mater.*, 211–212, 3–29.

Pérez-Estrada, L. A., Maldonado, M. I., Gernjak, W., Agüera, A., Fernández-Alba, A. R., Ballesteros, M. M., and Malato, S. (2005). “Decomposition of diclofenac by solar driven photocatalysis at pilot plant scale.” *Catal. Today*, 219–226.

Petrovic, M., Ginebreda, A., Acuña, V., Batalla, R. J., Elosegi, A., Guasch, H., Alda, M. L. de, Marcé, R., Muñoz, I., Navarro-Ortega, A., Navarro, E., Vericat, D., Sabater, S., and Barceló, D. (2011). “Combined scenarios of chemical and ecological quality under water scarcity in Mediterranean rivers.” *TrAC - Trends Anal. Chem.*, 30(8), 1269–1278.

Phanichphant, S., Nakaruk, A., and Channei, D. (2016). “Photocatalytic activity of the binary composite CeO₂/SiO₂ for degradation of dye.” *Appl. Surf. Sci.*, 387, 214–220.

Phoka, S., Laokul, P., Swatsitang, E., Promarak, V., Seraphin, S., and Maensiri, S. (2009). “Synthesis, structural and optical properties of CeO₂ nanoparticles synthesized by a simple polyvinyl pyrrolidone (PVP) solution route.” *Mater. Chem. Phys.*, 115(1), 423–428.

Postigo, C., and Richardson, S. D. (2014). “Transformation of pharmaceuticals during oxidation/disinfection processes in drinking water treatment.” *J. Hazard. Mater.*, 279, 461–475.

Pouretedal, H. R., Tofangsazi, Z., and Keshavarz, M. H. (2012). “Photocatalytic activity of

mixture of ZrO_2/SnO_2 , ZrO_2/CeO_2 and SnO_2/CeO_2 nanoparticles.” *J. Alloys Compd.*, 513, 359–364.

Rabiet, M., Togola, A., Brissaud, F., Seidel, J. L., Budzinski, H., and Elbaz-Poulichet, F. (2006). “Consequences of treated water recycling as regards pharmaceuticals and drugs in surface and ground waters of a medium-sized mediterranean catchment.” *Environ. Sci. Technol.*, 40(17), 5282–5288.

Rao, V. N., Reddy, N. L., Kumari, M. M., Cheralathan, K. K., Ravi, P., Sathish, M., Neppolian, B., Reddy, K. R., Shetti, N. P., Prathap, P., Aminabhavi, T. M., and Shankar, M. V. (2019). “Sustainable hydrogen production for the greener environment by quantum dots-based efficient photocatalysts: A review.” *J. Environ. Manage.*, 248(July), 109246.

Reza, K. M., Kurny, A., and Gulshan, F. (2017). “Parameters affecting the photocatalytic degradation of dyes using TiO_2 : a review.” *Appl. Water Sci.*, 7(4), 1569–1578.

Rizzo, L., Meric, S., Guida, M., Kassinos, D., and Belgiorno, V. (2009a). “Heterogenous photocatalytic degradation kinetics and detoxification of an urban wastewater treatment plant effluent contaminated with pharmaceuticals.” *Water Res.*, 43(16), 4070–4078.

Rizzo, L., Meric, S., Kassinos, D., Guida, M., Russo, F., and Belgiorno, V. (2009b). “Degradation of diclofenac by TiO_2 photocatalysis: UV absorbance kinetics and process evaluation through a set of toxicity bioassays.” *Water Res.*, 43(4), 979–988.

Rohani Bastami, T., Ahmadpour, A., and Ahmadi Hekmatikar, F. (2017). “Synthesis of Fe_3O_4/Bi_2WO_6 nanohybrid for the photocatalytic degradation of pharmaceutical ibuprofen under solar light.” *J. Ind. Eng. Chem.*, 51(2016), 244–254.

Sajjad, A. K. L., Sajjad, S., Iqbal, A., and Ryma, N. ul A. (2018). “ ZnO/WO_3 nanostructure as an efficient visible light catalyst.” *Ceram. Int.*, 44(8), 9364–9371.

Santos, J. L., Aparicio, I., and Alonso, E. (2007). “Occurrence and risk assessment of pharmaceutically active compounds in wastewater treatment plants. A case study: Seville city (Spain).” *Environ. Int.*, 33(4), 596–601.

Sarasidis, V. C., Plakas, K. V., Patsios, S. I., and Karabelas, A. J. (2014). “Investigation of diclofenac degradation in a continuous photo-catalytic membrane reactor. Influence of operating parameters.” *Chem. Eng. J.*, 239, 299–311.

Sarkar, U., Ravindra, K. C., Large, E., Young, C. L., Rivera-Burgos, D., Yu, J., Cirit, M., Hughes, D. J., Wishnok, J. S., Lauffenburger, D. A., Griffith, L. G., and Tannenbaum, S. R. (2017). “Integrated assessment of diclofenac biotransformation, pharmacokinetics, and omics-based toxicity in a three-dimensional human liver-immunocompetent coculture systems.” *Drug Metab. Dispos.*, 45(7), 855–866.

Sathishkumar, P., Meena, R. A. A., Palanisami, T., Ashokkumar, V., Palvannan, T., and Gu, F. L. (2020). “Occurrence, interactive effects and ecological risk of diclofenac in environmental compartments and biota - a review.” *Sci. Total Environ.*, 698, 134057.

Schwaiger, J., Ferling, H., Mallow, U., Wintermayr, H., and Negele, R. D. (2004). “Toxic effects of the non-steroidal anti-inflammatory drug diclofenac. Part I: Histopathological alterations and bioaccumulation in rainbow trout.” *Aquat. Toxicol.*, 68(2), 141–150.

Shahtalebi, A., Sarrafzadeh, M. H., and Rahmati, M. (2011). “Application of nanofiltration membrane in the separation of amoxicillin from pharmaceutical wastewater.” *Iran. J. Environ. Heal. Sci. Eng.*, 8(2), 109–116.

Shanmugam, G., Sampath, S., Selvaraj, K. K., Larsson, D. G. J., and Ramaswamy, B. R. (2014). “Non-steroidal anti-inflammatory drugs in Indian rivers.” *Environ. Sci. Pollut. Res.*, 21(2), 921–931.

Sharma, B. M., Bečanová, J., Scheringer, M., Sharma, A., Bharat, G. K., Whitehead, P. G., Klánová, J., and Nizzetto, L. (2019). “Health and ecological risk assessment of emerging contaminants (pharmaceuticals, personal care products, and artificial sweeteners) in surface and groundwater (drinking water) in the Ganges River Basin, India.” *Sci. Total Environ.*, 646, 1459–1467.

Shen, L., Luo, M., Liu, Y., Liang, R., Jing, F., and Wu, L. (2015). “Noble-metal-free MoS₂ co-catalyst decorated UiO-66/CdS hybrids for efficient photocatalytic H₂ production.”

Appl. Catal. B Environ., 166–167, 445–453.

SHU, Q., YANG, K., YU, J. C., CAO, F., YU, C., and LI, X. (2011). “Preparation of WO₃/ZnO Composite Photocatalyst and Its Photocatalytic Performance.” *Chinese J. Catal.*, 32(3–4), 555–565.

Snyder, S. A., Adham, S., Redding, A. M., Cannon, F. S., DeCarolis, J., Oppenheimer, J., Wert, E. C., and Yoon, Y. (2007). “Role of membranes and activated carbon in the removal of endocrine disruptors and pharmaceuticals.” *Desalination*, 202(1–3), 156–181.

Soufan, M., Deborde, M., and Legube, B. (2012). “Aqueous chlorination of diclofenac: Kinetic study and transformation products identification.” *Water Res.*, 46(10), 3377–3386.

Sousa, J. C. G., Ribeiro, A. R., Barbosa, M. O., Ribeiro, C., Tiritan, M. E., Pereira, M. F. R., and Silva, A. M. T. (2019). “Monitoring of the 17 EU Watch List contaminants of emerging concern in the Ave and the Sousa Rivers.” *Sci. Total Environ.*, 649, 1083–1095.

Stackelberg, P. E., Gibs, J., Furlong, E. T., Meyer, M. T., Zaugg, S. D., and Lippincott, R. L. (2007). “Efficiency of conventional drinking-water-treatment processes in removal of pharmaceuticals and other organic compounds.” *Sci. Total Environ.*, 377(2–3), 255–272.

Sturini, M., Speltini, A., Maraschi, F., Profumo, A., Pretali, L., Irastorza, E. A., Fasani, E., and Albini, A. (2012). “Photolytic and photocatalytic degradation of fluoroquinolones in untreated river water under natural sunlight.” *Appl. Catal. B Environ.*, 119–120, 32–39.

Subash, B., Krishnakumar, B., Sreedhar, B., Swaminathan, M., and Shanthi, M. (2013). “Highly active WO₃-Ag-ZnO photocatalyst driven by day light illumination.” *Superlattices Microstruct.*, 54(1), 155–171.

Sui, Q., Cao, X., Lu, S., Zhao, W., Qiu, Z., and Yu, G. (2015). “Occurrence, sources and fate of pharmaceuticals and personal care products in the groundwater: A review.” *Emerg. Contam.*, 1(1), 14–24.

Sun, J. H., Dong, S. Y., Wang, Y. K., and Sun, S. P. (2009). “Preparation and photocatalytic property of a novel dumbbell-shaped ZnO microcrystal photocatalyst.” *J. Hazard. Mater.*,

172(2–3), 1520–1526.

Tekin, H., Bilkay, O., Ataberk, S. S., Balta, T. H., Ceribasi, I. H., Sanin, F. D., Dilek, F. B., and Yetis, U. (2006). “Use of Fenton oxidation to improve the biodegradability of a pharmaceutical wastewater.” *J. Hazard. Mater.*, 136(2), 258–265.

Thiruppathi, M., Senthil Kumar, P., Devendran, P., Ramalingan, C., Swaminathan, M., and Nagarajan, E. R. (2018). “Ce@TiO₂ nanocomposites: An efficient, stable and affordable photocatalyst for the photodegradation of diclofenac sodium.” *J. Alloys Compd.*, 735, 728–734.

Tian, H., Ma, J., Li, K., and Li, J. (2008). “Photocatalytic degradation of methyl orange with W-doped TiO₂ synthesized by a hydrothermal method.” *Mater. Chem. Phys.*, 112(1), 47–51.

Tian, Z., Yu, N., Cheng, Y., Wang, Z., Chen, Z., and Zhang, L. (2017). “Hydrothermal synthesis of graphene/TiO₂/CdS nanocomposites as efficient visible-light-driven photocatalysts.” *Mater. Lett.*, 194(3), 172–175.

Tomita, O., Ohtani, B., and Abe, R. (2014). “Highly selective phenol production from benzene on a platinum-loaded tungsten oxide photocatalyst with water and molecular oxygen: Selective oxidation of water by holes for generating hydroxyl radical as the predominant source of the hydroxyl group.” *Catal. Sci. Technol.*, 4(11), 3850–3860.

Tröger, R., Klöckner, P., Ahrens, L., and Wiberg, K. (2018). “Micropollutants in drinking water from source to tap - Method development and application of a multiresidue screening method.” *Sci. Total Environ.*, 627, 1404–1432.

Turchi, C. S., and Ollis, D. F. (1990). “Photocatalytic degradation of organic water contaminants: Mechanisms involving hydroxyl radical attack.” *J. Catal.*, 122(1), 178–192.

Vieno, N. M., Härkki, H., Tuhkanen, T., and Kronberg, L. (2007). “Occurrence of pharmaceuticals in river water and their elimination in a pilot-scale drinking water treatment plant.” *Environ. Sci. Technol.*, 41(14), 5077–5084.

Vulliet, E., Cren-Olivé, C., and Grenier-Loustalot, M. F. (2011). “Occurrence of pharmaceuticals and hormones in drinking water treated from surface waters.” *Environ. Chem. Lett.*, 9(1), 103–114.

Wang, L., Ying, G. G., Zhao, J. L., Yang, X. B., Chen, F., Tao, R., Liu, S., and Zhou, L. J. (2010a). “Occurrence and risk assessment of acidic pharmaceuticals in the Yellow River, Hai River and Liao River of north China.” *Sci. Total Environ.*, 408(16), 3139–3147.

Wang, Q., Chen, G., Zhou, C., Jin, R., and Wang, L. (2010b). “Sacrificial template method for the synthesis of CdS nanosponges and their photocatalytic properties.” *J. Alloys Compd.*, 503(2), 485–489.

Webb, S., Ternes, T., Gibert, M., and Olejniczak, K. (2003). “Indirect human exposure to pharmaceuticals via drinking water.” *Toxicol. Lett.*, 142(3), 157–167.

Xekoukoulotakis, N. P., Xinidis, N., Chroni, M., Mantzavinos, D., Venieri, D., Hapeshi, E., and Fatta-Kassinos, D. (2010). “UV-A/TiO₂ photocatalytic decomposition of erythromycin in water: Factors affecting mineralization and antibiotic activity.” *Catal. Today*, 151(1–2), 29–33.

Xie, J., Zhou, Z., Lian, Y., Hao, Y., Liu, X., Li, M., and Wei, Y. (2014). “Simple preparation of WO₃-ZnO composites with UV-Vis photocatalytic activity and energy storage ability.” *Ceram. Int.*, 40(8 PART A), 12519–12524.

Yu, H., Nie, E., Xu, J., Yan, S., Cooper, W. J., and Song, W. (2013). “Degradation of Diclofenac by Advanced Oxidation and Reduction Processes: Kinetic Studies, Degradation Pathways and Toxicity Assessments.” *Water Res.*, 47(5), 1909–1918.

Yuan, Y. P., Yin, L. S., Cao, S. W., Gu, L. N., Xu, G. S., Du, P., Chai, H., Liao, Y. Sen, and Xue, C. (2014). “Microwave-assisted heating synthesis: A general and rapid strategy for large-scale production of highly crystalline g-C₃N₄ with enhanced photocatalytic H₂ production.” *Green Chem.*, 16(11), 4663–4668.

Yurdakal, S., Loddo, V., Augugliaro, V., Berber, H., Palmisano, G., and Palmisano, L. (2007). “Photodegradation of pharmaceutical drugs in aqueous TiO₂ suspensions:

Mechanism and kinetics.” *Catal. Today*, 129(1-2 SPEC. ISS.), 9–15.

Zhang, F., Wang, X., Liu, H., Liu, C., Wan, Y., Long, Y., and Cai, Z. (2019a). “Recent advances and applications of semiconductor photocatalytic technology.” *Appl. Sci.*, 9(12), 2489.

Zhang, K., Jin, L., Yang, Y., Guo, K., and Hu, F. (2019b). “Novel method of constructing CdS/ZnS heterojunction for high performance and stable photocatalytic activity.” *J. Photochem. Photobiol. A Chem.*, 380(April), 111859.

Zhang, W., Chen, X., Han, Y., and Yao, S. (2011). “Effect of SnO₂ addition on phase transformation of TiO₂ photocatalyst prepared by sol-gel method.” *Rare Met.*, 30(S1), 229–232.

Zhang, W., Zhou, L., and Deng, H. (2016). “Ag modified g-C₃N₄ composites with enhanced visible-light photocatalytic activity for diclofenac degradation.” *J. Mol. Catal. A Chem.*, 423, 270–276.

Zhang, W., Zhou, L., Shi, J., and Deng, H. (2017). “Fabrication of novel visible-light-driven AgI/g-C₃N₄ composites with enhanced visible-light photocatalytic activity for diclofenac degradation.” *J. Colloid Interface Sci.*, 496, 167–176.

Zhang, X., Wu, F., Wu, X., Chen, P., and Deng, N. (2008a). “Photodegradation of acetaminophen in TiO₂ suspended solution.” *J. Hazard. Mater.*, 157(2–3), 300–307.

Zhang, Y., Geißen, S. U., and Gal, C. (2008b). “Carbamazepine and diclofenac: Removal in wastewater treatment plants and occurrence in water bodies.” *Chemosphere*, 73(8), 1151–1161.

PUBLICATIONS

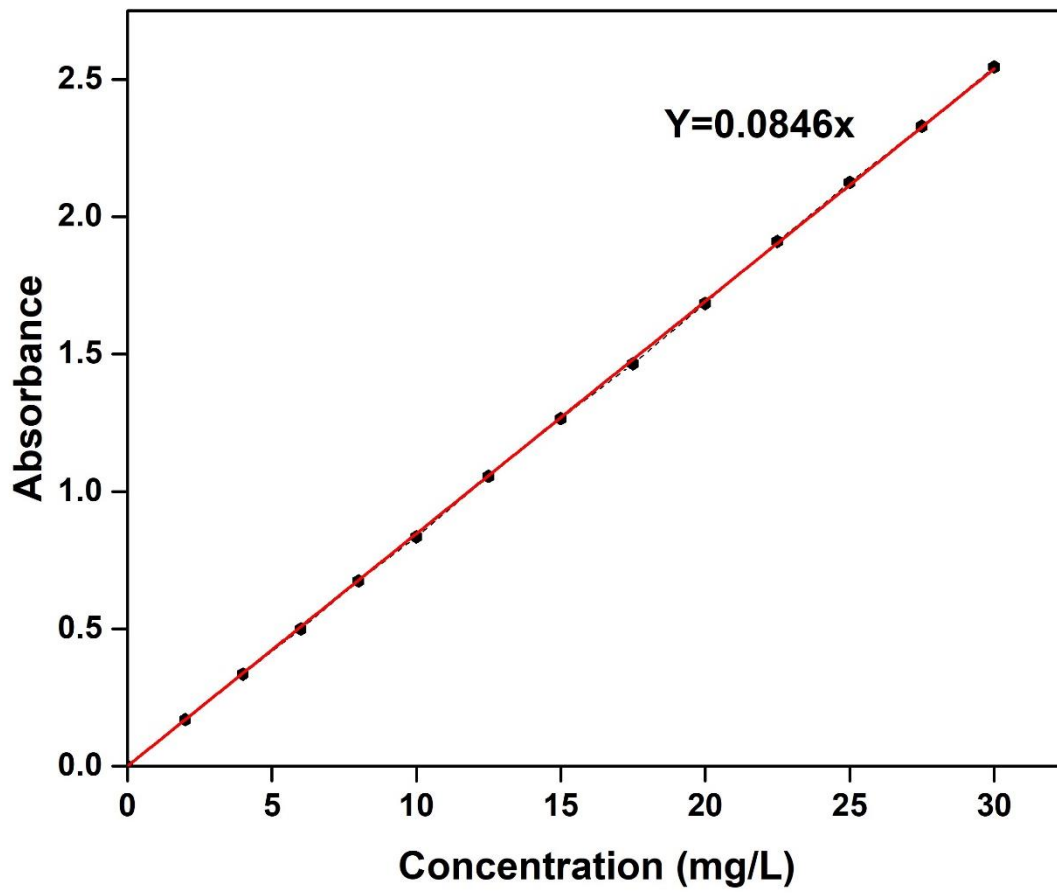
- ❖ **E. Mugunthan**, M. B. Saidutta, and P. E. Jagadeeshbabu, (2017). “Photocatalytic degradation of diclofenac using TiO₂–SnO₂ mixed oxide catalysts.” *Environ. Technol.*, 40(7), 929–941.
- ❖ **E. Mugunthan**, M. B. Saidutta, and P. E. Jagadeeshbabu, (2018). “Visible light assisted photocatalytic degradation of diclofenac using TiO₂-WO₃ mixed oxide catalysts.” *Environ. Nanotechnol. Monit. Manag.*, 10, 322–330.
- ❖ **E. Mugunthan**, M. B. Saidutta, and P. E. Jagadeeshbabu, (2019). “Photocatalytic activity of ZnO-WO₃ for diclofenac degradation under visible light irradiation.” *J. Photochem. Photobiol. A Chem.*, 383, 111993.
- ❖ **E. Mugunthan**, M. B. Saidutta, and P. E. Jagadeeshbabu, (2021). “Photocatalytic degradation of diclofenac using TiO₂-CdS heterojunction catalysts under visible light irradiation.” *Environ. Sci. Pollut. Res.*, <https://doi.org/10.1007/s11356-020-11538-w>.

CONFERENCE PRESENTATIONS

- ❖ **E. Mugunthan**, Saidutta, M. B., and Jagadeeshbabu, P. E., (2016). “Photocatalytic oxidation of diclofenac using TiO₂–SnO₂ mixed oxide catalysts.” *5th International Conference on Research Frontiers in Chalcogen Science and Technology*, December 19-21, Dona Paula, Goa.

APPENDIX

DICLOFENAC CALIBRATION CURVE



BIO-DATA

Name	Mugunthan E
Registration Number	148022CH14F07
Course Name	Ph.D. (Chemical Engineering)
Institution	National Institute of Technology Karnataka, Surathkal
Permanent Address	10, Arkadu Village Palaiyur Post Cheyyur Taluk Chengalpattu District Tamil Nadu-603302
Date of Birth	07-09-1990
Email ID	mugunthanke@gmail.com
Mobile	+91-9600838732